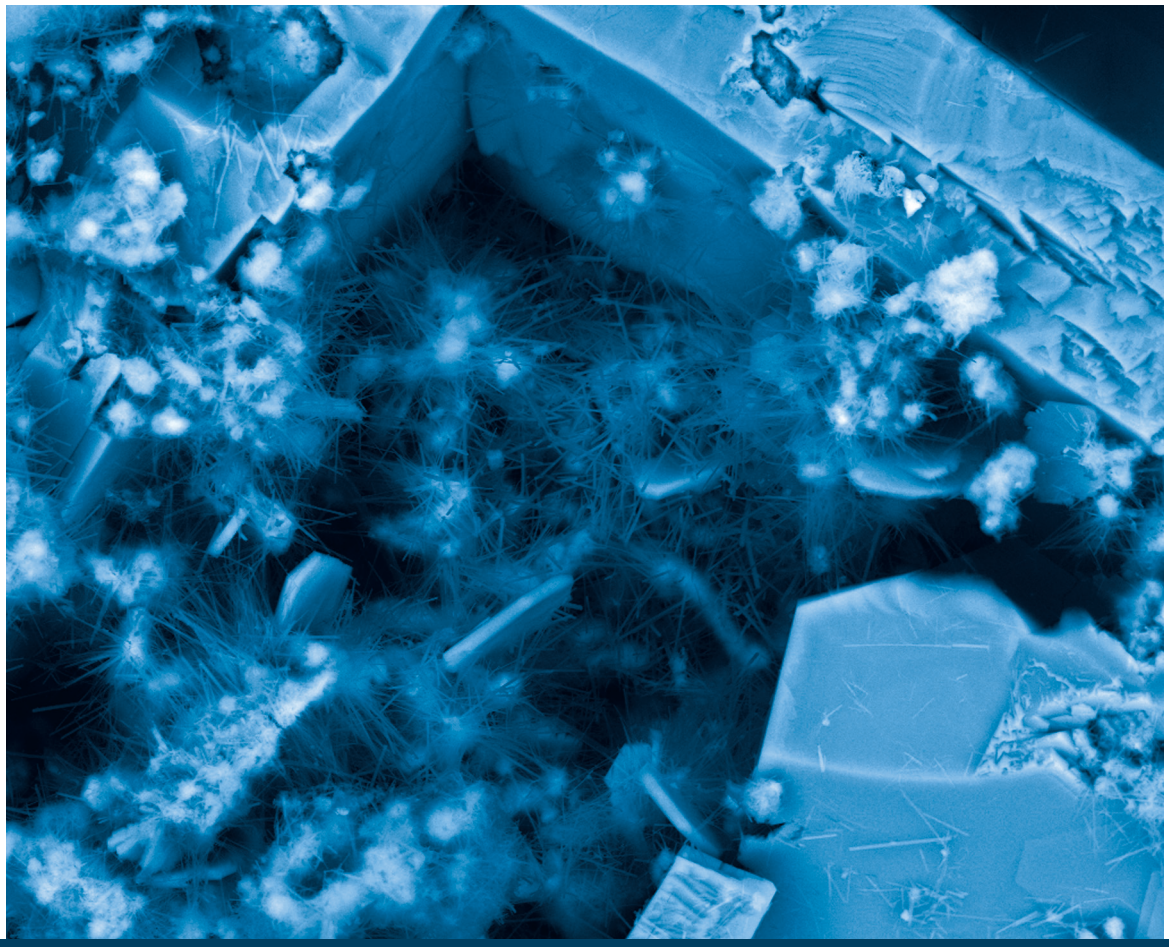

Structural uptake and retention of safety relevant radionuclides by cementitious materials

Steve Lange

Energie & Umwelt / Energy & Environment
Band / Volume 480
ISBN 978-3-95806-437-9

Mitglied der Helmholtz-Gemeinschaft

JÜLICH
Forschungszentrum

Schriften des Forschungszentrums Jülich
Reihe Energie & Umwelt / Energy & Environment Band / Volume 480

Forschungszentrum Jülich GmbH
Institute of Energy and Climate Research
Nuclear Waste Management and Reactor Safety (IEK-6)

Structural uptake and retention of safety relevant radionuclides by cementitious materials

Steve Lange

Schriften des Forschungszentrums Jülich
Reihe Energie & Umwelt / Energy & Environment Band / Volume 480

ISSN 1866-1793 ISBN 978-3-95806-437-9

Bibliografische Information der Deutschen Nationalbibliothek.
Die Deutsche Nationalbibliothek verzeichnet diese Publikation in der
Deutschen Nationalbibliografie; detaillierte Bibliografische Daten
sind im Internet über http://dnb.d-nb.de abrufbar.

Herausgeber und Vertrieb:	Forschungszentrum Jülich GmbH Zentralbibliothek, Verlag 52425 Jülich Tel.: +49 2461 61-5368 Fax: +49 2461 61-6103 zb-publikation@fz-juelich.de www.fz-juelich.de/zb
Umschlaggestaltung:	Grafische Medien, Forschungszentrum Jülich GmbH
Druck:	Grafische Medien, Forschungszentrum Jülich GmbH
Copyright:	Forschungszentrum Jülich 2019

Schriften des Forschungszentrums Jülich
Reihe Energie & Umwelt / Energy & Environment, Band / Volume 480

D 82 (Diss. RWTH Aachen University, 2019)

ISSN 1866-1793
ISBN 978-3-95806-437-9

Vollständig frei verfügbar über das Publikationsportal des Forschungszentrums Jülich (JuSER)
unter www.fz-juelich.de/zb/openaccess.

Abstract

Cement-based materials are widely used in nuclear waste management, for example for the solidification of low and intermediate level wastes, as barrier materials in nuclear waste repositories, or in certain waste containers. However, the barrier function of the applied cementitious materials with respect to the migration of safety relevant radionuclides is not completely understood. In general, the migration behavior of radionuclides in cementitious materials is controlled by radionuclide solubility phenomena at high pH conditions, diffusion, interface processes such as surface complexation, or incorporation of radionuclides into solid phases, including the formation of solid solutions. Within this thesis, open issues regarding the uptake of selected safety relevant long-lived fission and decay products such as ^{129}I, ^{99}Tc and ^{226}Ra in cementitious systems are investigated, using advanced micro analytical and spectroscopic tools. The objective of these investigations is to enhance the mechanistic understanding of the radionuclide uptake and retention in cementitious materials and to evaluate the relevance of cement alteration processes, such as carbonation, with regards to the solid speciation of radionuclides in aged concrete. To unravel the contributions of individual hydrate phases on the radionuclide retention behavior of complex multiphase cementitious materials, a bottom-up approach is adopted here, studying the radionuclide interaction with synthesized hydration phases (model phases) present in cementitious materials, such as calcium silicate hydrates (C-S-H) with different Ca/Si ratios, monosulphate (AFm) and ettringite (AFt) phases, in addition to hardened cement pastes of different composition (e.g. CEM I and CEM V).

The model phases were synthesized under argon atmosphere, using well established procedures. Uptake kinetic and distribution ratios (R_d) of selected safety relevant long-lived radionuclides (RN) such as ^{129}I, ^{99}Tc, Mo and ^{226}Ra were studied in static batch experiments under anoxic conditions. Uptake kinetics and retention mechanisms (anion/cation exchange, electrostatic sorption and phase formation) that contribute to the retention of RN in complex cement systems were identified and investigated. Here, a systematic study of the retention of RN for all relevant cement hydration phases was performed, in particular for systems where data are scarce or lacking to date. The results of this study enhance the understanding of the uptake and retention mechanisms of safety relevant radionuclides in cementitious barriers and materials and thus contribute to the scientific basis of the safety case for deep geological disposal of nuclear wastes.

Kurzzusammenfassung

Zement-basierte Materialien werden vielfältig im Bereich der nuklearen Entsorgung und der Endlagerung radioaktiver Abfälle verwendet, wie zum Beispiel zur Verfestigung von schwach- und mittelaktiven Abfällen oder als Abschirmung in Abfallbehältern. Des Weiteren finden Beton und Mörtel als Konstruktionsmaterial in oberflächennahen und tiefengeologischen Endlagern und als Verfüllstoff Verwendung und sind somit Bestandteil der geotechnischen Barrieren in einem tiefengelogischen Endlager. Das Migrationsverhalten von langzeitsicherheitsrelevanten Radionukliden, wie ^{129}I, ^{99}Tc, ^{93}Mo und ^{226}Ra (RN), ist bisher nicht ausreichend untersucht und die Langzeitwirksamkeit der Barrierefunktion der zementbasierten Materialien nicht vollständig verstanden. Generell wird das Migrationsverhalten von Radionukliden in zementgebunden Materialien durch deren Löslichkeit unter hochalkalischen Bedingungen, sowie durch Diffusionsprozesse, Sorption, Inkorporation in Hydrationsphasen oder auch durch Bildung von Mischkristallen beeinflusst. In dieser Arbeit wurden Sorption und Einbau von langzeitsicherheitsrelevanten Radionukliden, wie ^{129}I, ^{99}Tc, ^{93}Mo und ^{226}Ra in Zementsystemen mit Hilfe mikoanalytischer und spektroskopischer Methoden untersucht. Ziel dieser Arbeit war es ein besseres Verständnis für den Mechanismus der Aufnahme und Rückhaltung der Radionuklide in Zementsystemen zu generieren. Weiterhin soll der Einfluss von Alterationsprozessen auf die Rückhaltung der an den Feststoffen sorbierten Radionuklide untersucht werden. Um den Einfluss der individuellen Zementhydratphasen in komplexen multi-phasigen Zementsystemen auf das Retentionsverhalten der einzelnen Radionuklide zu bestimmen, wurde ein bottom-up Ansatz verwendet, und die Interaktion der Radionuklide mit einzelnen synthetisierten Zementhydratphasen (Zementmodellphasen), wie z. B. Calciumsilikathydrat (C-S-H) mit unterschiedlichen Calcium zu Silizium Verhältnis, Monosulfatphasen (AFm) und Ettringit (AFt) sowie mit verschiedenen ausgehärteten Zementpasten (z. B. CEM I und CEM V) untersucht.

Die verwendeten Zementmodellphasen wurden hierbei auf Basis von in der Literatur beschriebenen Methoden unter Argonatmosphäre synthetisiert. Die Reaktionskinetik und Gleichgewichtsverteilung (R_d) von ausgewählten langzeitsicherheitsrelevanten Radionukliden in Systemen mit Zementmodellphasen und Zementstein wurden insbesondere in statischen Batchexperimenten unter anoxischen Bedingungen (Inertgas Atmosphäre) untersucht. Hierbei wurde die Sorptionskinetik untersucht und die Mechanismen (An-/Kationenaustausch,

elektrostatische Sorption und Phasenbildung), die einen Beitrag zur Rückhaltung von RN in Zementsystemen leisten, identifiziert. In dieser Arbeit wurde zum ersten Mal eine systematische Untersuchung zur Rückhaltung der o. g. RN an allen relevanten Zementhydratationsprodukten durchgeführt.

Die Ergebnisse dieser Arbeit tragen zu einem verbesserten Verständnis der Aufnahme und Retention von langzeitsicherheitsrelevanten Radionukliden in Zement-basierten Barrieresystemen bei und liefern damit einen wissenschaftlichen Beitrag zur Langzeitsicherheitsbetrachtungen für die Endlagerung radioaktiver Abfälle.

Table of Contents

List of abbreviations

ACW	Artificial cement pore water
AFm	Al_2O_3-Fe_2O_3-mono
AFt	Al_2O_3-Fe_2O_3-tri
ANDRA	Agence Nationale pour la Gestion des Déchets Radioactifs (France)
BET	Brunauer–Emmett–Teller (BET) theory
BFS	Blast furnace slag
C_2S	Dicalcium silicate (belite)
C_3A	Tricalcium aluminate
C_3AH_6	Hydrogarnet
C_3S	Tricalcium silicate (alite)
CAC	Calcium aluminate cement
C-S-H	Calcium silicate hydrates
DEF	Delayed ettringite formation
EDS	Energy-dispersive X-ray spectroscopy
EXAFS	Extended X-ray absorption fine structure
FS	Fumed silica
GRS	Gesellschaft für Reaktorsicherheit (Germany)
HAC	High alumina cement
HCP	Hardened cement paste
HTS	Haute teneur en silice (High silica content)
ICP-MS	Inductively coupled plasma mass spectrometry
ICP-OES	Inductively coupled plasma optical emission spectrometry
LA	Low alkalinity
LDH	Layered double hydroxide
LDPE	Low density polyethylene
LMA	Long-lived intermediate level waste (Langlebige Mittelaktive Abfälle)
LSC	Liquid scintillation counting

MH	Medium heat generating
MoFAP	Mobile Fission and Activation Products
NAGRA	National Cooperative for the Disposal of Radioactive Waste (Switzerland)
NDA	Nuclear Decommissioning Authority (UK)
ONDRAF/NIRAS	Belgian Agency for Radioactive Waste and Enriched Fissile Materials
NRVB	Nirex Reference Vault Backfill
OPC	Ordinary Portland cement
PFA	Pulverized fuel ash
PSI	Paul-Scherrer-Institut
SAED	Selected area electron diffraction
SEM	Scanning electron microscope
SKB	Swedish Nuclear Fuel and Waste Management Co
SR	Sulfate resisting
SRPC	Sulfate resisting Portland cement
TEM	Transmission electron microscopy
ToF-SIMS	Time of flight secondary ion mass spectrometry
UBA	Cladded concrete shielded container made by GRS
VTT	Technical Research Centre of Finland Ltd
XRD	X-ray diffraction
XRF	X-ray fluorescence

1. Introduction

The peaceful use of nuclear power during the last decades created an increasing amount of nuclear waste. The majority of the nuclear waste is produced by commercial nuclear power plants in operation and in particular during decommissioning. Moreover, civil research in nuclear technology, nuclear medicine, reprocessing of nuclear waste and nuclear fuel production contribute to the quantity of radioactive waste (WNA, 2018). From the many disposal strategies that have been suggested over time, the disposal of radioactive waste in deep geological repositories using a multi-barrier concept is the most favored, in particular for intermediate-level (ILW) and high-level radioactive wastes (HLW) (Committee on Radioactive Waste Management, 2006; European Union, 2011; Kommission Lagerung hoch radioaktiver Abfallstoffe, 2016; NAGRA, 2006). At the technical and scientific level, it is generally agreed that this concept represents the safest and most sustainable option for the management of high-level radioactive waste and spent nuclear fuel. Research and development work on disposal concepts for a save enclosure of the waste has been performed for several decades. However, it remains a challenging task to demonstrate the long-term safety of a deep geological repository for the required timescales of up to one million years.

In the last decades, significant progress has been made on the development of waste management and disposal strategies in many countries and the siting process for geological repositories. In the United Kingdom, the Nuclear Decommissioning Authority (NDA) became operational in 2005 and is now responsible for the decommissioning of 17 nuclear sites. Furthermore, the NDA is also responsible for the development of an underground Geological disposal facility (NDA, 2017), although a site for a repository for higher activity waste has not been selected yet. In 2015 the Environmental Agency accepted the low level waste (LLW) Repository Ltd.'s proposal permitting the continued disposal of low level radioactive waste repository (LLWR) in Cumbria, UK (Environment Agency, 2015). The German Konrad mine site repository was granted in 2007 for low level and intermediate level waste, a former iron ore mine, was licensed under nuclear law and permission for construction and operation as final repository for radioactive waste with negligible heat generation (BfS, 2008). Konrad is planned to be operational in 2027 (BGE, 2018). A German repository site for high level radioactive, heat generating waste will be selected in a stepwise, science-based and transparent process within the framework of the Repository Site Selection Act within the next decades (StandAG, 2017).

Swedish, Swiss, French and Finnish projects on deep geological repositories are making fast progress. The Finnish Government has granted the nuclear waste management organization Posiva in 2015 (Mokka, 2015), as well as the Finnish Radiation and Nuclear Safety Authority in 2016 (Heinonen and Isaksson, 2016) a construction license for a deep geological disposal facility. In the Finnish disposal strategy, a deep geological repository for high level nuclear waste in granite host rock, is located at Olkiluoto. Crystalline host rocks, like granite, are one of three favored potential host rocks, beside clay and salt, for deep geological repositories (IAEA, 2009). Granite has a very low intrinsic permeability, as long as the repository is placed outside of fracture zones, a high heat resistance, but thermal diffusivity and radionuclide retention capacity are mediocre. In the current French and Swiss concepts, clay rocks are explored as host rock for a repository, due to their very low permeability and the high retention potential for radionuclides. On the other hand, the lower thermal resistance results in a larger footprint and needs to be considered in the siting progress. Moreover, higher technical efforts are required for the stabilization of drifts and disposal tunnels (e.g. by shotcreting), due to the lower geomechanical stability of clay rocks. Salt, as an undisturbed host rock, is practically impermeable to water, and exhibits high heat resistance and thermal diffusivity. Tunnels and shafts drilled in salt do not need to be supported by secondary structures and due to the viscosity of salt small holes and gaps will be closed with time (Deutsches Atomforum e.V., 2015; Geckeis et al., 2012).

Irrespective of the host rock, the general concept for the deep geological disposal involves a multi barrier concept. In the multi barrier concept, various engineered barriers (engineered barrier system EBS) in combination with the geological barrier are present to isolate the waste from the biosphere (Ojovan and Lee, 2014). The barrier system consists of a number of components. Design and materials of the barrier system used, depend on the host rock and disposal concept itself, but they can generally be described by the waste matrix, the waste container, the buffer or backfill material, repository walls or tunnel linings and the host rock itself. The engineered barrier system acts to protect the primary waste container that is initially containing the nuclear waste. In case of a container failure, the barriers should limit and delay the release of long-lived radionuclides from the repository near-field into the host rock and the biosphere. Materials considered for waste canisters comprise steel, copper, and concrete materials of various compositions, whereas the selection of backfill materials like bentonite clays, crushed salt, or cementitious materials (e.g. OPC based mortars, Nirex Reference Vault Backfill or Sorel cement) depends on the host rock and disposal concept

(ANDRA, 2008; Bamforth et al., 2012; Crossland and Vines, 2001; ONDRAF/NIRAS, 2001; Schatz and Martikainen, 2012).

Cementitious materials are applied for various tasks in nuclear waste management and disposal due to their radionuclide immobilization potential, including low solubility of many metals at high pH (Ochs et al., 2016). Beside the use of cement for the solidification of liquid wastes or bulk materials, concrete is used as shielding in double walled waste containers or as a container material on its own (ANDRA, 2005; Kugel and Möller, 2017; Poyet, 2006). Furthermore, cementitious materials are widely used in the construction of near surface and deep geological repositories. Tunnels and shafts drilled into clay host rock need to be supported by an engineered lining along the tracks, mostly steel supported shotcrete structures, to avoid break down of material or collapse of engineered structures, providing an additional barrier for the long-term safety of the final repository. Moreover, cementitious backfill materials are intended to be used in the Swiss repository for low and intermediate level waste in Opalinus clay (Figure 1) as well as the Belgian high-level waste repository in Boom Clay (NAGRA, 2008; ONDRAF/NIRAS, 2001). In the latter concept, a HLW container containing a concrete buffer, the so-called "Supercontainer" is used (cf. Bel et al., 2006). In case of the Swedish and Finnish repositories in crystalline rocks, cementitious materials will be used for sealing of fractures to control and limit groundwater inflow.

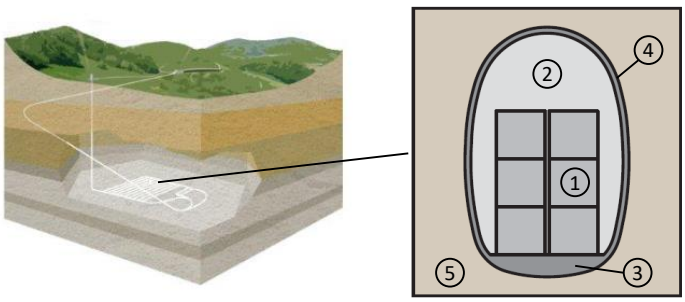

Figure 1 *Schematic view of Swiss LMA/SMA repository concept for geological disposal of low and intermediate level wastes (NAGRA. 2008).1) Waste container; 2) Mortar; 3) Construction concrete; 4) Shotcrete lining; 5) Clay host rock (Opalinus Clay). (Copyright Nagra, NTB 08-01, Fig. 3.9)*

Cement grouting of the rock was discovered to be the main tool in controlling water ingress into the underground tunnels of the final repository and the applied cementitious materials will also act as a barrier material in case of a canister failure (Kronlöf, 2003). Salt concrete (i.e. concrete using OPC and fly ash as binder and crushed salt as aggregate) and magnesia-based Sorel cements are used for drift and shaft seals and partly as backfill material in repositories in salt rocks (Mauke and Herbert, 2015; Ranft et al., 2010). Due to this widespread usage of cementitious materials in the repository near-field, an in-depth understanding of the migration behavior of safety-relevant radionuclides, in particular mobile fission and activation products (MoFAPS such as ^{135}Cs, ^{129}I, ^{99}Tc, ^{93}Mo or ^{79}Se) in cementitious environments is important with respect to the long-term safety of the repository.

The migration behavior of radionuclides in cementitious materials is controlled by radionuclide solubility phenomena at high pH conditions, diffusion, interface processes such as surface complexation, or incorporation of radionuclides into solid phases, including the formation of solid solutions. The phase composition and the physical properties like porosity and strength of cementitious materials depend on various factors such as the type and composition of the cement, the usage of cement additives amount of water used for the hydration, hydration time, the cement composition and cement additives, the retention of radionuclides can vary in terms of retention potential or even in terms of the mechanism itself. Over the last decades, a large number of studies focused on the uptake and retention of radionuclides by hardened cement pastes or concretes (cf. Atkins et al., 1994; Atkins and Glasser, 1992; Atkins et al., 1991a; Berner, 1992; Evans, 2008; Glasser and Atkins, 1994; Hinchliff, 2015; Holland and Lee, 1992; Jantzen et al., 2010; Kim et al., 2011; Ochs et al., 2016; Wieland, 2014 and reviews by Evans, 2008; Glasser, 2011; Glasser, 1997; Gougar et al., 1996; Jantzen et al., 2010). Within these studies, the retention potential of various cement formulations and effects of the admixture of blast furnace slag or fly ash etc. on the barrier function of cementitious materials were investigated (Allen et al., 1997b; Atkins and Glasser, 1992; Smith and Walton, 1993; Sugiyama and Fujita, 1999). Using batch uptake or diffusion experiments, radionuclide distribution coefficients and diffusion coefficients were obtained in these studies for a variety of cementitious materials, leading, inter alia, to the development of various sorption coefficient databases (e.g. Heath et al., 2000; Ochs et al., 2016; Wang, 2013; Wieland, 2014; Wieland and Van Loon, 2002). However, the mechanisms governing the immobilization of various safety relevant radionuclides by cementitious materials on the molecular scale are still not completely

understood and detailed data for safety relevant radionuclides (e.g. ^{226}Ra, ^{129}I, ^{99}Tc, ^{93}Mo, ^{79}Se) from scientific and applied perspective are scarce or lacking.

2. Cementitious materials and their application in nuclear waste management

2.1. Composition and properties of cementitious materials

Concrete is a composite material composed of fine and coarse aggregates bonded together with a fluid cement paste, often based on ordinary Portland cement (OPC), which hardens over time. Hydraulic cements like Portland cement set and become adhesive due to a chemical reaction between the dry ingredients (cement clinker) and water, which results in the formation of various hydration phases.

For the production of OPC clinker sources of calcium oxide and silicon oxide are needed, as well as small amounts of aluminum oxide and iron oxide. Since it is produced from natural resources, the final composition of cement varies slightly, depending on the source of raw materials (e.g.: limestone, clay or shale). For the production of Portland cement clinker typically limestone and a clay or shale, providing CaO and SiO_2 respectively, are mixed and ignited (Taylor, 1997). Reactions taking place during heating the material in a rotary kiln to 1450°C can be divided into three subgroups (Figure 2). The first step below 1300°C can be described by the decomposition of calcite and clay minerals, where water and CO_2 are removed from the system. In this stage the major product formed is a dicalcium silicate (belite, Ca_2SiO_4). At temperatures above 1300°C the belite is reacting with remaining lime to form the tricalcium silicate alite (Ca_3SiO_5). Furthermore, a melt is formed consisting of aluminate and ferrite. After cooling, the clinker material forms it final phase assembly. The agglomerated clinker contains 45-80% tricalcium silicate (alite), 0-32% dicalcium silicate (belite), 4-14% calcium aluminoferrite, 7-15% tricalcium aluminate and to some minor extend free CaO as well as MgO (Taylor, 1997; Verein Deutscher Zementwerke, 2002). After cooling, the clinker is ground into a fine powder. During grinding, additives like polycarboxylether can be added to limit coating of the mill and enhance workability. Gypsum is added during grinding to slow down setting of the cement after the addition of water.

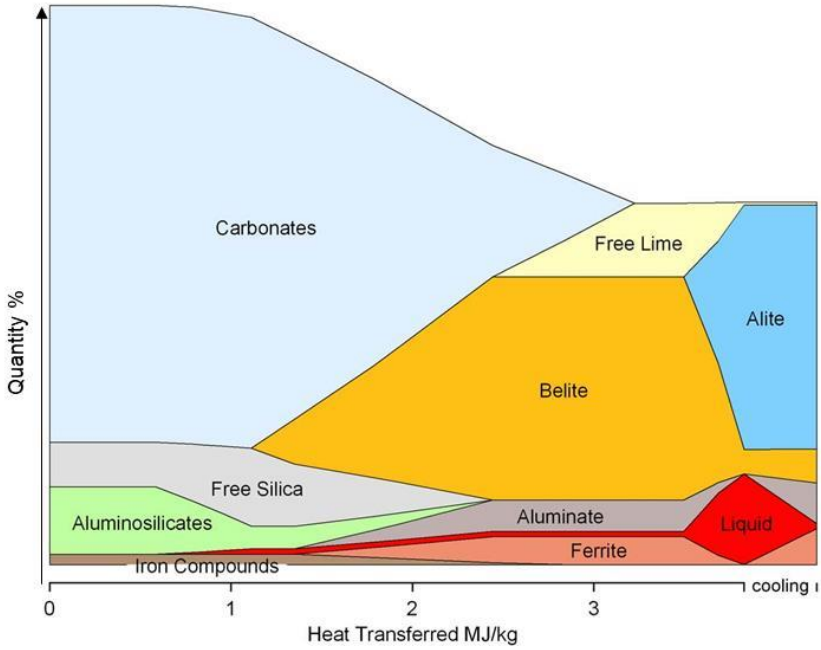

Figure 2 *Composition of cement clinker material in a rotary kiln as a function of heat transferred. (Source: www.cementkilns.co.uk/ckr_therm.html: 28.08.2017, modified)*

The properties of Portland cement based materials like setting time, flow workability, heat production on hydration, mechanical strength etc. can be adjusted to fit the requirements for the final concrete product by blending the Portland cement clinker with other materials. DIN EN 197-1 defines five main types of cement (CEM I – CEM V) comprising 27 different cement formulations with varying in the kind and amount of constituent (volcanic ash glasses, calcined clays and shale). Pozzolans itself are used in cement chemistry to reduce pH of cement pore water and add mechanical strength. BFS containing cements develop strength more slowly than OPC, however, due to the reactivity of BFS, BFS cement develops higher strength after 28 days compared to OPC. The addition of fly ash enhances the workability of the cement paste and gives a lower porosity in the HPC. Furthermore, to increase or decrease setting retardation or acceleration agents can be added.

Cement formulations are selected in most cases to address specific requirements regarding mechanical properties, heat of hydration, and resistance or workability. However, also solute transport and diffusion properties can be adjusted, e.g. by addition of silica fume or by reducing/increasing the water to cement ratio. Even though cement properties are adjustable

to fit the needs for most applications, in some cases special cement formulations are needed to fulfill specialized tasks. Hence, several special cement formulations like low pH cement (low in sodium, potassium and portlandite), sulfate resisting Portland cement SRPC (low in alumina), and HTS cements ("haute teneur en silice" a cement rich in silica), non OPC based cements like CAC (calcium aluminate cement), salt cement and Sorel cement (also known magnesium oxychloride cement) are used for specific purposes. HTS cement can be produced by addition of fumed silica to cement. This also effects, beside the acceleration of the clinker hydration, the density of the final paste a higher mechanical strength as well as lower permeability due to filling of small spaces by fine material used. In contrast to OPC, CAC cement is made from limestone and bauxite or other materials low in SiO_2. The educts are complete reacted at temperatures between 1450°C and 1600°C to give various calcium aluminates like CA ($CaAl_2O_4$), $C_{12}A_7$ ($Ca_{12}Al_{14}O_{33}$) and CA_6 ($CaAl_{12}O_{37}$) (Taylor, 1997). Beside rapid strength formation, CAC cements are usually more resistant to sulfate and many other chemical attacks. Sorel cement on the other hand differs quit strongly from the previously described cement formulations. Sorel cement is a magnesia based binder obtained by mixing magnesium oxide and magnesium chloride with water. The final hydration product is a magnesium oxychloride. This cement is used for production of backfill material in the Asse repository (The Federal Office for Radiation Protection, 2009).

2.2. Cement hydration

OPC is a complex mixture of alite, belite, calcium aluminoferrite, tricalcium aluminate, free CaO and MgO (chapter 2.1). Its hydration behavior and chemistry and the hydration products formed have been addressed in many studies (Atkins et al., 1991a; Baquerizo et al., 2015; Bennett et al., 1992; Berner, 1988; Blanc et al., 2010a, b; Breval, 1976; Damidot et al., 2011; Lothenbach and Wieland, 2006; Matschei et al., 2007; Merlini et al., 2007; Scrivener et al., 2015; Tuerker et al., 2003; Wei and Yao, 2013).

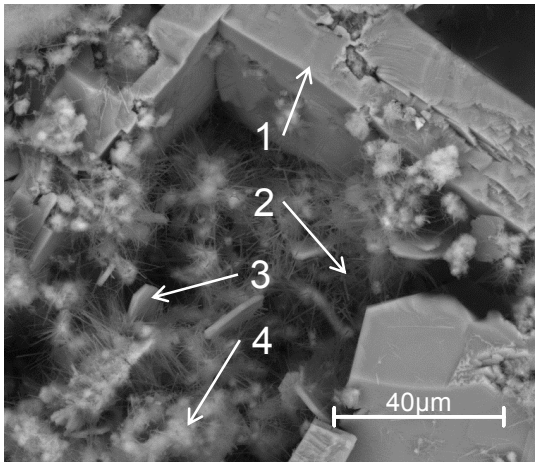

Figure 3 *SEM picture of OPC-based HCP hydrated for 3 days. Large crystals are portlandite (1), needles are ettringite (AFt) (2), hexagonal sheet-like crystals are AFm phases (3), cloudy material surrounding small grains are C-S-H phases (4).*

Hardened cement pastes from OPC containing cements generally consist of a complex heterogeneous mixture of various hydrated phases, mainly nanocrystalline calcium-silicate-hydrates (C-S-H), portlandite ($Ca(OH)_2$), and calcium aluminate/ferrate compounds (AFm/AFt) (cf. Figure 3; Glasser, 2001; Taylor, 1997). The composition of a specific cementitious material and its microstructure (e.g. pore size distribution and pore structure) depend on the cement types and the mixing and curing processes (Taylor, 1997). In Table 1, the calculated composition of different hardened cement pastes is given.

Hydration of cement starts when the grinded clinker material is mixed with water. This mixture is called cement paste; the typical water to cement ratio is in the range of 0.3 L kg^{-1} to 0.6 L kg^{-1} for concretes used for construction purposes. Higher water to cement ratios will increase the porosity of the final HCP increasing its diffusivity and reducing mechanical strength. From the four main clinker phases C_3A is the most reactive. When water is added it reacts quickly and exothermic into a alumina rich gel, which will react with dissolved sulfate ions to give $Ca_4(Al,Fe)_2(OH)_{12}SO_4 \cdot xH_2O$ (AFm). This reaction is the main reason for the very rapid development of strength (Taylor, 1997). The speed of hydration strongly depends on the initial water soluble sulfate concentration, typically increased by the addition of gypsum. Without gypsum the cement paste would rapidly develop strength and workability is decreased (Verein Deutscher Zementwerke, 2002).

Table 1 *Calculated weight proportions of hydrated phases in OPC based hardened cement pastes.*

Hydrate phase	OPC[1] wt.-%	OPC[2] wt.-%	CEM I 52.5 N[3] wt.-%	CEM I 42.5 N[3] wt.-%	NRVB[4] wt.-%
C-S-H	50 - 60	64.6	51	40	24.8
Calcium hydroxide	20 - 30	25.4	20	18	23.2
AFt	0 - 10	5.2	8.9	13.5	-
AFm	0 - 10	18.4	9.77	12.7	-
Hydrotalcite		2.9	1.6	2.9	-
Hydrogarnet		5.5	-	-	10
Calcium carbonate		-	1.1	1.1	42

[1] Glasser (1997)
[2] Taylor (1997)
[3] Lothenbach and Wieland (2006)
[4] Wilson et al. (2017)

The time between initial mixing and strength development should be between 45 and 75 minutes, according to DIN EN 197-1. The amount of gypsum admixed has to match the stoichiometry of ettringite ($Ca_6(Al,Fe)_2(OH)_{12}(SO_4)_3 \cdot 26\ H_2O$; also termed AFt). At this composition the C_3A will react mainly towards hexagonal rod like ettringite crystals within the period of early hydration. The concentration of ettringite will peak at approximately 24 to 48 hours of hydration and decrease afterwards. Release of sulfate from ettringite is giving raise in AFm concentration which finally leads, together with ongoing C-S-H formation, to strength development in the hydrated cement paste.

The hydration of the calcium silicate phases basically forms gel-like calcium silicate hydrates (C-S-H). The hydration reaction of alite (C_3S) and belite (β-C_2S) differ in speed, with the hydration reaction of alite being faster. Typically, 70% of this clinker phase is reacted within the first 28 days of hydration and, more than 99% are reacted after 1 year. Belite (β-C_2S) is reacting slower and responsible for the later strength development. Within the first 28 days of hydration, approximately 30% have reacted and 90% within 1 year (Garbev, 2004). The products formed by the hydration of C_3S and β-C_2S are C-S-H and portlandite ($Ca(OH)_2$). Due to its stoichiometry, hydration of C_3S produces more portlandite. Figure 4 provides an overview of the time dependent hydrate phase development in OPC.

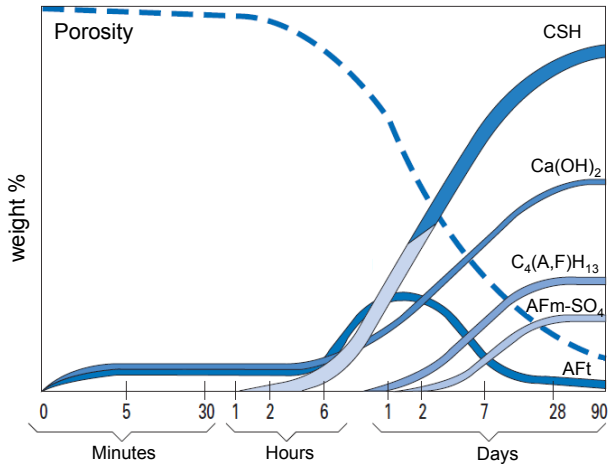

Figure 4 *Schematic view of time dependent hydrate phase development in OPC based cementitious materials (Verein Deutscher Zementwerke (2008), modified).*

The hydration products obtained from cements containing blast furnace slags (e.g. CEM III or CEM or CEM V) are very similar to OPC, although the higher content of alumina and magnesia in BFS containing cement formulations increases the contents of aluminate phases (AFm/AFt) and hydrotalcite ($Mg_6Al_2[(OH)_{16}|CO_3]\cdot 4H_2O$) in the HCP. The addition of fly ash also affects the kinetics of cement hydration. In the early stage of hydration, fly ash slows down the hydration reaction of alite, whereas the additional nucleation sites provided by fly ash accelerate the hydration reaction in later stages (Taylor, 1997). Furthermore, the formation of aluminates and ferrites are also accelerated. In early stages, the content of portlandite is higher compared to OPC, whereas in later stages of hydration, portlandite is consumed due to the pozzolanic reaction.

Calcium aluminate cements (CAC) have similar hydration kinetics and strength development compared to cementitious materials based on Portland cement. Due to the lack of silicon, here the hydration products are mostly calcium aluminates. The actual hydration products of CAC are depending on curing time and curing temperature. At low temperatures and young ages, various calcium aluminates are formed, whereas the major hydration product at curing temperatures above 30°C and at later ages are hydrogarnet type phases (C_3AH_6) and aluminum hydroxides. Since, the retention of radionuclides is a function of the types and amounts of phases formed during hydration, the differences in phase composition of HCP

from various cement formulations are essential to predict the retention potential, based on a component additive approach.

2.3. Major cement hydration phases

2.3.1. C-S-H

Calcium silicate hydrates (C-S-H), with the general formula xCaO·SiO$_2$·yH$_2$O, are the main hydration phase in hardened OPC based cement paste. C-S-H is a nano crystalline material with low long-range order, exhibiting only a few very diffuse structural reflexes in X-ray diffraction analysis, that has been intensively studied in the last decades (Atkins et al., 1992; Chen et al., 2004; Fuji and Kondo, 1981; Grutzeck et al., 1989; Henocq et al., 2014; Lothenbach and Nonat, 2015; Roller and Ervin, 1940; Sugiyama, 2008; Taylor, 1950). The structure of C-S-H is related to the mineral 14Å tobermorite and can be described by a defect tobermorite structure (Lothenbach and Nonat, 2015; Richardson, 2014; Richardson, 2004). C-S-H phases are either formed by hydration of C_2S and C_3S or formed by reaction of calcium hydroxide and silicon oxide, by the pozzolanic reaction. C-S-H gels are characterized according to their calcium to silicon ratio. The two most clearly definable phases were thought to be C-S-H I at low Ca/Si ratios and C-S-H II at high Ca/Si ratios, which are structurally imperfect forms of their natural analogues, namely tobermorite and jennite respectively (Richardson, 2004; Richardson, 2008; Taylor, 1997). However, more recent studies indicate that the environment of Ca and Si is independent of the Ca/Si ratio hence, the tobermorite like structure seems to be preserved (Lothenbach and Nonat, 2015; Sezen et al., 2012).

In general, the C-S-H structure consists of a calcium oxide layer (octahedral layer) with repeating chains of silica dreierketten attached on both sites, providing exchange sites for sorption (Figure 5). With increasing calcium to silicon ratio in C-S-H phases the bridging tetraeder of the silicon dreierketten is missing resulting in the imperfect tobermorite structure. Based on the structural model of Bonaccorsi et al. (2005), all of the silica chains are connected via a bridging tetraeder at Ca/Si ratio of 0.83; at Ca/Si = 1.4 the silica layer is consisting of silicon tetraeder dimers only.

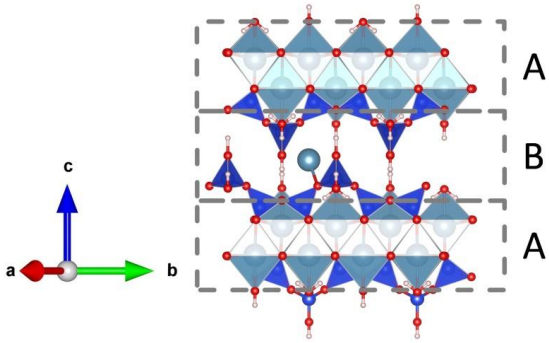

Figure 5 Schematic representation of the C-S-H structure with octahedral CaO_2 layers (A) and the interlayer (B) (Hamid (1981)).

Synthetic C-S-H produced by pozzolanic reaction of calcium hydroxide and silica fume in a batch reaction is limited to a maximum Ca/Si ratio of 1.45 (Lothenbach and Nonat, 2015). This limit can be described by the maximum activity of calcium ions fixed by the solubility of portlandite. Excess calcium will precipitate as $Ca(OH)_2$, if the initial concentration is higher. For Ca/Si ratios below 0.7 the activity of silicon as silicic acid is limiting the lower end giving a mixture with (amorphous) silica at lower Ca/Si ratios. Higher Ca/Si ratios in C-S-H obtained from the hydration of ordinary Portland cement is due to the hydration of alite. On the reaction of alite and water, the solution is supersaturated with respect to calcium, resulting in a C-S-H with a Ca/Si ratio between 2.2 – 1.8 (Lothenbach and Nonat, 2015; Taylor, 1950). In mature cement pastes the Ca/Si ratio is usually between 1.2 and 0.9 (Garbev, 2004).

Beside the dependency of the mean silica chain length and the water content of the C-S-H gels on the Ca/Si ratio, also the equilibrium pH varies with respect to the calcium content in the C-S-H gel (Lothenbach and Nonat, 2015). More precisely, a solution in equilibrium with C-S-H0.9 has a lower pH (pH = 11; c(Ca) = 4 mmol L^{-1}) than a solution in equilibrium with C-S-H1.4 (pH = 12.3; c(Ca) = 21 mmol L^{-1}). Furthermore, due to the difference in surface structure at the different calcium to silicon ratios, the zeta potential changes. The surface charge is created by deprotonation of silanol groups by binding of alkalis and alkaline earths (Na, K, Ca). Calcium can balance the negative charge and is also capable of over compensating the surface charge in the form of $\equiv SiOCa^+$ surface species, resulting in a positive charge at higher Ca/Si ratios (Labbez et al., 2007; Labbez et al., 2011). Therefore, C-S-H1.45 has a positive and C-S-H 0.83 a negative surface charge. The point of zero charge

is at Ca/Si = 1.2 (Ochs et al., 2016). This provides for an increasing anion sorption potential for C-S-H high in calcium and a better cation sorption potential for C-S-H low in calcium. Incorporation of bivalent cations into the C-S-H interlayer as an additional uptake mechanism has been discussed previously by various authors (Komarneni et al., 1986; Komarneni and Tsuji, 1989; Missana et al., 2017; Shrivastava and Glasser, 1986; Shrivastava and Komarneni, 1994; Tits et al., 2006a). Uptake of large cations like radium and barium by C-S-H is usually attributed to cation exchange with calcium and potentially also by silanol-like sorption sites at the C-S-H surface (Missana et al., 2017; Tits et al., 2006a), whereas the uptake of these ions into the C-S-H interlayer has been debated. In general, it was concluded that cations smaller than calcium (e.g. Ni, Co or Zn) as well as Sr can replace calcium in the C-S-H interlayer, whereas the uptake of cations larger than calcium was limited to sorption at surface sites. However, more recent investigations on the uptake of Np(VI/V) and U(VI) by C-S-H suggested that also large cations can be incorporated into the C-S-H interlayer spacing (Gaona et al., 2011; Gaona et al., 2012; Tits et al., 2014; Tits et al., 2011).

2.3.2. AFm and AFt

The aluminate (and ferrite) sulfate phases in hydrated cement pastes are usually termed AFm/AFt, based on their chemical composition. AFm refers to a Al_2O_3-Fe_2O_3-mono-(sulfate) and AFt to a Al_2O_3-Fe_2O_3-tri-(sulfate) phase in cement chemistry terminology. The letter m/t refers to mono or tri substitution of the phase by (monovalent) anions giving the general formula $Ca_2Al(OH)_6^+ X^-$ for AFm phases and $Ca_3Al(OH)_6^+ X^-_3$ for AFt (Taylor, 1997). Beside the similarities in chemical composition, both phases comprise different structures (Figure 6).

In cementitious materials a variety of layered double hydroxides (LDH) phases can be formed depending on the ions present in the hydrated cement paste. LDH in general have received considerable attention in the last decade due to their high anion exchange capacity. The AFm phases in HCP can be structurally described as CaAl-LDH. They are composed of alternating positively charged brucite-type layers and negatively charged layers of anions (interlayer), forming lamellar structured, hexagonal, or pseudohexagonal plates (Figure 6). The hydroxide layers structurally related to brucite (or portlandite) are built from octahedrally coordinated divalent metal cations, with one third of the divalent metal cations replaced by trivalent cations (Matschei et al., 2006). Due to the abundance of calcium and aluminum, the hydroxide layer is occupied by Ca^{2+} and Al^{3+}/Fe^{3+} like in AFm-SO_4

($Ca_4Al_2(OH)_{12}SO_4 \cdot xH_2O$), whereas the anion interlayer can be composed of SO_4^{2-}, OH^-(AFm-OH), or CO_3^{2-}(AFm-CO_3). Friedel's salt (AFm-Cl_2) can be formed due to the ingress of chloride ions into cementitious materials. Furthermore, due to the magnesium contained in the cement formulations, the formation of small amounts of hydrotalcite, a Mg^{2+}-Al^{3+}/Fe^{3+} LDH containing carbonate ions in the interlayer, is often very likely (cf. Taylor, 1997).

AFt, which is structurally related to ettringite ($Ca_6Al_2(OH)_{12}(SO_4)_3 \cdot 26\ H_2O$) on the other hand has a rod and channel like structure whereas the rods contain the tri- and divalent metal cations (Ca^{2+}-Al^{3+}/Fe^{3+}). The anions are located in the channels formed in between the rods. Due to this structure, the anion substituted ettringite-structured end members with AsO_4^{3-}, $B(OH)_4^-$, CO_3^{2-}, CrO_4^{2-}, OH^-, SeO_4^{2-}, SO_3^{2-}, VO_4^{3-} can be synthesized (Baur et al., 2004).

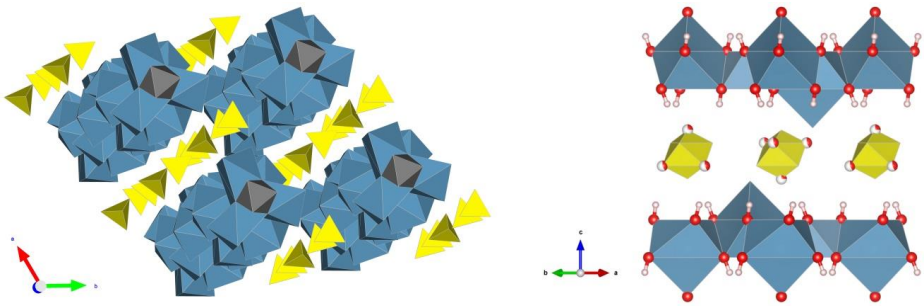

Figure 6 *Schematic view of the column like crystal structure of ettringite (left) and the lamellar structure of AFm-SO_4 (right).*

2.3.3. Hydrogarnet

In the cement literature hydrogarnet is usually defined as the silicon-free composition $Ca_3Al_2(OH)_{12}$ (Figure 7). However, in real cement pastes hydrogarnet often includes Si (Taylor and Newbury, 1984) similar to the mineral katoite ($Ca_3Al_2(SiO_4)_{3-x}(OH)_{4x}$, x = 1.5 to 3).

Hydrogarnet is the thermodynamic stable phase in the CaO-Al_2O_3-H_2O system (Brisi et al., 1986; Pommersheim and Chang, 1986). Hydrogarnet is formed by the reaction of C_3A with water. It has been shown that the direct products of this hydration reaction are C_2AH_8 and C_4AH_{19}, which are subsequently converted into C_3AH_6 (Hydrogarnet) (Taylor, 1997). At elevated temperatures (> 40°C) it is observed that the hydration gives C_3AH_6 directly (Verein Deutscher Zementwerke, 2002). Uptake of RN by hydrogarnet is rarely investigated. Sorption on hydrogarnet may be through ion substitution, e.g. Cr(III) may replace Al in hydrogarnet (Glasser, 2002; Ochs et al., 2016).

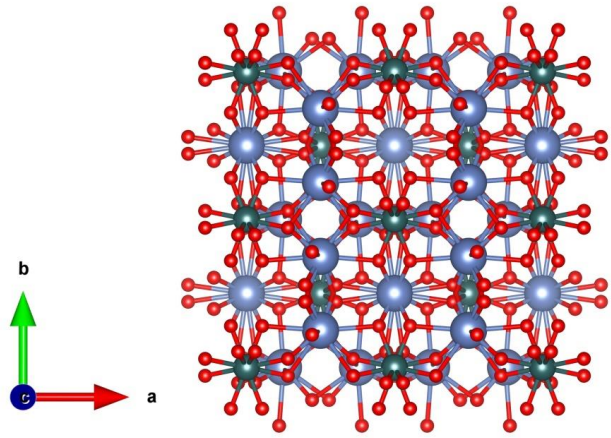

Figure 7 *Structure of hydrogarnet (C_3AH_6). Light blue: calcium, grey: aluminium, red: oxygen. (Lager et al., 1987)*

2.4. Cement alteration

The alteration of cementitious materials like concrete in aqueous environments with time is a complex phenomenon, depending on initial phase assemblage and the type of water in contact with the material. Cementitious materials are generally not in equilibrium with their environment. Hence, phase composition, pore water composition, as well as micro structure and transport properties are changing with proceeding aging or alteration of the cementitious materials. The alteration of the material can be linked to different phenomena. Either, essential elements (e.g. Na, K, Ca) are leached and removed by out-diffusion or advective transport, resulting in decreasing pH and depletion of buffer phases (cf. section 2), resulting in a weaker structure and higher porosity. This process referred to as leaching and has been subject to a large number of studies regarding the long-term behavior of cementitious systems for a range of scenarios (e.g. Baur et al., 2001; Borkel et al., 2014; Brodda and Xu, 1989; Harris et al., 2002; Mattigod et al., 2001; Trägårdh and Lagerblad, 1998; Yang et al., 1995).

On the other hand, addition or in-diffusion of elements and molecules capable of chemically reacting with the phases present in the cementitious matrix can result in alteration processes leading to deleterious effects, like expansion or cracking, or loss of mechanical strength. As previously mentioned, sulfate is a common cement additive used for retardation of cement hardening. If the hardening material reaches an internal temperature of more than 60°C, delayed ettringite formation can occur, if certain other factors are satisfied as well (e.g. alkali- and MgO content) (Taylor, 1997). Due to the large molar volume of ettringite, the hardened cement paste develops cracks resulting in a higher porosity and weaker structure. In contrast, an external attack of sulfate ions will occur, if hardened cement pastes come into contact with sulfate containing ground water. Here, the chemical reaction between the ground water and the HCP will also result in cracking of the cement, due to formation of expansive phases, with an inwards moving reaction front. The products of the chemical reaction are often a mixture of gypsum and ettringite (Taylor, 1997). If sulfate and carbonate anions are present at the same time, thaumasite ($Ca_3Si(OH)_6(CO_3)(SO_4)\cdot 12H_2O$) can be formed (Taylor, 1997). Moreover, microstructural changes can also occur due to the ingress of chloride or carbonate ions or gaseous CO_2, respectively. The reaction of aluminate phases like AFm with chloride is known as chloride attack (Taylor, 1997). The product of this reaction is Friedel's salt, an AFm type phase ($Ca_2Al(OH)_6(Cl)\cdot 2H_2O$).

A more complex alteration mechanism is observed by reactions with carbonate, derived either from gaseous carbon dioxide or due to high concentrations of dissolved carbonate anions, i.e. carbonation. The solubility of CO_2 is higher at high pH, consequential CO_2 has a higher affinity to be dissolved in high pH cement pore water. Carbonation is a common alteration process of cementitious materials (Taylor, 1997; Trägårdh and Lagerblad, 1998) leading to changes in the phase assemblage due to formation of calcite, in particular at the expense of portlandite, decalcification of C-S-H and subsequent calcite formation, and formation of amorphous silica gels, accompanied by decreasing alkalinity and pH of the pore solution. Moreover, carbonate ions are also capable of substituting for sulfate ions in AFm phases to form AFm-CO_3 as alteration product.

C-S-H acts as a buffer material maintaining a high pH (pH > 11) whereas the actual pH is depending on the Ca/Si-ratio of the C-S-H itself. The incongruent dissolution of C-S-H maintains the equilibrium pH and consumes calcium ions, either directly from C-S-H phases or from cement pore water, resulting in continuously decreasing Ca/Si-ratios (Harris et al., 2002). This is obtained by the continuously exchange of pore water or simple leaching of dissolved elements. Within the exchange, mobile or soluble components are removed as described in IAEA (2013) (Figure 8). These components, namely sodium, potassium and calcium, are in equilibrium with the different minerals phases in HCP. These solids buffer the concentration according to their solubility limit until they are entirely dissolved. Alkalis (Na, K), responsible for the high pH (pH>13) in young cements, are very mobile. In a first phase (Stage 1), if pore water is exchanged continuously, a drop in pH of approximately 13.5 to about 12.5 is observed, which can be understood as a complete removal of sodium and potassium from the leached cement paste (Ochs et al., 2016). In a second phase, portlandite is buffering the pH around 12.5, providing for a Ca-concentration of approximately 20 mmol L^{-1} in the pore solution. Large amounts of portlandite in OPC are responsible for the constant pH over the prolonged time of stage II. In the third phase, the pH and chemistry of the pore solution is controlled by the (incongruent) dissolution of C-S-H, whose initial Ca/Si ratio depends on the type of cement used. As a consequence of the incongruent dissolution of the C-S-H with preferential calcium leaching, the pH of the pore solution decreases continuously with ongoing alteration, until the calcium ions in the C-S-H phases are depleted below Ca/Si = 0.83. At this point the further leaching will lead to congruent dissolution of C-S-H (Harris et al., 2002). In the second part of Stage III, the pH is buffered by the individual hydration phases of the cement pastes giving different pH. A similar result is obtained by

cement leaching with slightly carbonated ground water (Jacques et al., 2008; Ochs et al., 2016).

The duration of these different stages of pore-water evolution in cementitious materials in the disposal environment are depending on different factors (e.g. hydraulic conductivity of the host rock, composition and porosity of the cementitious material, and ground water composition) and it is generally expected to take tens of thousands of years to decrease the pH in the cementitious material to approx. pH 10. Simulations regarding cementitious repository materials in clay host rock, which is expected to maximize the durability, performed for the Belgian super container concept, show that a pH above 12.5 will last for 80,000 years (Wang, 2009). For the Swiss L/ILW repository these high pH values are calculated to last for hundred thousand to million years in Opalinus clay, due to the large amounts of cement used in the Swiss concept and the low permeability of the clay host rock (Wersin et al., 2003). Calculations made for the UK cementitious repository concept indicate that a pH above 12.5 will be maintained over 100,000 years and a pH above 10.5 for over a million years (Kursten et al., 2004).

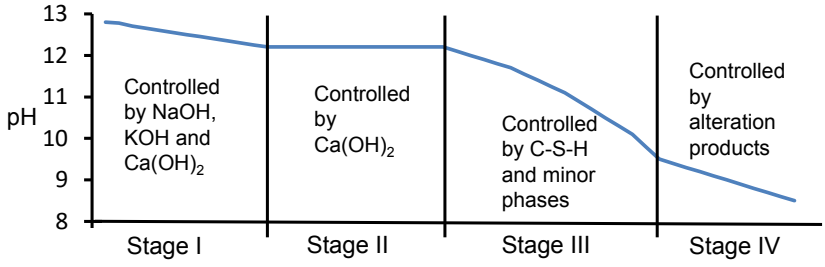

Figure 8 *Schematic view of cement evolution under simple leaching conditions in disposal environment (IAEA, 2013).*

2.5. Cementitious materials in Nuclear Waste Management

Geological disposal facilities are designed to fulfill the safety functions in different ways over different timescales to ensure that the contained radionuclides are isolated from the biosphere by using a multi-barrier system. A barrier is a physical entity like the waste package and the backfill or the host rock acting as geological barrier. The different barriers can be divided into two groups, the near field and the far field (Ojovan and Lee, 2014). In contrast to the repository far field, strong chemical and thermodynamic gradients are expected in the repository near field, in particular at the interfaces between different barrier materials. The barrier function of cementitious materials, with respect to the retention and mobility of radionuclides, strongly depends on its mechanical, physical and chemical properties. These properties correlate with the cement formulation, including the additives used, and hydration conditions of the hardened cement paste. Changes in phase composition of the applied cementitious barriers are also observed in correlation with aging and alteration effects.

Nuclear waste management is taking profit from the easy and universal applicability of cementitious materials for a large variety of tasks, e.g. solidification of low and intermediate level waste, radiation shielding by cement or as barrier materials. By the solidification of nuclear waste raw material, either a liquid or bulk material is converted into a solid and stable waste form by the admixing of cement (Figure 9). Beside the use in stabilizing waste, cement is applied in container claddings as shielding material. An example is the cladded concrete shielded container (UBA) by GRS. This cask is produced for storage and transport purposes of a maximum load of 1500 kg dry solid waste or up to 400 liter of waste, approved for disposal in the Konrad repository beside a variety of conventional containers are produced where either the container is entirely made out of concrete or concrete is used as shielding (Kugel and Möller, 2017). The "Supercontainer", a concept designed by the Belgian Agency for Radioactive Waste and Enriched Fissile Materials (NIRAS/ONDRAF), is designed as a package for spent nuclear fuel and vitrified high-level radioactive waste. It is a multiple barrier system constructed of a 6 mm stainless steel envelope, a concrete buffer and carbon steel over pack of 30 mm. The dimensions of the container are 420 cm in height and 193 cm in width giving an ordinary Portland cement based buffer of approximately 70 cm to each side (Poyet, 2006).

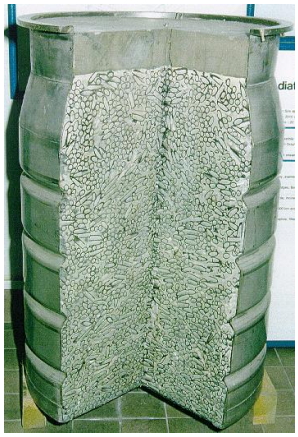

Figure 9 *Drum containing encapsulated cladding waste (Fairhall and Palmer, 1997; Copyright © by WM Symposia. All Rights Reserved. Reprinted with permission).*

Furthermore, cementitious materials and concrete are foreseen for the construction, stabilization and closure of most repositories for radioactive wastes. During construction of a repository in clay host rocks, concrete and/or shotcrete are used as gallery liners and supports of tunnels and shafts (ANDRA, 2005; Geckeis et al., 2012; Wacquier, 2012). In crystalline host rocks, cementitious materials are used for stabilization of the rocks in fracture zones as well as for grouting of fractures and cracks as an additional barrier against water ingress (Kronlöf, 2003). Furthermore, during repository closure cementitious materials will be used as confinement for backfilling in particular in L/ILW repositories and for sealing of shafts and drifts using cement plugs (ANDRA, 2005). Moreover, a cementitious backfill is also intended to be used in the Belgian high-level waste repository, for compatibility with the cement-based buffer in the "Supercontainer" (Bel et al., 2006).

Also the Belgium near surface repository concept for short lived low activity wastes involves a wide range of cement and cementitious materials to be used in construction. Main components are cementitious engineered barrier, the immobilization mortar, fiber-reinforced concrete, lightly reinforced concrete, and the backfill material (Wacquier, 2012). The auxiliary structures in a final repository require large amounts (several hundred tons) of cementitious materials (Barcena and Garcia-Sineriz, 2008). The recent Belgium concept includes prefabricated, wedge shaped blocks of concrete applied as gallery lining (Van Cotthem et al., 2012). During improvements of German Konrad mine to fulfill the requirements of a final repository for low and intermediate level waste, cementitious materials

and concrete, mainly shotcrete, are used to stabilize tunnels and shafts and to grant safe construction and operation. The applied consolidation layer consist of a 3 cm thick reinforced layer of shotcrete and an outer lining thickness of 20 cm slotted shotcrete lining supported by the use of 2 m bolts each square meter (Groll et al., 2015).

2.6. Chemical conditions in a cementitious near field

The chemical conditions in the near-field of cemented wastes or cementitious repository materials (e.g. structural material or backfill) will be determined by the dissolution of soluble constituents in the hydrated cement and the non-equilibration conditions between the groundwater and the altering cementitious material (cf. chapter 2.4). Soluble components of the cement like sodium and potassium hydroxide will dissolve and dominate the near-field chemistry giving rise to a so called alkali plume having a high pH (De Windt et al., 2004; Martin et al., 2016). The near field pH will be controlled by the cementitious material and its state of alteration. A pH >13 will be maintained initially due to the leaching of very mobile alkalis. Subsequently, the pH in the near-field will be buffered at a pH >12 by the excess of portlandite present in cementitious material, whose initial amount depends on the cement formulation used. In some cases a reduction in alkalinity is foreseen to reduce the alkaline plume, which is affecting the host rock material. The low pH cement formulations will maintain equilibrium pH according to their composition for the majority of the time (Bach et al., 2013; Garcia Calvo et al., 2010; Lothenbach et al., 2012). In the longer term, after depletion of portlandite, the pH will be controlled by the incongruent dissolution of C-S-H, resulting in a continuous decrease in pH, until the pH of the surrounding groundwater will be reached.

The redox potential in the repository near field is controlled by the corrosion of steel and iron present in the repository (e.g. in the waste, as container material, or rebar in construction concrete). After closure of a repository, the redox conditions are oxidizing due to the remaining contents of oxygen in the repository. This oxygen will be consumed by corrosion of steel and microbial processes until reducing conditions are reached. At this point reducing conditions are maintained by the anoxic corrosion of the large quantities of iron contained. The lowest redox potentials are obtained as long as uncorroded iron and steel is present. Based on thermodynamic considerations, the redox potentials under post-closure conditions in cementitious repository systems are thought to be in the range from -30 to -800 mV

(Hummel et al., 2002; Wang, 2013). Anyhow, the corrosion rate of steel embedded in cementitious material will be rather slow under anoxic conditions at high pH.

2.7. Mechanisms of radionuclide uptake in cementitious materials

In this work the uptake of radionuclides by different cementitious materials and model phases is studied. The underlying mechanisms for the radionuclide uptake are based on sorption and structural incorporation. Sorption refers to the accumulation of a sorbate at the surface or in a sorbent. In general sorption is divided into three phenomena namely absorption, adsorption and ion exchange. Absorption describes the incorporation of a gaseous or liquid adsorbate into a liquid or solid, respectively. The absorption of carbonate by calcium hydroxide followed by calcite precipitation and the absorption of water by cement are processes that include a chemical reaction of the sorbate with the sorbent. In absorption a chemical process takes place, whereas in adsorption the physical adherence to the surface of the adsorbent is caused by electrostatic interactions, polarization interactions, and hydrophobic expulsion (Stumm, 1992). Adsorption is the accumulation of atoms or molecules at the surface of a solid from either a liquid or gaseous phase, without the formation of a three-dimensional arrangement. Absorption may occur after adsorption, due to recrystallization or diffusion, if the incorporation of previously sorbed molecule or atom will result in a thermodynamic favorable homogenous crystal or solid solution. Ion exchange describes the phenomena where ions are exchanged between two electrolytes, an electrolyte and a complex or the exchange of cations on surfaces or in clay interlayers or anion exchange in the interlayer between two positively charged oxide layers. Adherence of a molecule or atom onto a surface by sorption can be distinguished into inner- and outer-sphere complexes, surface precipitation, and solid solution formation. Whereas in an outer-sphere complex one or more water atoms are between the solute cation and the Lewis base at the surface, in inner-sphere complexes surface functional groups act as σ-donor ligand to form chemical bonds. By this direct contact to the surface the electron density of the coordinated cation increases and therefore chemical properties, like redox potential changes. Furthermore, reactivity of the surface is also affected by inner-sphere complexes (Stumm, 1992).

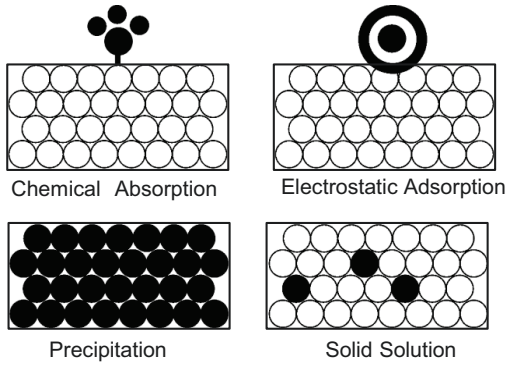

Figure 10 *Sketch of ab-/adsorption, solid solution formation and precipitation.*

A further relevant aspect in this context that needs to be discussed is the surface charge of solids that has a very important factor regarding sorption. The charge, whether positive or negative, determines the possible attraction and accumulation of ions onto the surface. The surface charge itself strongly depends on the pH of the surrounding media, may arise from a chemical reaction, or is a permanent charge like on the surface of clay minerals or the hydroxide layer of LDH-type phases. For instance, the surface charge of a solid containing OH groups (e.g. Fe- or Al-hydroxides) depends on the proton transfer to a functional group and consequently on the pH of the medium. Therefore, a positive surface charge is dominant at low pH ($-OH_2^+$), negative at high pH ($-OH^-$) and neutral in-between, whereas the actual point of zero charge depends on the nature of the solid and describes the pH, at which the net electrical charge at the surface is zero. In addition, a deprotonation reaction of hydroxyl groups by reaction with divalent metal cations can also lead to a positive surface charge. The electric charge of a hydrous oxide is dependent on the acid base behavior of its solid surface. Furthermore, the surface charge of a solid can also be caused by replacement of ions in the bulk solid. Since the substitution of an atomic with different valence in the lattice of a solid can create a charged framework. As an example, related to cement hydration phases, due to the substitution of the divalent calcium atoms in the hydroxide layer like in LDH-type AFm phases by trivalent aluminum atoms, the hydroxide layer exhibits an excess of positive charges. Therefore the layer is positively charged and anions are located in between two hydroxide layers.

Sorption isotherms are often used to describe the dependency of the concentration, more precise the activity of the adsorbate, on the absorbed amount at equilibrium state for of a

specific substance at constant temperature. A variety of models are available to fit the observations, differing in assumptions about sorption processes and materials properties. At low solution concentrations, a simple linear sorption isotherm (termed K_d or R_d) can often by applied. A BET-isotherm, developed by Stephen Brunauer, Paul Emmett and Edward Teller, is often used for the determination of surface area by adsorption of a gas on the surface of a solid. The sorption at the solid/liquid interface is often described in terms of Langmuir- or Freundlich-isotherms. The exponential Freundlich-isotherm refers to the decreasing sorption with increasing loading of the surface, although a saturation of the surface by the sorbent is not accounted for. In Langmuir-isotherms it is assumed that all places on the surface are equal and that a maximum loading of the surface can be achieved by a monomolecular layer. Although the sorption isotherms can describe the experimental findings, the application of isotherms provides no insight into the uptake mechanism and does not clarify between uptake/sorption and structural incorporation.

2.8. Retention of radionuclides by cementitious materials

The uptake and binding of radionuclides to cementitious materials have been investigated in a large number of studies over the last decades (e.g., see reviews by Evans, 2008; Gougar et al., 1996; Glasser, 1997; Glasser, 2011; Jantzen et al., 2010). However, the behavior of a number of safety relevant radionuclides in cementitious environments, the mechanisms of their uptake by various hydration phases or the effects of long-term alteration processes on radionuclide migration behavior are not completely understood so far.

In the context of direct disposal of spent nuclear fuel, but also with respect to the disposal of other uranium rich waste streams (e.g. depleted uranium), the uranium daughter nuclide radium is relevant to the long-term safety of a repository. Recent assessments show that ^{226}Ra can emerge as one of the main contributors to the biosphere dose in the long-term (i.e. after more than 100,000 years) in some scenarios (cf. NAGRA, 2002; ONDRAF/NIRAS, 2001; SKB, 2011). Since most of the backfill materials used in engineered barriers (e.g. Bentonite and hydrated cements consisting mainly of C-S-H) have negatively charged surfaces, they are unlikely to retard radionuclides in anionic forms, such as I^-, MoO_4^{2-} and TcO_4^-, which are generally deemed to be rather mobile in the repository near and far field, and emerge often as relevant contributors to the radiological risks in post closure

safety assessments. Thus in this work, the interaction of ^{226}Ra as well as I^-/IO_3^-, MoO_4^{2-} and TcO_4^- with cementitious materials was investigated in detail.

2.8.1. Radium

^{226}Ra is a daughter nuclide of ^{238}U, the most abundant uranium isotope. Therefore, with respect to the direct disposal of spent nuclear fuels, ^{226}Ra can be a main contributor to dose in the long-term (i.e. after more than 100,000 years) due to the high concentrations of uranium present within the waste inventories (SKB, 2010).

However, up to now detailed investigations on the uptake of radium by cementitious materials have been rather scarce, and are limited to uptake/sorption of radium by HCP and C-S-H-phases (Bayliss et al., 1989; Holland and Lee, 1992; Tits et al., 2006a). For example, the uptake of radium by hardened cement paste was investigated by Bayliss et al. (1989) in cement equilibrated water. Experimental results indicated that the concentration of radium remained constant after adding sulfate to the cement-equilibrated solution in contrast to the thermodynamically predicted solubility limit calculated for $RaSO_4$. This phenomenon was explained by the lack of sufficient nucleation sites. In the same work Bayliss et al. (1989) also studied the uptake of radium by a sulfate resistant Portland cement (SRPC) and an ordinary Portland cement (OPC) blended with blast furnace slag (BFS), indicating higher uptake of radium by OPC/BFS. Higher sorption by OPC/BFS was explained by formation of $RaSO_4$. Holland and Lee (1992) investigated the sorption of radium to SRPC/BFS, SRPC/PFA, high alumina cement (HAC), OPC, SRPC and tobermorite as a C-S-H surrogate. Distribution ratios or partition coefficients (R_d) obtained in these sorption experiments were highest for HAC and lowest for SRPC. Although these results show that the addition of BFS to SRPC increased the retention of Ra, PFA caused even greater enhancement onto SRPC. Sorption of radium onto tobermorite was studied in simulated pore water (pH 13.1), saturated lime solution (pH 12.6) and SRPC equilibrated water (pH 12.4). The highest distribution ratio was obtained in saturated lime solutions. Tits et al. (2006a) investigated the interaction of radium with C-S-H and hydrated cement pastes (HCP). In this study, calcium silicate hydrates with different calcium to silicon ratios were synthesized to represent the composition of the C-S-H phases expected at different stages of the evolution of cement pastes. It was demonstrated that the uptake of radium by C-S-H is fast and reaches completion within one week of continuously shaking. The uptake kinetics showed no differences regarding the calcium to

silicon ratio, but the distribution ratios decreased with increasing calcium content of the C-S-H phases, indicating competitive interactions between calcium and radium. Studies on the liquid to solid ratio used in the batch experiments showed that almost no influence on the distribution of radium was observed by varying the liquid to solid ratio. Tits et al. (2006a) also investigated desorption of radium from the above mentioned phases and observed that radium sorption onto C-S-H phases is linear and reversible. Based on results obtained for the sorption of Sr^{2+} to C-S-H phases, it was stated that the sorption of radium can be described in terms of a cation exchange model (Tits et al., 2006a; Tits et al., 2006b; Wieland et al., 2008). Furthermore, it was found that, in the case of HCP, the sorption of radium is much slower with fresh HCP compared to the very fast uptake of degraded HCP.

2.8.2. Technetium

^{99}Tc is a long-lived fission product with a half-life of 211.100 years with a high fission yield that is produced by the decay of primary fission products in a reactor. Therefore, it is typically present in nuclear waste such as ion-exchange resins, contaminated liquid, filters and sluges (Ochs et al., 2016). Tc can occur in environmental systems as Tc(IV) and Tc(VII). Since technetium is very redox sensitive, the redox potential and pH will have a major influence on its mobility (Figure 11). The speciation calculations show that the solubility of technetium will be controlled by hydrous TcO_2 in presence of corroding iron (Eh approx. -800mV) at concentration levels of about 10^{-7} to 10^{-6} mol L^{-1} in the pH range relevant for cementitious conditions, while the anionic form TcO_4^- will be dominant in cementitious systems with less reducing conditions. Generally, irrespective of the redox state, dissolved Tc in cementitious environments will be present predominantly in anionic form (i.e. either as $Tc^{IV}O(OH)_3^-$ or as $Tc^{VII}O_4^-$). In previous studies, it was observed that the pertechnetate anion is mobile in young and mature cementitious environments due to the negatively charged surfaces of C-S-H (Brodda and Xu, 1989; Corkhill et al., 2012; Evans et al., 2008; Mattigod et al., 2004; Mattigod et al., 2001; Smith and Walton, 1993; Tallent et al., 1987). The major mechanism of retention of technetium in cementitious systems was found to be the reduction to less mobile Tc(IV) or Tc(0) by reducing agents present in cementitious materials (Allen et al., 1997a; Allen et al., 1997b).

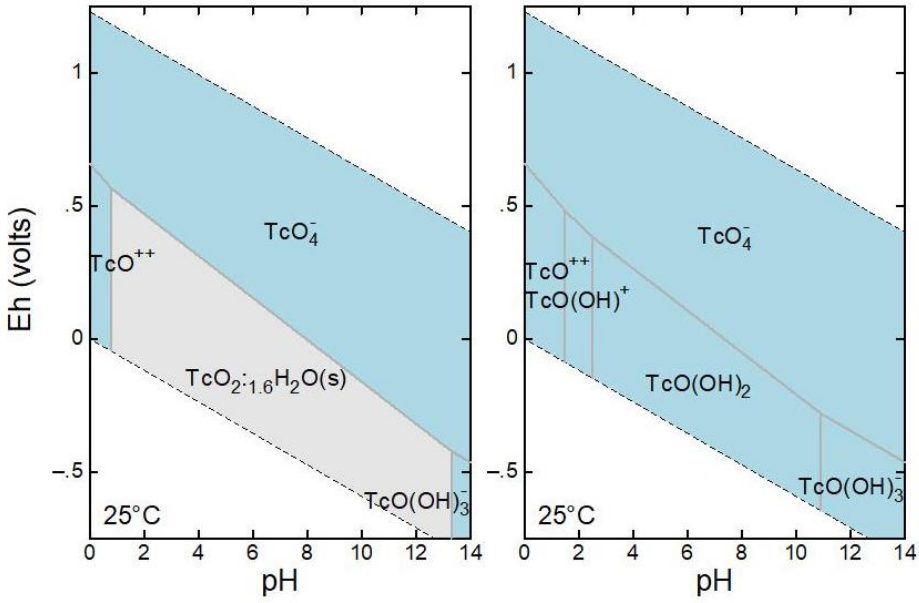

Figure 11 *Eh – pH diagram of technetium for c(Tc) = 10^{-6} M with solid phases supressed on the right (Database: PSI/NAGRA 12/07, Thoenen et al., 2014).*

Tallent et al. (1987) studied the influence of grout composition on the leachability of technetium containing cementitious matrices. They demonstrated that leachability decreases with increasing mix ratio, grout fluid density and blast furnace slag content. Later, Gilliam et al. (1990) showed that the effective technetium diffusivity of cement based waste forms decreases by five orders of magnitude on the addition of BFS. A further decrease of the leach coefficient in water and brine was achieved by addition of sodium sulfide, as reported by Brodda and Xu (1989) who concluded that technetium seemed to be chemically fixed. Thermodynamic calculations carried out by Smith and Walton (1993) suggested that the leachability of the highly mobile anionic pertechnetate species decreased as a result of reaction with sulfur present in BFS and reductive formation of Tc_2S_7. Allen et al. (1997b) conducted extended X-ray absorption fine structure (EXAFS) studies on the effect of sodium and iron sulfides on technetium speciation in cementitious environments. In contrast to the thermodynamic predictions of Smith and Walton (1993), the study of Allen et al. (1997b) demonstrated that the addition of BFS to a cement formulation leads to an in situ partial reduction of pertechnetate anions, whereas the addition of Na_2S or FeS results in complete reduction to the less mobile Tc(IV). Furthermore, Allen et al. (1997b) measured

Tc-S and Tc-Tc distances in the presence of Na_2S or FeS, observing bond distances in agreement with an oligomeric structure similar to that found in TcS_2 and concluded that sulfide containing species are the active reducing agents in BFS. These findings were in agreement with previous work done by Gilliam et al. (1990) and the reduction of Tc(VII) by FeS and Fe_2O_3 found by Yalcintas et al. (2016).

Layered double hydroxides (LDHs) have also been suggested as potential host phases for technetium in its anionic form. Berner (1999) suggested that binding and/or incorporation of TcO_4^- into the alumina ferric mono/tri-sulfate (AFm/AFt) phases of cement systems could be also expected, by analogy to other oxo-anions such as SO_4^{2-} or MoO_4^{2-} (and possibly also SeO_3^{2-}), although experimental and quantitative evidence confirming this hypothesis is lacking to date (Ochs et al., 2016).

2.8.3. Molybdenum

^{93}Mo is a neutron activation product of ^{92}Mo, a stable naturally occurring Mo isotope, and forms as an activation product in irradiated components in nuclear installation (Lidman et al., 2017). ^{93}Mo has a half-life of about 4,000 years. The aqueous speciation of molybdenum is dominated by the molybdate anion (MoO_4^{2-}) (Grivé and Olmeda, 2015). In strongly reducing conditions and under high pH conditions, reduction to Mo(+IV) can be observed although the solubility-controlling phase under cementitious conditions is powellite ($CaMoO_4$) (Kindness et al., 1994). The solubility of powellite is sensitive to the calcium concentration in solution and thus be higher in cement degradation stage I (pH 13.5) than in the portlandite buffered stage II (pH 12.5) as well as in stage III (Table 2).

The interaction of molybdenum with cementitious materials has received little attention so far. The immobilization of molybdenum in ordinary Portland cement and single model phases was studied, conducting experiments on the uptake of Mo onto OPC, slag cements, C_3S and AFt (Kato et al., 2002; Kindness et al., 1994; Minocha and Goyal, 2013; Minocha et al., 2004). The results of the batch experiments of Kindness et al. (1994) suggested that, disregarding cement formulation, the uptake of molybdenum appeared to be controlled by a precipitation mechanism (Kindness et al., 1994).

Table 2 *Solubility of molybdate in cementitious pore water for the different cement alteration stages (Grivé and Olmeda, 2015).*

Stage	$c(MoO_4^{2-})$ mol kg^{-1}
I	$3 \cdot 10^{-4}$
II	$5.5 \cdot 10^{-6}$
III	$8.5 \cdot 10^{-6}$

The precipitation of powellite as process for immobilization of molybdate in OPC was confirmed by EXAFS measurements conducted by Minocha and Goyal (2013). Further investigations on synthesized Mo-bearing cement phases demonstrated that two solubility limiting phases could be identified; $CaMoO_4$ isostructural with powellite and a Mo-AFm phase (Kindness et al., 1994). Zhang (2000) studied the incorporation of molybdate by hydrocalumite and ettringite. It was demonstrated that a solid solution of molybdate and hydrocalumite could be synthesized and that molybdate formed a solid solution with AFm-OH (Zhang, 2000). Furthermore, Marty et al. (2018) demonstrated that molybdate binds to AFm by replacing chloride ions in the interlayer mid-plane. The mechanisms of Mo incorporation by AFm phases were studied by EXAFS and found to be concentration dependent. At low Mo concentrations (10^{-8} M) edge site complexes were observed/formed. At intermediate concentrations (10^{-6} M) anion exchanges at the interlayer occurred and $CaMoO_4$ precipitation was observed with increasing Mo concentration in solution (Ma et al., 2017).

2.8.4. Iodine

Various iodine isotopes are produced by thermal fission of ^{235}U in nuclear reactors; however, besides stable ^{127}I only ^{129}I exhibits a half live ($1.57\ 10^7$ y) that is relevant for the long-term safety of repositories for nuclear wastes. The speciation of iodine in cementitious systems is rather simple. Iodide (I^-) is the most stable form under repository relevant conditions whereas iodate (IO_3^-) becomes only dominant under highly oxidizing conditions (Figure 12). Thus in literature, it is generally agreed that the majority of iodine in the repository environment will be present in the form of iodide (Aimoz et al., 2012a; Atkins and Glasser, 1990; Bonhoure et al., 2002; Curtius and Kattilparampil, 2005; Mattigod et al., 2001; Shirai et al., 2011; Toyohara et al., 2002). However, in the case of iodine containing wastes originating from reprocessing and off gas treatment, larger amounts of iodate (IO_3^-) will be solidified in cementitious materials. Off gas treatment in a reprocessing plant utilizes silver

nitrate ($AgNO_3$) filters to adsorb ^{129}I in the chemical form of silver iodide (AgI) or silver iodate ($AgIO_3$), exhibiting approximately 6% (w/w) (Tanabe et al., 2010). According to thermodynamic considerations, the oxidized form of iodine will be reduced under the premise that sufficient reducing agents are present, while the timeframe needed for this reduction is unclear. A number of studies have been carried out investigating the immobilization of I^- in cementitious materials using a range of experimental approaches: (i) through-diffusion (Atkinson and Nickerson, 1984; Sarott et al., 1992; Chida and Sugiyama, 2008; Felipe-Sotelo et al., 2014) and (ii) out-diffusion (Mattigod et al., 2001).

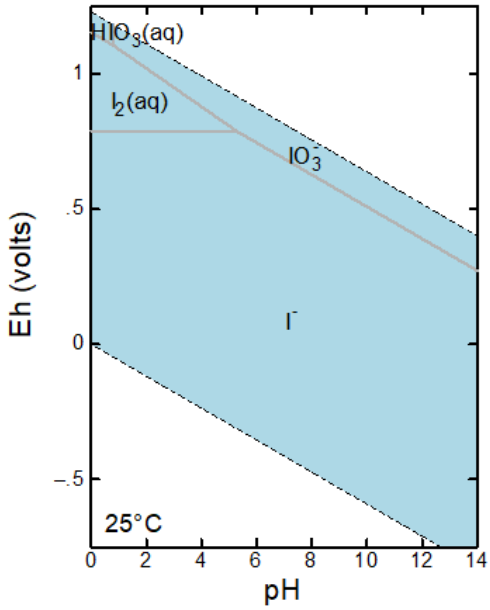

Figure 12 *Eh-pH diagram of iodine for c(I) = 10^{-6} M. (Database: PSI/NAGRA 12/07, Thoenen et al., 2014).*

The diffusion of I^- in cementitious materials correlates strongly with the water to cement ratio of the cement paste. An increase in the w/c ratio from 0.2 to 0.7 can lead to an increase of the diffusion coefficient by 3 orders of magnitude, which may be attributable to the increased porosity (Atkinson and Nickerson, 1984). Whilst changes in porosity of the cements at high w/c ratios may account for some of the impact on diffusivity, the authors suggested that other parameters, such as changes in constrictivity could also contribute to the observed differences (Atkinson and Nickerson, 1984). Uptake and retention mechanisms of iodine by various cement formulations and different cement model phases were intensively studied in

the last decades (Aimoz et al., 2012a; Aimoz et al., 2012b; Atkins and Glasser, 1990; Atkins and Glasser, 1992; Bonhoure et al., 2002; Chida and Sugiyama, 2008; Curtius and Kattilparampil, 2005; Fuhrmann et al., 1998; Holland and Lee, 1992; Idemitsu et al., 2013; Iwaida et al., 2001; Mattigod et al., 2004; Mattigod et al., 2001; Niibori et al., 2012; Rapin et al., 1999; Shirai et al., 2011; Tanabe et al., 2010; Toyohara et al., 2002). Iodide can be retained in cementitious systems by sorption onto C-S-H or by incorporation into crystalline cement phases (Aimoz et al., 2012a; Bonhoure et al., 2002; Shirai et al., 2011). The solidification of iodate bearing wastes by the use of cement increased the final contents of ettringite from 12% (w/w) to approximately 80% (w/w), indicating a shift of the sulfate phases equilibrium (AFt/AFm) by iodate (Tanabe et al., 2010). Idemitsu et al. (2013) pointed out that iodate is incorporated into the structure of ettringite. Mattigod et al. (2001) observed a decrease of the leachability of iodine in cementitious material containing steel fibers, which was suggested to be due to the reduction of IO_3^- to I^-. Iodide sorption onto cement has been shown to increase with increasing Ca/Si ratios in C-S-H gels in spite of an increased competition from OH^- for sorption sites, suggesting I^- is sorbed electrostatically (Glasser et al., 1989; Pointeau et al., 2008). However, in general, the retention of iodide by cementitious systems was found to be weak (e.g. Ochs et al., 2016).

3. Aim of this work

Cementitious materials play an important role in nuclear waste management and form part of the engineered barrier systems in near surface and deep geological disposal facilities for nuclear waste. Over the last decades, the retention of radionuclides by cementitious materials has been investigated in terms of K_d-values or diffusion coefficients, leading to the development of various sorption coefficient databases (e.g. Kato et al., 2002; Ochs et al., 2016; Wieland and Van Loon, 2002). However, the mechanisms governing uptake and binding of various safety relevant radionuclides by cementitious materials are not completely understood and detailed data for safety relevant radionuclides (e.g. ^{226}Ra, ^{129}I, ^{99}Tc, ^{93}Mo) are scarce or lacking. Thus the aim of this work is to enhance the mechanistic understanding of the radionuclide uptake and retention in cementitious materials. The relevance of cement alteration processes, such as carbonation, is evaluated with regard to the solid speciation of radionuclides in aged concrete. Specific radionuclides were selected for these investigations with focus on radioelements for which insufficient information is available and rather large uncertainties exist with respect to the retention processes in cementitious systems. Thus, the focus of this study was set on retention mechanisms of radium, technetium, molybdenum and iodine in cementitious materials.

A systematic bottom-up approach was used to unravel the contributions of all relevant individual hydration phases of cement on the retention of radionuclides in complex multiphase cementitious materials. Here, the radionuclide interaction with synthesized phases present in cementitious materials (model phases), such as calcium silicate hydrates (C-S-H) with different Ca/Si ratios, monosulfate (AFm) and ettringite (AFt) phases, was studied. In addition the radionuclide uptake by hardened cement pastes of different compositions (e.g. CEM I and CEM V) was investigated. Potential radionuclide retention mechanism were identified and characterized. The distribution of the safety relevant radionuclides was studied by advanced microanalytical techniques, to distinguish between sorption/uptake mechanisms and solubility limitations by solid phase formations. Moreover, the relevance of aging effects such as leaching and carbonation on radionuclide uptake and retention by cementitious materials was investigated. Potential changes in the barrier functions in the post closure phase of a repository were taken into account. The generated data and the improved understanding of the contribution of individual hydration phases to the retention of safety relevant radionuclides in the different stages of system evolution aim at an improvement of the

knowledge base to perform long-term assessments of the function of cementitious barriers based on a diversity of cement formulations in the repository environment.

Only few publications are available regarding the uptake of radium in cementitious systems, and no other data on the uptake of radium by cement hydration phases other then C-S-H have been published so far. Thus in this work, it was identified to which degree other hydration phases are involved in radium retention process in cementitious materials. Furthermore, computational methods were used to improve the understanding of radium uptake and retention mechnisms.

Technetium as TcO_4^- is known to interact only weakly with cementitious materials and is therefore very mobile in cementitious environments. However, the potential contributions of individual hydration phases to Tc(VII) retention have not been investigated so far and were addressed in this study. Potential uptake and retention processes, other than reduction of Tc(VII) to less mobile Tc(IV), by various cement hydration phases were investigated.

Very limited systematic knowledge is available regarding the retention of MoO_4^{2-} in cementitious systems and its uptake by hydration phases, in particular C-S-H. Thus sorption and solid solution formation with various hydration phases are studied to outline retention mechanisms beside powellite formation at higher molybdenum concentrations and advanced microanalytical methods were used to study the underlying retention mechanisms.

Although immobilization of iodine in cement has been a topic in various investigations in the past, within this work a systematic study regarding the interactions of iodine with cement hydration phases was conducted for the first time. A systematic approach was used to identify the potential mechanisms for the retention and uptake of iodine supported by the use of advanced microanalytical methods.

4. Materials and Methods

4.1. Synthesis of model phases

The various model phases used in the present study were synthesized according to procedures described in the literature (Aimoz et al., 2012b; Atkins et al., 1992; Atkins et al., 1991a; Baur et al., 2004). However, in many cases these procedures were optimized in terms of chemical yield and purity of the hydration phases. Phase synthesis and sample preparation was carried out in an argon glove box at $c(CO_2) < 10$ ppm, to avoid carbonation of the material; details on the chemicals used are compiled in Table 3.

C-S-H phases with Ca/Si ratios of 0.7 and 1.4 were prepared following the procedure of Atkins et al. (1992), by mixing freshly produced CaO obtained from the ignition of $CaCO_3$ (>7 hours of calcination at 1000 °C) with SiO_2 in the desired ratio. The solids were carefully suspended in deionized water to achieve a water/solid ratio of 20. The reaction mixture was shaken intensively during the first days and once a day until the product was purified after one month. The product were washed by centrifugation (30 min at 4500 rpm) and resuspended in deionized water three to five times, followed by vacuum filtering using a Büchner funnel and a paper filter (Whatman). Drying was carried out over saturated $CaCl_2$ solution using a desiccator.

Table 3 *Details of chemical substances used in the synthesis of the model phases.*

Compound	Product description	Provider
$CaCO_3$	analytical grade, EMSURE	Merck Millipore
$Al_2(SO_4)_3 \cdot 18\ H_2O$	AnalaR normapur	VWR chemicals
SiO_2	fumed silica (395 m²/g)	Sigma Aldrich
Al_2O_3	99.5% purity based on trace metals analysis	Sigma Aldrich
$CaSO_4 \cdot 2H_2O$	analytical grade, EMSURE	Merck Millipore

Ettringite ($Ca_6Al_2(SO_4)_3(OH)_{12}\cdot 26H_2O$) synthesis was carried out according to the method described by Atkins et al. (1991b) and Baur et al. (2004), respectively. CaO was suspended in water and cooled to 4°C. A stoichiometric solution (Ca/Al ratio = 3) of $Al_2(SO_4)_3\cdot 18\ H_2O$ was added and mixed with the CaO suspension having a water-to-solid ratio of 10. The suspension was stirred for 4 hours at approximately 4°C and cured for one month at room temperature. The obtained product was washed 5 to 10 times by re-suspending the solids in deionized water, followed by filtration until gypsum impurities were fully removed. Drying was conducted over saturated $CaCl_2$ solution using a desiccator.

AFm ($Ca_4Al_2(OH)_{12}(X^{2-})\cdot 6H_2O$) phases were obtained using tricalcium aluminate (C_3A, i.e. $3CaO\cdot Al_2O_3$) and $CaSO_4\cdot 2H_2O$ or $CaCO_3$ as reagents, respectively, depending on the desired interlayer anion (X^{2-}) in the AFm, according to the procedures described by Baur et al. (2004) and Matschei et al. (2006). C_3A was synthesized, as described by Atkins et al. (1991b) and Mondal and Jeffery (1975), by calcination of a mixture $CaCO_3$ and Al_2O_3 with a Ca/Al ratio = 1.5 at 1000°C for 2 h in a Pt/Au (5% Au) crucible, followed by ignition at 1450°C for 1 h. The product was cooled to room temperature, crushed and ground using an agate mortar to obtain a homogeneous reaction mixture and ignited in a second cycle at 1450°C for 48 h. The AFm were prepared by suspending freshly prepared C_3A and $CaSO_4\cdot 2H_2O$ or $CaCO_3$ (Ca/Al ratio = 2) in deionized water at 4°C and stirring them for 4 h. The products were cured for 1 to 5 months at room temperature, depending on the expected reactivity of the calcium salts used. The obtained products were washed by re-suspending 3 times in deionized water to remove impurities and dried over a saturated $CaCl_2$ solution.

AFm-CO_3 was prepared by suspending freshly prepared of C_3A and $CaCO_3$ and cured for 4 months. Additionally, cooling was applied in the first hours of reaction and compared to reactions conducted in the glove box under argon blanket. Due to the larger experimental effort, cooling of the reaction was conducted outside the glove box. Two AFm-CO_3 products were resulting from these syntheses, named 1-AFm-CO_3 for the cooled product and 2-AFm-CO_3 for the product not cooled in the first hours of reaction.

Three different approaches were used to synthesize molybdate bearing AFm-type phases that might be relevant to the Mo-uptake in AFm and hydrogarnet-bearing systems. The formation Mo bearing AFm phase was studied in highly alkaline conditions by adjusting the pH with either KOH or NaOH to 13.5 and curing for 2 months, or by suspending C_3A with $CaMoO_4$ at room temperature and curing for 1 month.

Hydrogarnet ($Ca_3Al_2(OH)_{12}$) was synthesized from freshly prepared C_3A that was immersed in deionized water and cured at 90°C for two weeks. Portlandite ($Ca(OH)_2$) was prepared by the reaction of CaO, obtained from the ignition of $CaCO_3$, with deionized water. Calcite ($CaCO_3$) was used as provided by Merck Millipore (analytical grade, EMSURE).

4.2. Preparation of HCP

Hardened cement paste samples were prepared under CO_2-free conditions in a glove box under argon atmosphere. A HCP based on ordinary Portland cement was produced from a commercial Portland cement (CEM I 32.5 R; Heidelberger Zement) using a water/cement ratio of w/c = 0.4 L kg^{-1}. Cast cement monoliths were cured for at least 28 days, submerged in water, under anoxic conditions. A low pH cement formulation developed by the Finnish waste management organization Posiva for deposition tunnel end plugs was provided by VTT Technical Research Centre of Finland Ltd. In addition to Portland cement (CEM I), the ternary mix comprised blast furnace slag and silica fume as well as a quartz filler (Table 4). The cement paste was prepared with a w/c-ratio of 0.25 and hydrated for 90 days in a saturated KOH solution to prevent any leaching.

After hydration, the HCP samples were stored under argon atmosphere at ambient conditions. For the use in batch sorption experiments, the HCP was mechanically crushed, followed by BET surface area determination prior to the sorption experiments. The BET surface area of the crushed HCP was 24.2 m^2 g^{-1} (CEM I paste) and 5.9 m^2 g^{-1} (VTT reference paste), respectively.

Table 4 *Composition of the VTT low-pH HCP (Vehmas et al., 2017).*

CEM I 42.5	468 kg m^{-3}
Silica fume	491 kg m^{-3}
Blast furnace slag	290 kg m^{-3}
Quartz filler	517 kg m^{-3}
Plasticizer (from total binder weight)	6.0 %
Water (effective)	312 kg m^{-3}

4.3. Batch uptake experiments

Analyte distribution ratios (R_d-values) between solid and liquid phases and radionuclide uptake kinetics were determined in static batch experiments under anoxic conditions. Generally, batch sorption experiments were carried out in 20 mL LDPE bottles using a L/S-ratio between 0.005 and 0.1 kg L^{-1} (10 - 200 L kg^{-1}), depending on the type of experiment. Uptake kinetics were investigated at a S/L-ratio of 0.005 kg L^{-1}, whereas equilibrium R_d-values were determined at a S/L-ratio of 0.04 kg L^{-1}. The initial determination of uptake kinetics at a low S/L-ratio of 0.005 kg L^{-1} was chosen to obtain measurable equilibrium concentrations in the supernatant solutions, to be able to follow the uptake process in time. Due to the known high mobility and low uptake of pertechnetate, uptake experiments with technetium were generally performed at a L/S-ratio of 0.04 kg L^{-1}. Batch sorption experiments with the model phases were carried out for up to 100 days, employing different solutions. First, weighted amounts of dried solids were equilibrated with deionized water (18.2 MΩ) to obtain equilibrium solutions (ES). To achieve equilibrium, suspensions were stored at room temperature for up to 14 days under anoxic conditions. After equilibrium was reached, the liquid phase was separated from the solids by filtration. The pH of these respective equilibrium solutions is provided in Table 5.

Table 5 *pH of aqueous solutions equilibrated with various cement hydration phases.*

Phase	C-S-H0.9	C-S-H1.4	AFm-SO_4	AFm-CO_3	Ettringite	C_3AH_6	$Ca(OH)_2$	$CaCO_3$
pH_{ini}	11.9±0.2	12.1±0.2	12.0±0.2	11.3±0.2	11.1±0.2	12.1±0.2	12.3±0.2	7.5±0.2

For the sorption experiment weighted amounts of the respective fresh phase were added to the equilibrium solution at the same S/L-ratio and stored for additional 14 day, prior to the addition of radiotracers. Kinetics were monitored for up to 100 days. The timeframes for experiments to determine R_d-values were defined based on the time needed to reach stable distribution ratios. In addition to the solutions equilibrated with the respective solids (equilibrium solutions, ES) and to address conditions representative for concrete degradation stages I and II, experiments using an alkali-rich artificial young cement water (ACW, pH >13) and a solution saturated with portlandite (CH) were performed. ACW, representative for young cementitious materials, was prepared by filtration and dilution of highly concentrated alkali hydroxide solutions (NaOH and KOH; i.e. pH ~13.5) (Wieland et al., 1998).

The solution was stored over $Ca(OH)_2$ to precipitate remaining carbonates, following the procedure of Sipos et al. (2000). The resulting solution at a pH of 13.3, containing c(NaOH) = 0.114 mol L^{-1} and c(KOH) = 0.18 mol L^{-1}, was filtered prior to use.

The tracer concentrations used were $c(^{226}Ra^{2+}) = 10^{-6}$ - 10^{-8} mol L^{-1}, $c(^{99}TcO_4^-) = 10^{-5}$ - 10^{-7} mol L^{-1}, $c(I^-) = 10^{-6}$ - 10^{-7} mol L^{-1} and $c(MoO_4^{2-}) = 10^{-6}$ - 10^{-7} mol L^{-1}. Sorption to the reaction vessels and filters was tested prior to the sorption experiments and was found to be negligible. Prior to the analysis of the analyte concentration in solution, liquid and solid phases were separated by filtration using USY-1 ultrafilters (10,000 Da, Advantec).

The radionuclide uptake by the respective solids is described in terms of the distribution ratio R_d between solid and liquid phase according to:

$$R_d = \frac{A_{ini} - A_t}{A_t} \cdot \frac{V}{m} \qquad \text{eq 1}$$

with

A_t: concentration in liquid phase at time t (Bq or mol L^{-1})

A_{ini}: initial concentration in liquid phase (Bq or mol L^{-1})

V: volume of liquid phase (L)

m: mass of solid phase (kg).

In case of C-S-H phases the mass of solid was based upon a dry weight after ignition at 1000°C.

In-situ uptake experiments were performed to get insights into the effects of potential structural changes during drying on the radionuclide uptake by C-S-H. Here, the radiotracers directly added to the suspended phases during C-S-H synthesis at the end of the curing time (S/L-ratio 0.01 kg L^{-1}). Duplicate samples were produced under identical conditions. After synthesis, one of the batches was sacrificed for solid phase characterization (XRD-analyses) and liquid phase analysis. The others were spiked with the radiotracer and studied with respect to the radionuclide uptake, avoiding microstructural changes upon purification and drying.

4.4. Uptake experiment using HCP monoliths

In addition to batch uptake experiments, in-diffusion experiments using HCP monoliths based on CEM I were used to address the migration and retention behavior of Ra, Tc, Mo and I in cementitious systems. Cylindrical CEM I monoliths were prepared with at a w/s ratio = 0.4 L kg^{-1} with a diameter of 12.2 mm and a height between 14 mm and 15 mm. The monolith samples were cured in an inert gas atmosphere for 28 days. The initial tracer concentration used was 10^{-6} mol L^{-1} for RN studied. After termination of the experiments, the monoliths were cut perpendicular to the length axis and the elemental distributions on the obtained cross sections were investigated by autoradiography, SEM/EDS and/or ToF-SIMS.

4.5. Carbonation experiments

To address the fate of radium sorbed to C-S-H during carbonation, a C-S-H phase with a Ca/Si ratio of 1.4 was contacted with ACW (S/L-ratio 0.006 kg L^{-1}) containing 2.5 10^{-7} mol L^{-1} ^{226}Ra in an autoclave (Parr Instruments Company). After attaining a stable Ra-concentration in solution, carbonation of the C-S-H was initiated by pressurizing the autoclave with pure CO_2 at 1 bar overpressure. The solution pH and the ^{226}Ra activity in solution were monitored by taking aliquots of the suspension (1 mL) for the solid phase and liquid phase analyzation after separation by filtration, using USY-1 ultrafilters (10,000 Da, Advantec).

Figure 13 *Parr autoclave used for alteration of cement and C-S-H phases under pressurized CO_2 conditions.*

Moreover, the behavior of radium during carbonation of HCP was investigated, using HCP monoliths prepared from CEM I. Prior to carbonation, the monoliths were immersed for 28 days in 40 mL CEM I equilibrium solution containing 1.2 10^{-6} mol L^{-1} ^{226}Ra under inert gas atmosphere. One monolith was retained for comparison, whereas a second was placed in an autoclave under 2.5 bar CO_2 overpressure for 13 d, to initiate carbonation of the HCP. After cessation of the experiment, the monoliths were cut perpendicular to their length axis and the distributions of radium and various other elements on the obtained cross sections were investigated by autoradiography, SEM/EDS and ToF-SIMS.

4.6. Solution analyses

Concentrations of ^{226}Ra in solution were determined by γ-spectroscopy (186 keV γ-line) using 500 µL sample aliquots in a 2 mL borosilicate glass vial placed in a high-purity germanium coaxial N type detector system (type: EGC 35-195-R), from Eurisys Mesures, equipped with a spectrometer system from EG & G Ortec. Analysis of the spectra was performed with the GammaVision® Modell A66-B32 software (version 5.20). Liquid scintillation counting (LSC) measurements of ^{99}Tc were performed using a 1220 Ultra low level Quantulus™ LSC device (Perkin Elmer), equipped with the WinQ software (version 1.2). Aliquots of 50 – 1000 µL were diluted in a 20 mL polyethylene Vial with 15 mL Ultima Gold™ LSC-cocktail (Perkin Elmer). Concentrations of inactive elements (I, Mo) were determined by ICP-MS or ICP-OES (Thermo Scientific iCAP7600; conducted by an external contractor). Aliquots of the samples were diluted to a concentration of 1 to 100 ppb and measured by ICP-MS using an Elan 6100 DRC (Perkin Elmer) equipped with the Elan software (version 3.4).

4.7. Phase characterization

Purity and composition of the final products was confirmed by XRD using a D4 Endeavour spectrometer (Bruker AXS GmbH) with a θ-2θ geometry employing CuK_α –radiation (λ = 0.15406 nm) at a power setting of 40 kV and 40 mA. Powder XRD patterns were collected at ambient conditions in the 2θ range from 5° to 80° using a step size of 0.02°/2θ and a counting time of 2 s per step. Phases sensitive to carbonation in air atmosphere were covered using polyimide film (Kapton, DuPont) and silica grease sealing

prior to the measurements. XRF-analyses were conducted by an external service company (Terrachem GmbH), respectively.

Phase morphology and sample microstructure was studied by SEM analyses performed with a Quanta 200F SEM from FEI, equipped with a field emission cathode. Energy dispersive spectroscopy (EDS) was performed with an Apollo X Silicon Drift Detector (SDD) from EDAX. Point and multipoint measurements, line scans, element mapping and particle analysis were carried out with the Genesis software. Samples were prepared on sticky carbon pads which were glued to an aluminum sample holder. SEM analysis was carried out under low vacuum (60 Pa), where a coating of the samples was not required.

Transmission electron microscopy (TEM), selected area electron diffraction (SAED) and energy dispersive X-ray spectroscopy (EDS) were performed on a FEI Technai G2 F20 transmission electron microscope at the Ernst-Ruska-Centre for Microscopy and Spectroscopy with Electrons (ER-C) at Forschungszentrum Jülich. The transmission electron microscope was operated at 200 kV accelerating voltage with a total beam current of about 2 nA. The samples present in form of few micrometer sized crystallites were supported by a hexagonal copper grid for analyses. TEM images and SAED patterns were recorded from parts of the crystallites exposed over the free grid space with the incident electron beam perpendicular to the platelet normal. EDS spectra were recorded with the samples tilted by 15° towards the spectrometer.

Time-of-Flight Secondary Ion Mass Spectrometry (ToF-SIM) was performed on a ToF-SIMS IV provided by IONTOF, at the Central Institute for Engineering, Electronics and Analytics (ZEA-3) at the Forschungszentrum Jülich GmbH. Prior to the measurement a thin gold coating was applied to increase conductivity. The elemental composition was measured using negative polarity. Sputtering was performed at a voltage of 2000 V using a Cs source.

4.8. Autoradiography

The 2D radionuclide distribution in monolithic samples was determined using a HD-CR 35 NDT Autoradiograph (DÜRR NDT GmbH & Co. KG) equipped with CR-Reader software version 1.4.1. Sample evaluation was conducted using AIDA image analyser software (v. 4.50) obtained from Raytest Isotopenmessgeräte GmbH. Samples were polished

and embedded in epoxy resin prior to autoradiography. The sample diameters were calculated from pixel size (12.5 μm) and the numbers of pixels.

4.9. Thermodynamic modelling

To support the interpretation of the sorption experiments, aqueous solution speciation and saturation indices were calculated using the geochemical code PhreeqC Ver. 3.4.0 (Parkhurst and Appelo, 2013). The ANDRA Thermochimie v.9a thermodynamic database was used for the thermodynamic modeling (Giffaut et al., 2014; Grivé et al., 2015). This database includes the thermodynamic data on cement phases from Blanc et al. (2010a, b).

4.10. Ab-initio calculations of cation exchange in C-S-H

Ab-initio calculations of cation exchange reactions in C-S-H were performed using the Density Functional Theory (DFT)-based plane-wave Quantum-ESPRESSO simulation package (Giannozzi et al., 2009) applying the PBE exchange-correlation functional (Perdew et al., 1996). To achieve a good convergence of the computed energies a plane-wave energy cutoff of 30 Ryd was applied. The core electrons of the atoms were represented by ultra-soft pseudopotentials (Vanderbilt, 1990). During the calculations, the lattice parameters and the ionic structure of the C-S-H-phases were optimized to the equilibrium values, assuming zero pressure with a tolerance of 0.01 GPa and a total force smaller than 0.0001 a.u.. To account for the effects of the aqueous solution, for the calculation of the aqueous species (Ca^{2+} and Ra^{2+}) the ENVIRON module (Andreussi et al., 2012; Giannozzi et al., 2017) was applied, assuming a water relative static permittivity constant of 78.3 (Andreussi et al., 2012). Here, we assumed that both aqueous cations (Ca^{2+} and Ra^{2+}) are coordinated by 8 water molecules (as $[M(H_2O)_8]^{2+}$) in the first hydration sphere (Jalilehvand et al., 2001; Matsuda and Mori, 2014a, b). The enthalpies of the aqueous species were derived by combining the computed energies of the isolated (gas phase) Ca^{2+} and Ra^{2+} and measured hydration enthalpies. The computed hydration energy for Ca^{2+} and Ra^{2+} was 1635 kJ mol^{-1} and 1320 kJ mol^{-1}, respectively. This corresponds well to the measured values of 1577 kJ mol^{-1} and 1266 kJ mol^{-1} (Smith, 1977). Most importantly, the computed difference in the hydration energies between Ca^{2+} and Ra^{2+} of 315 kJ mol^{-1} matches well the experimentally derived value of 311 ± 12 kJ mol^{-1}.

The solid C-S-H phases were represented by model structures based on the structure of the (crystalline) natural C-S-H phase 11 Å tobermorite ($Ca_{2.25}[Si_3O_{7.5}(OH)_{1.5}])H_2O$) from Hamid (1981) that corresponds to a Ca/Si ratio of 0.75. C-S-H structures with higher Ca/Si-ratios were derived by adding calcium atoms in the interlayer space of the C-S-H structure in a random manner; the respective supercells used in the simulations contained between 285 and 300 atoms. Radium atoms were introduced into the C-S-H by replacing calcium atoms in different structural positions, i.e. exchanging calcium in the interlayer (and Ca sorbed to the surface) as well as calcium bound in the octahedral layer; the formation enthalpies for the different configurations were calculated and compared.

4.11. Calculation of selectivity coefficients

A quantitative evaluation of the experimental data on the ^{226}Ra uptake by C-S-H was performed, assuming cation exchange with calcium (cf. Tits et al., 2006a) according to:

$$\text{C-S-H-(Ca)} + Ra^{2+} \leftrightarrow \text{C-S-H-(Ra)} + Ca^{2+} \qquad \text{(eq. 2)}$$

with C-S-H-(Ca) referring to the exchangeable calcium in the C-S-H structure. The selectivity coefficient, K_c, for this reaction can then be defined as follows:

$$K_c = \frac{N_{Ra} \cdot a(Ca^{2+})}{N_{Ca} \cdot a(Ra^{2+})} \qquad \text{(eq. 3)}$$

where $a(Ca^{2+})$ and $a(Ra^{2+})$ are the activities of the cations in the aqueous phase and N_{Ra} and N_{Ca} represent the equivalent fractional occupancies defined as:

$$N_M = \frac{2 \cdot M_s^{2+}}{CEC} \qquad \text{(eq. 4)}$$

where M_s^{2+} is amount of the divalent cations sorbed (mol kg^{-1}), and *CEC* the cation exchange capacity of the C-S-H phase in eq kg^{-1}. For homovalent cation exchange, the activity coefficients for both cations are the same and the activities in Eq. (4) can be substituted by concentrations:

$$K_c = \frac{N_{Ra} \cdot [Ca^{2+}]}{N_{Ca} \cdot [Ra^{2+}]} \qquad \text{(eq. 5)}$$

if sorption is attributed only to cation exchange, the relation between the distribution coefficient R_d (Eq. 1) of radium and the selectivity coefficient for the Ra-Ca exchange can be formulated as:

$$R_{\mathrm{d}} = \frac{0.5 \cdot CEC \cdot K_{\mathrm{c}}}{[\mathrm{Ca}^{2+}]} \qquad \text{(eq. 6)}$$

5. Results

5.1. Characterization of solids

5.1.1. C-S-H

XRD and SEM investigations were performed to confirm the nature and purity of the synthesized phases and to assess their microstructure before and after the uptake experiments. The C-S-H phases exhibit the typical fine-grained cloudy microstructure, corresponding to their nanocrystalline nature (Figure 14). XRD patterns of the C-S-H phases, shown in Figure 15, exhibited the typical diffuse reflexes at 29.1, 31.8, 49.8, 55.1 and 66.4°/2θ, respectively (e.g. Baur et al., 2004; Chen et al., 2004; Lachowski et al., 2000; Nonat, 2004), despite the higher background below 22°2 θ due to the kapton foil sealing used. The XRD investigations exhibited no evident portlandite reflexes. Therefore, portlandite impurities are expected to be lower than 1% (w/w). Lothenbach and Nonat (2015) reported difficulties of synthetizing C-S-H phases at Ca/Si-ratios above 1.45, without (co)precipitation of portlandite with the applied synthesis procedure. The XRF-analysis affirmed generally the intended Ca/Si-ratios of the C-S-H phases of about 0.9 and 1.4 respectively, with a slightly higher Ca/Si ratio of 0.96 for the phase with the lower Ca/Si ratio (Table 6).

The BET-data show the expected high surface area of the C-S-H gels with surface areas of 126 m^2 g^{-1} (C-S-H0.9) and 109 m^2 g^{-1} (C-S-H1.4), respectively. These surface areas are slightly lower than those determined by Tits et al. (2006b) (148 m^2 g^{-1}) and Missana et al. (2017) (144 ± 40 m^2 g^{-1}) for C-S-H having Ca/Si-ratios ranging from 0.9 to 1.6. Despite the fact that the synthesized C-S-H gel appeared to be dry, the water content was 78% for C-S-H0.9 and 53% for C-S-H1.4 due to the gentle drying procedure. The aqueous solutions in equilibrium with the C-S-H phases had a pH of 12.1 (C-S-H0.9) and pH 12.6 (C-S-H1.4), which is in the typical range of literature values for these C-S-H compositions (Lothenbach and Nonat, 2015).

Table 6 *Detailed data of the synthesized C-S-H0.9 and C-S-H1.4 phases.*

Phase	C-S-H0.9	C-S-H1.4
water content [%]	77.8	53.0
Surface area [m²/g]	125.7	109.6
Ca/Si ratio	0.96	1.41
supernatant solution		
c(Ca) [mmol L^{-1}]	4.8	19.6
c(Si) [mmol L^{-1}]	0.046	<0.01
pH	12.1	12.6
Eh [mV]	-33	-69

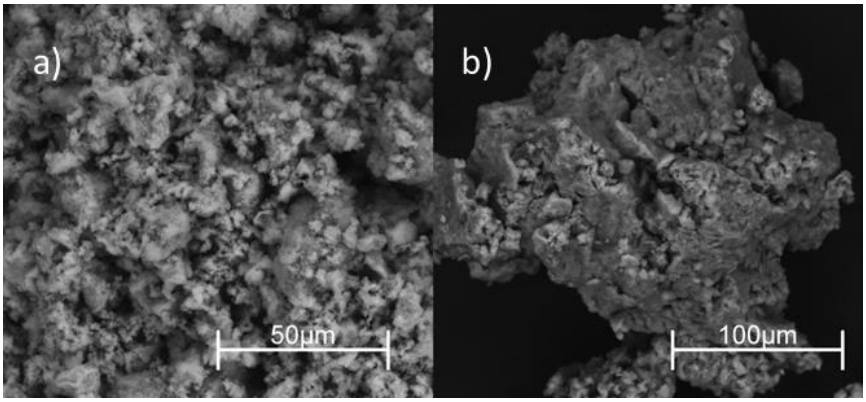

Figure 14 *SEM images of C-S-H0.9 (a) and C-S-H1.4 (b).*

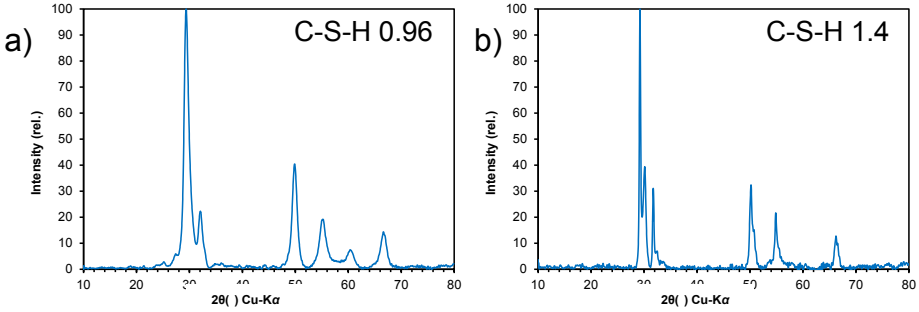

Figure 15 *XRD patterns of C-S-H0.9 (a) and C-S-H1.4 (b).*

5.1.2. AFm

5.1.2.1. Tricalcium aluminate C_3A precursor

Tricalcium aluminate, a precursor for AFm and C_3AH_6, of sufficient yield and quality, was obtained by a pre temperature treatment at 1000°C followed by heating once to 1450°C (Mondal and Jeffery, 1975). Heating in smaller steps lead to increased mayenite contents. Mayenite ($C_{12}A_7$) is faster hydrating compared to C_3A and will also result in the formation of hydrogarnet; however, due to the calcium aluminum stoichiometry, hydration of mayenite would result in additional $Ca(OH)_2$ formation (Taylor, 1997).

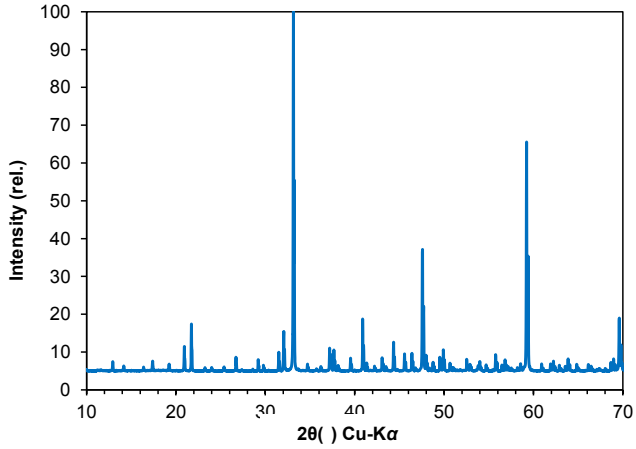

Figure 16 *XRD pattern of the synthesized C_3A product.*

5.1.3. AFm-SO_4

The synthesis of these layered double hydroxides was in principle be achieved by the reaction of C_3A ($3CaO{\cdot}Al_2O_3$) and a calcium salt containing the anion that will be located in the interlayer ($CaSO_4$, CaI_2, $CaCl_2$, $CaCO_3$). However, for the synthesis of AFm-SO_4 it should be noted that the use of C_3A and $CaSO_4$ will lead to mixture of AFm and (minor) ettringite. The coexistence of these two phases is caused by the thermodynamic stability of ettringite and is obtained also if the Al/SO_4 is set exactly to match AFm. However, it was found that these AFt impurity can be overcome by the fact that ettringite is very soluble at elevated temperatures above 40°C (Jimenez and Prieto, 2015). Therefore, a phase pure AFm was observed by Matschei et al. (2006), who performed the AFm-SO_4 synthesis at 85°C.

Here, a phase pure AFm-SO_4 product was achieved by the reaction of C_3A and $CaSO_4 \cdot 2\ H_2O$. The obtained AFm-SO_4 shows the typical hexagonal sheet like micro structure, with crystal sizes varying between a few µm up to 50 µm in diameter (Figure 17); the BET surface area was 1.12 $m^2\ g^{-1}$ (Table 7). The SEM and XRD investigations revealed no evidence of AFt impurities (cf. Figure 18). Due to the preferential orientation of the platelets, the two reflexes representing the basal spacing (003, 006) have a very high intensity; thus most of the reflexes at higher angles are comparatively small and not resolvable in some cases. The measured reflexes at 9.9 °2Θ (003) and 19.9 °2Θ (006) are in agreement with the literature values for the basal spacing of AFm-SO_4 (Matschei et al., 2006).

Table 7 *Detailed data for synthesized AFm-SO_4.*

Nr. Phase	AFm-SO_4
water content [%]	35.1
Surface area [m²/g]	1.12
supernatant solution	
pH	11.9

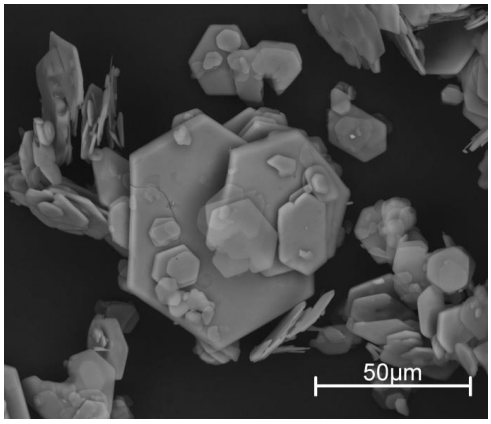

Figure 17 *SEM image of the synthesized AFm-SO_4.*

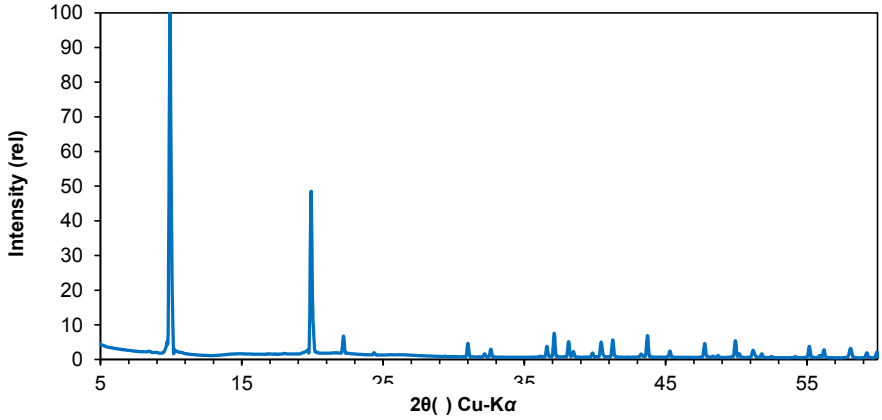

Figure 18 *XRD pattern of the synthesized AFm-SO_4.*

5.1.4. AFm-CO_3

Synthesis of AFm-CO_3 was achieved by reaction of C_3A and $CaCO_3$, with and without initial cooling during the synthesis procedure (cf. chapter 4.1). The different AFm-CO_3 products resulting from these syntheses were named 1-AFm-CO_3 for the cooled product and 2-AFm-CO_3 for the product not cooled in the first hours of reaction. The XRD patterns with strong reflexes at 11.8 °2theta in the indicate well crystalline AFm-CO_3 having typical basal spacing (Aimoz et al., 2012b; Baquerizo et al., 2015; Francois et al., 1998; Matschei et al., 2006), reflexes observed at 10.8° 2theta revealed the presence of minor amounts of hemicarbonate ($Ca_4Al_2[(OH)(CO_3)_{0.5}]\cdot xH2O$) and portlandite, respectively. SEM observations show that AFm-CO_3 synthesized with initial cooling exhibits a poorly developed micro structure and low grain size (Figure 19). XRD diffraction patterns and SEM investigations on 2-AFm-CO_3 synthesized without initial cooling revealed higher crystallinity but C_3AH_6 impurities; thus this material was rejected for the uptake experiments.

Table 8 *Detailed data for synthesized 1-AFm-CO_3.*

Nr.	
Phase	AFm-CO_3
water content [%]	n.d.
Surface area [m²/g]	n.d.
supernatant solution	
pH	11.3

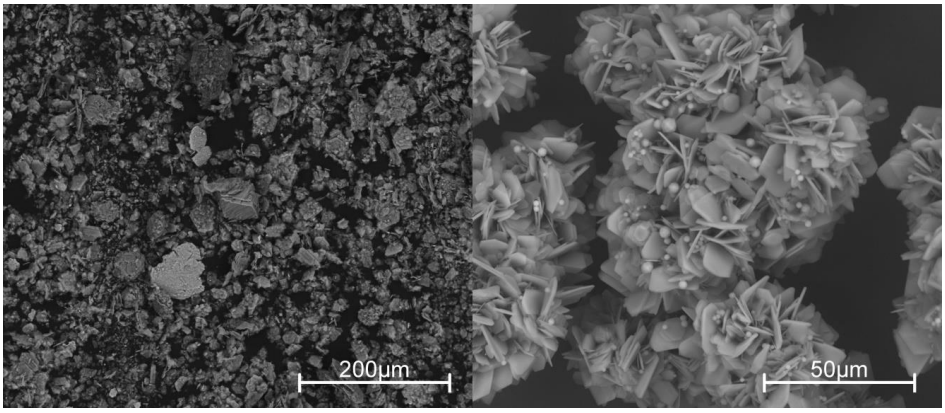

Figure 19 *SEM image of the synthesized AFm-CO_3; 1-AFm-CO_3 (left) and 2-AFm-CO_3 (right).*

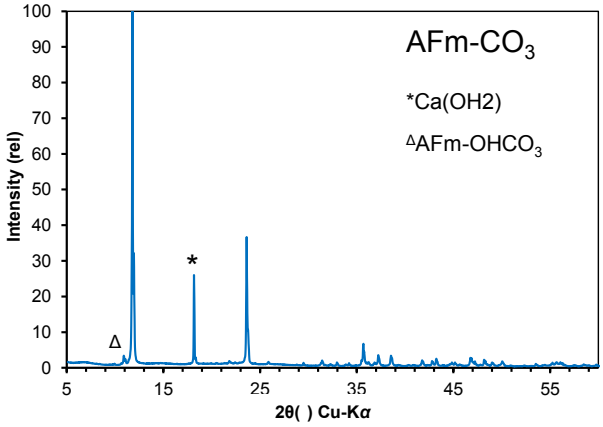

Figure 20 *XRD pattern of the synthesized AFm-CO_3.*

5.1.5. Ettringite (AFt)

The XRD data obtained for ettringite (Figure 20) revealed a typical XRD pattern for this phase (cf. Baur et al., 2004; Iwaida et al., 2001; Jimenez and Prieto, 2015; Terai et al., 2007; Zhou and Glasser, 2000) without discernable impurities. The crystal size of the synthesized ettringite was determined by SEM measurements to be < 2µm (cf. Figure 22); the BET surface area was 13.6 m^2 g^{-1} (Table 9). The relatively high sulfate concentration in the supernatant solution is due to the presence of gypsum in the product prior to purification. Sulfate concentrations in equilibrium solutions of purified ettringite were in agreement with thermodynamic calculations for the ettringite-water system.

Table 9 *Detailed data for synthesized ettringite.*

Phase	ettringite
water content [%]	61.1
Surface area [m²/g]	13.55
supernatant solution	
c(Al) [mmol L^{-1}]	0.12
c(Ca) [mmol L^{-1}]	16.5
c(S) [mmol L^{-1}]	16.8
pH	10.4
Eh [mV]	205

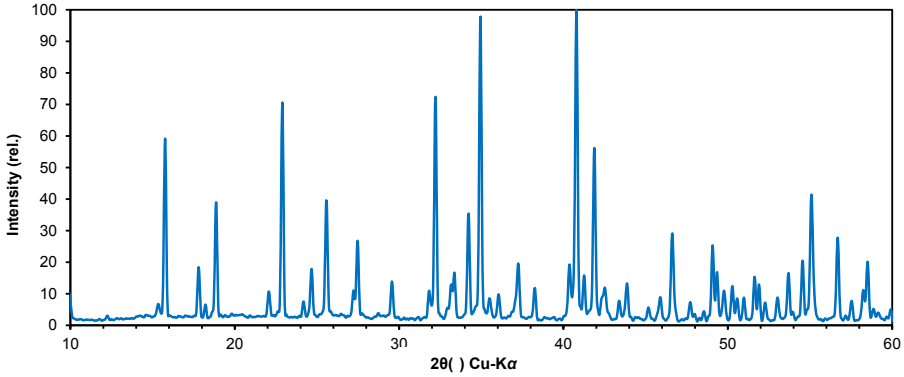

Figure 21 *XRD pattern of the synthetic ettringite.*

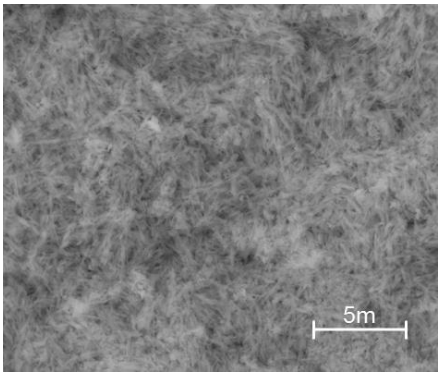

Figure 22 *SEM image of the synthetic ettringite (AFt).*

5.1.6. Hydrogarnet

The hydrogarnet C_3AH_6 cured at 90°C revealed good crystallinity occurred as agglomerates of idiomorphic crystals with up to 30 µm in size, with a surface area of 1.5 $m^2 g^{-1}$ (Table 10, Figure 23). Typical XRD patterns were obtained (Figure 24) indicating the absence of impurities.

Table 10 *Detailed data for synthesized hydrogarnet.*

Phase	Hydrogarnet (C_3AH_6)
water content [%]	25.6
Surface area [m^2/g]	1.46
supernatant solution	
c(Al) [mmol L^{-1}]	0.02
c(Ca) [mmol L^{-1}]	13.8
pH	12.5
Eh [mV]	-74

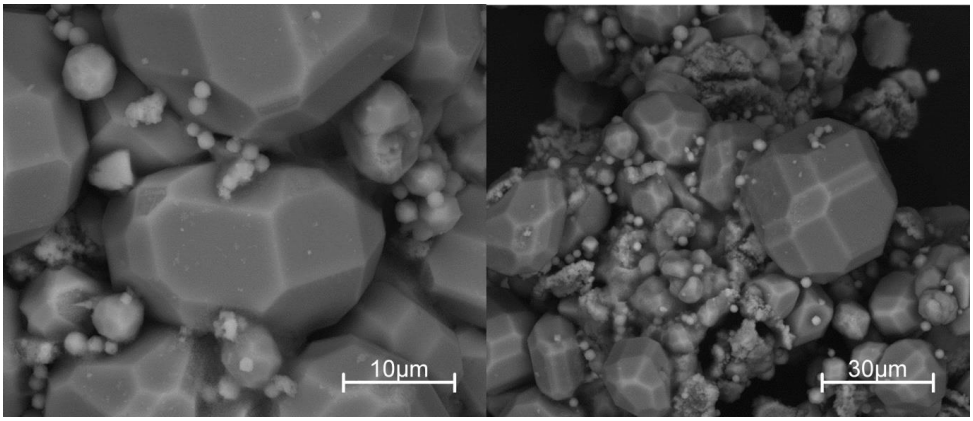

Figure 23 *SEM image of synthesized C_3AH_6.*

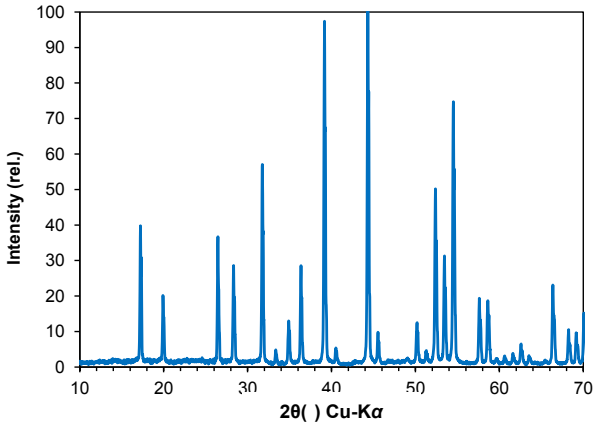

Figure 24 *XRD pattern of synthesized* C_3AH_6.

5.1.7. Hardened cement pastes (HCP)

Two different cement formulations were used in this study, namely pastes based on CEM I and a low pH cement paste. The chemical composition of the unhydrated CEM I cement clinker is given in Table 11.

Table 11 *Oxide distribution of CEM I 32.5 R used for uptake studies (n.d.; not determined).*

Oxide	w%
CaO	63.4
SiO_2	20.5
Al_2O_3	5.5
SO_3	2.9
Fe_2O_3	2.5
MgO	1.5
K_2O	0.8
TiO_3	0.3
Na_2O	0.2
Mn_2O_3	0.1
P_2O_5	0.1
Cl	<0.1
S	n.d.
Other	0.2
Loss on ignition	2
Total	100

According to information from the cement producer (Heidelberger Zement), the initial phase distribution in the clinker is C_3S 53.1 wt.%, C_2S 18.9 wt.%, C_3A 10.2 wt.%, C_4AF 7.6 wt.% and free CaO 0.7 wt.%. Prior to the experiments the initial phase assemblage and the micro structure of the HPC was characterized. According to the powder XRD patterns of the ground HCP samples, the phase assemblage of the CEM I paste comprised minor amounts of ettringite, various AFm-phases (i.e. mainly AFm-SO_4 accompanied by minor amounts of AFm-CO_3 and hemicarbonate) besides C-S-H and portlandite. In general, modern CEM I pastes are expected to contain about 60–70 wt.% C-S-H, about 25 wt.% portlandite and less than 10 wt.% each of ettringite, AFm and other minor hydration phases (Glasser, 1997; Glasser, 2001).

Figure 25 depicts the results of SEM/EDS investigations of the hydrated CEM I paste. Based on their lower density, the dark gray regions in the SEM picture were assigned to be hydration phases, whereas the light gray areas represent unreacted clinker phases. The hydration phases are mainly consisting of C-S-H. A clear assignment of the hydration phases based on gray scales and elemental composition was not possible in most cases. In EDS measurements, the electron beam hitting the surface is expanding to a width of approximately 5 µm and therefore limiting the resolution for small crystals. In the unreacted clinker material, the stoichiometry obtained by EDS was used to distinguish between alite and belite. SEM/EDS elemental mapping (Figure 25) shows that the majority of iron and alumina is located in the unreacted clinker phases and can be attributed to C_3A and C_4AF. Sulfur was mainly located in the hydration phases due to its high mobility in cement pore water. The local difference in the sulfur concentration was not sufficient to allow for a clear assignment of AFm or AFt phases. In general, at hydration times exceeding 90 days, the ettringite content should be below 1% (Taylor, 1997; Verein Deutscher Zementwerke, 2002).

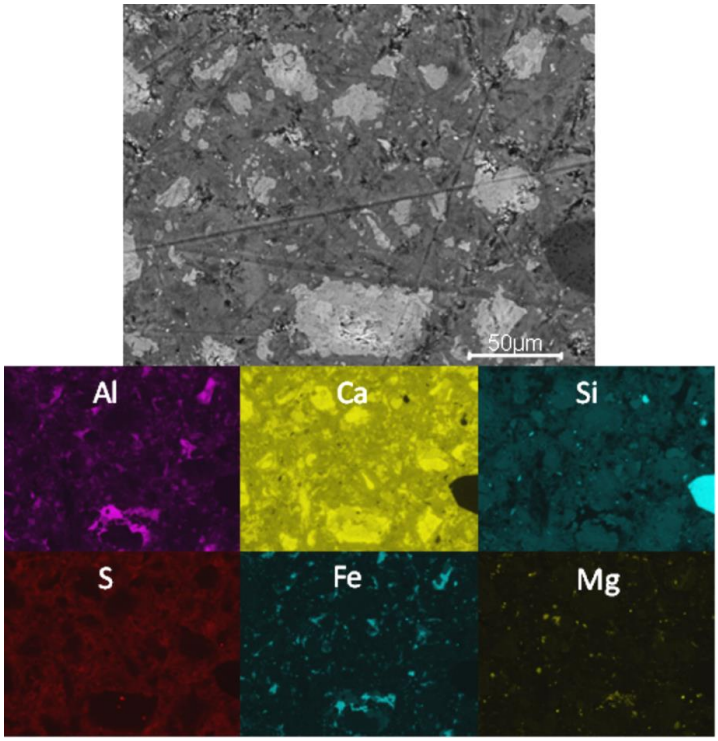

Figure 25 *SEM/EDS mapping of hardened CEM I paste.*

For a more detailed visualization of the microstructure of the HCP, a false color map was obtained from the EDS element mapping, based on a least square method, where the phase with the highest calculated probability was assigned to the respective pixel (Figure 26). Thus a phase distribution was obtained that matches the SEM/EDS observations. A minor drawback was the low contrast on sulfur. Sulfur was mainly located in regions rich in C-S-H. In fact, no AFm/AFt could be assigned. It should be noted that also the regions designated as AFm/AFt marked comprise mainly C-S-H, since AFm phases formed in OPC pastes are poorly crystalline and intimately mixed with C-S-H (Taylor, 1997). Anyhow, the image reveals the typical distribution of clinker and hydration phases for the studied hardened CEM I paste.

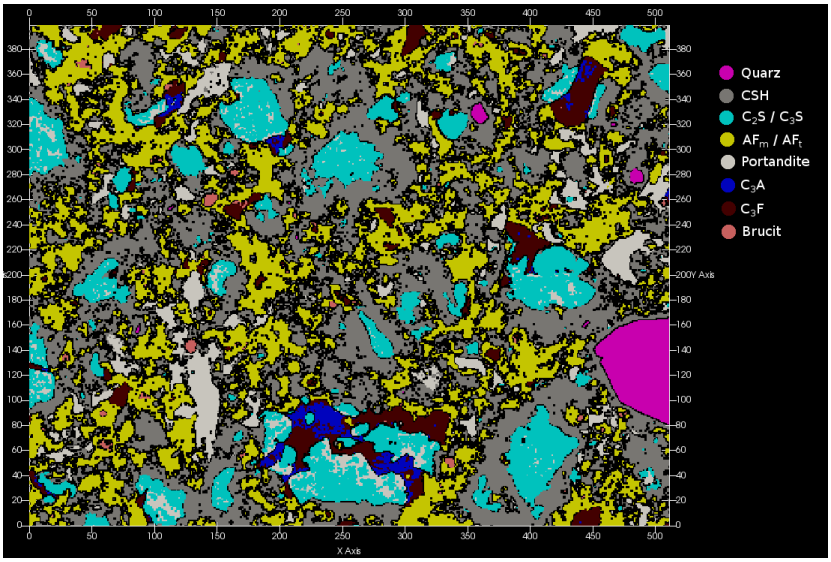

Figure 26 *False color mapping of hardened CEM I paste based on EDS mapping data.*

Table 12 *Oxide distribution in cement clinker and BFS used in the VTT reference paste.*

CEM I 42,5 MH/SR/LA		Blast furnace slag	
Oxide	w%	Oxide	w%
CaO	65	CaO	36 – 42
SiO_2	22	SiO_2	36 – 40
Al_2O_3	3.5	Al_2O_3	8 – 10
Fe_2O_3	4.5	K_2O	0.5 – 1.0
K_2O	0.6	Na_2O	0.5 – 1.0
Na_2O	0.1	MgO	10 – 12
MgO	1.0	S	1.5 – 2
SO_3	2.0	Ti	0.9 – 1.3

The other hardened cement paste under investigation is a low pH cement paste, based on a ternary mix of binder (CEM I) with blast furnace slag and silica fume, containing additional quartz filler. The oxide compositions of the binder (CEM I) and the blast furnace slag are given in Table 12.

The XRD patterns of the ground VTT low pH cement paste show, beside intense reflexes of the quartz filler, only weak reflexes of crystalline hydration phases, mainly ettringite, and amorphous C-S-H. Simulations of the hydration process of the VTT low pH cement by Idiart (2017) suggested that after 1 year of hydration the paste contains predominantly C-S-H with low Ca/Si-ratios <1 and only small amounts of other hydration phases, besides unreacted clinker, silica fume and blast furnace slag. The SEM/EDS mapping of the polished surface of a HCP monolith made from VTT low pH cement is shown in Figure 27. The micro analytical investigations reveal the presence of unhydrated clinker material, mainly C_2S, unreacted quartz filler, and blast furnace slag. Investigation on the educts used reveal that the fumed silica used is main source of carbon present in the reference cement paste. Moreover, iron rich phases such as iron oxides and iron sulfides were identified, which can provide for the immobilization of redox-sensitive radionuclides in the hardened cement paste. Beside very few large cavities that are caused by trapped air bubbles, the pore size of the material are below resolution level of SEM. The pH of the equilibrium solutions produced with crushed HCP was found to be 12.6 (CEM I) and 12.5 (VTT low pH cement), respectively. The comparatively low equilibrium pH for the crushed CEM I compared to the pH of young cement pore waters in Portland cement based systems is attributed to the low S/L-ratio used in the experiments, resulting in a low inventory of alkalis.

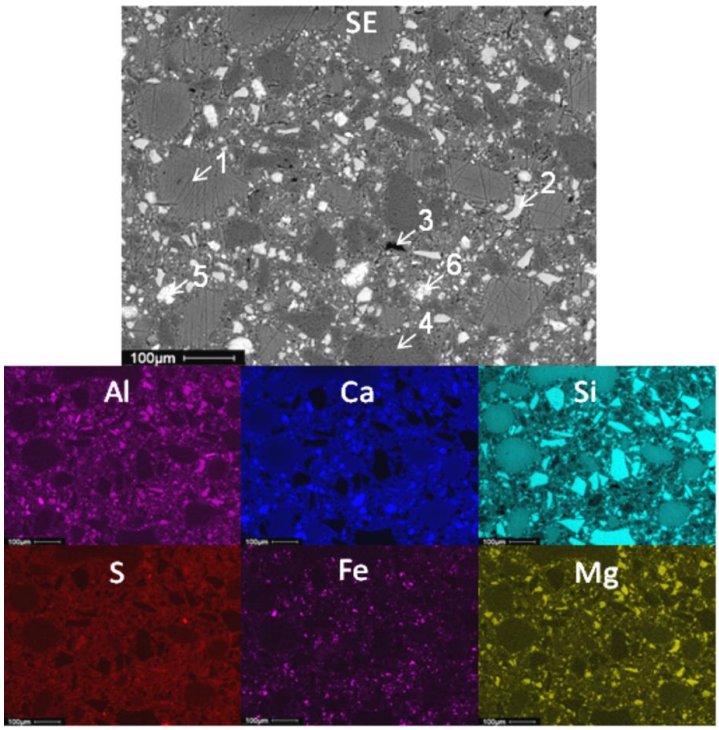

Figure 27 *SEM/EDS mapping of the hardened VTT reference paste (BSED); 1) fumed silica, 2) blast furnace slag, 3) carbon, 4) quartz, 5) iron oxide, 6) unhydrated clinker.*

5.2. Radium uptake in cementitious systems

5.2.1. Uptake kinetics

The kinetics of the radium uptake by the model hydration phases were determined at a S/L-ratio of 0.005 kg L^{-1} in the absence and in the presence of alkalis for up to 100 days. The results of the sorption tests as a function of time are shown in Figure 28. The pH in the respective solutions was found to be constant over the time of the experiments. A significant uptake of radium is only observed for the C-S-H phases; uptake of radium in systems with AFt and AFm phases is distinctively lower. For C-S-H, a dependency of the radium uptake on the alkali content in solution and the Ca/Si-ratio of the solids were observed. The uptake of radium by the various phases is rather fast and sorption equilibrium was attained within 10–28 days, irrespective of the solutions used in the experiments. The uptake of radium by C-S-H0.9 and C-S-H1.4 reached a steady state at 28 days. Since drying and purifying of C-S-H might lead to an agglomeration of the nano-crystalline C-S-H material, effects of potential structural changes and the dehydration of the C-S-H on the radionuclide uptake were addressed in in situ experiments.

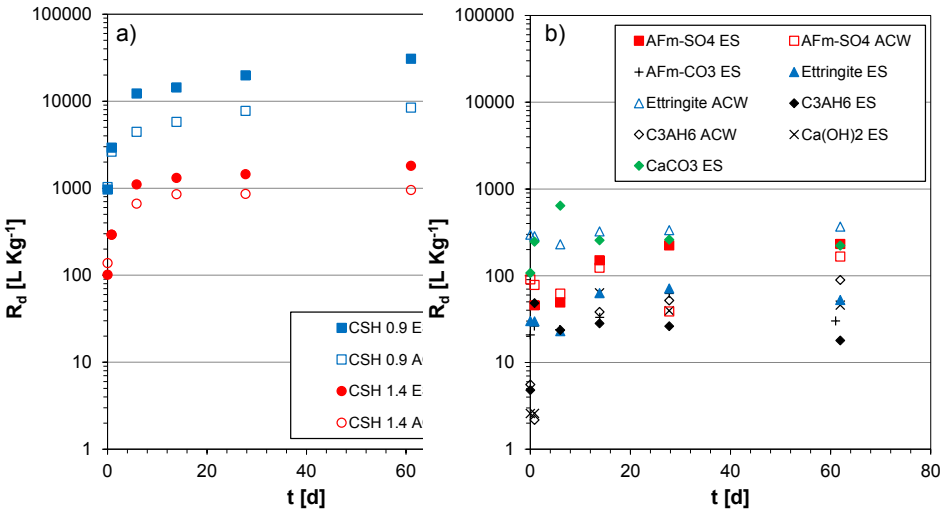

Figure 28 *Uptake kinetics of radium by a) C-S-H phases and b) other phases for different solutions used (ES: equilibrium solution; ACW: artificial young cement water (pH 13.3); error bars are omitted for the sake of clarity.*

Here radiotracers were added directly at the end of the curing time, without separation of the solid and liquid phase. Figure 28 shows the uptake of radium by C-S-H in the in situ experiments which was found to be considerably faster, with steady state concentrations established within less than 8 days. The faster uptake in the in situ experiments can be attributed to the time required for the rehydration of the C-S-H interlayer when using dried material, since the water content in the interlayer of the C-S-H significantly impacts the mobility of ions in C-S-H and the accessible surface area. The rehydration time of C-S-H generally depends on the actual water content in the interlayer (Maruyama et al., 2015). The addition of alkalis in the in situ experiments accelerated the radium uptake by the C-S-H. Here, sorption equilibria were attained within one day, comparably to the results obtained by Tits et al. (2006a) in similar experiments.

The R_d-values obtained in the in situ experiments were generally rather similar to those obtained using dried and purified C-S-H. Distribution ratios obtained from in-situ experiments were found to be $R_d = 12200 \pm 500$ L kg^{-1} for C-S-H0.9 and $R_d = 850 \pm 28$ L kg^{-1} for C-S-H1.4. Distribution ratios in ACW were lower in general, with $R_d = 4000 \pm 140$ L kg^{-1} for C-S-H0.9 and $R_d = 640 \pm 29$ L kg^{-1} for C-S-H1.4 and reached steady state conditions within 1 day. Hence, it can be concluded that the effect of drying and purifying of C-S-H have an accelerating effect on uptake kinetics, whereas the equilibrium distribution ratios are rather similar.

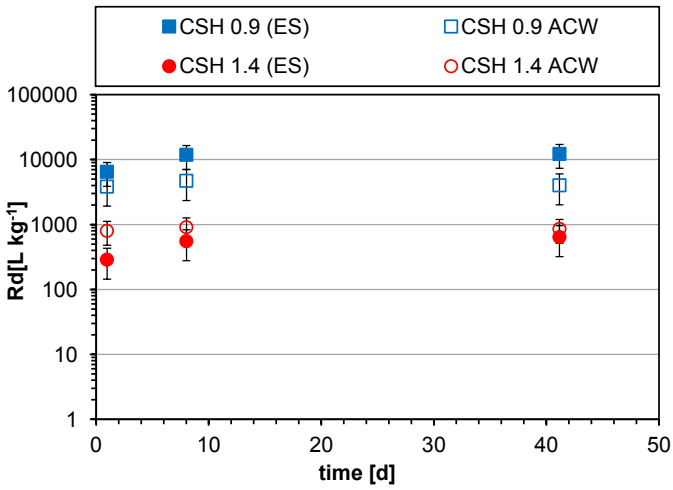

Figure 29 *Kinetics of radium uptake by C-S-H0.9 and C-S-H1.4 in in situ experiments (ES: equilibrium solution; ACW: artificial young cement water, pH 13.3).*

5.2.2. Equilibrium distribution ratios

Results regarding the R_d values for the uptake of radium by the various cement hydration model phases determined at a S/L-ratio of 0.04 L kg^{-1} are shown in Figure 30 and detailed in Table 13. The results show that C-S-H is the only hydration phase providing for an effective retention of radium in cementitious systems. Weak contribute of aluminate phases AFm and ettringite are expected (in general R_d <50 L kg^{-1}). The slightly more pronounced radium uptake by calcite (R_d = 200 to 260 L kg^{-1}) indicates a potential additional radium retention mechanism in carbonated cementitious materials.

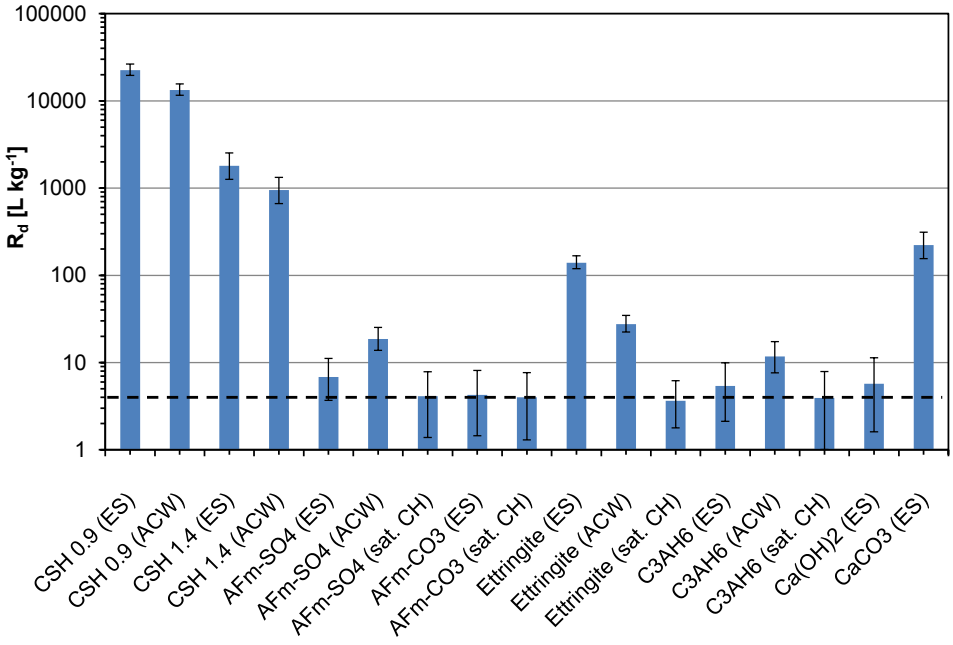

Figure 30 *Distribution ratios R_d of radium for various hydration phases in different solutions (ES: equilibrium solution; ACW: artificial young cement water (pH 13.3); CH: portlandite saturated solution (pH 12.3). Dashed line indicates the lowest discernible Rd based on the detection limit and counting statistics.*

Table 13 *Distribution ratios R_d of radium for various hydration phases in different solutions (ES: equilibrium solution; ACW: artificial young cement water (pH 13.3); CH: portlandite saturated solution (pH 12.3).*

Phase	R_d [L kg^{-1}]		
	ES	ACW	CH
C-S-H0.9	22,529 ± 3,980	13,328 ± 2,356	
C-S-H1.4	1,805 ± 722	951 ± 380	
AFm-SO_4	7 ± 4.3	19 ± 6.7	4 ± 3.7
AFm-CO_3	4 ± 3.9		4 ± 3.7
Ettringite	139 ± 28	28 ± 7.1	4 ± 2.5
Hydrogarnet C_3AH_6	5 ± 4.5	12 ± 5.6	4 ± 3.9
Portlandite			6 ± 5.6
Calcite	223 ± 89		

5.2.2.1. Calcium silicate hydrates

C-S-H was the only investigated hydration phase showing a significant uptake of radium. The R_d was found to depend on the Ca/Si ratio of the C-S-H phases as well as on pH and alkali content in solution. Stronger uptake of radium was observed for low calcium to silicon ratio exhibiting a distribution ratio of $R_d = 2.3 \cdot 10^4$ L kg^{-1} in equilibrium solution, whereas the C-S-H with Ca/Si ratio of 1.4 exhibit a maximum at $R_d = 1.8 \cdot 10^3$ L kg^{-1}. This effect is probably due to the change in surface charge from negative at Ca/Si <1.2 to positive at Ca/Si > 1.2, allowing for a more pronounced uptake of cations at Ca/Si < 1.2 (Labbez et al., 2007; Lothenbach and Nonat, 2015; Tits et al., 2006a). Similar trends were observed by Tits et al. (2006a) with R_d values decreasing from about $2 \cdot 10^3$ L kg^{-1} for Ca/Si ratio of 0.96 to about 100 L kg^{-1} for Ca/Si ratio of 1.6. Despite the higher BET surface area, R_d-values obtained by Tits et al. (2006a) for C-S-H with similar compositions were about one order of magnitude lower than our values.

The radium uptake by C-S-H in ACW, representative for young cementitious materials (stage I, pH ~13.5), was generally smaller, by a factor of approximately 2, compared to the uptake in the equilibrium solution (ES). The distribution coefficients found for C-S-H0.9 and C-S-H1.4 in ACW were $R_d = 13 \cdot 10^4$ L kg^{-1} (ACW) was $R_d = 0.95 \cdot 10^3$ L kg^{-1}, respectively. Similar trends were observed also by Tits et al. (2006a). The lower uptake in ACW can most probably be explained by alkalis, taking part as competing ions for sorption sites (Tits et al., 2006a). Furthermore, surface charge and speciation of C-S-H, due to the higher pH, and the increasing fraction of $RaOH^+$ complexes in solution (<2.5% at pH 12, ~22% at pH 13.3) may contribute to this trend. These results suggest a higher mobility of

radium in young cementitious materials (stage I) compared to alkali free, aged cementitious systems (stage II; portlandite stage). Therefore, lower Ca/Si-ratios of C-S-H in low pH cementitious materials should provide a higher retention potential for radium compared to young Ordinary Portland Cement (OPC) based systems.

Moreover, the radium uptake by C-S-H was studied as function of S/L-ratio for S/L between 0.005 and 0.l kg L^{-1} in equilibrated solutions (Figure 31), to exclude significant effects of different S/L-ratios on the uptake of radium by C-S-H. The uptake by C-S-H phases was found to be rather independent of the S/L-ratio used. The distribution ratios for radium uptake by C-S-H0.9 are in good agreement with results stated earlier (R_d > 10,000 L kg^{-1}). Distribution radios obtained for C-S-H1.4 indicate a slight decrease in the R_d-value at high S/L-ratios. This is similar to the observations of Tits et al. (2006a) for a Ca-rich C-S-H phase (Ca/Si 1.6).

Uptake of radium (and barium) by C-S-H has generally been explained in terms of cation exchange with calcium and sorption to two silanol-like sites at the C-S-H surface (Missana et al., 2017; Tits et al., 2006a). To calculate the selectivity coefficient (Kc) for radium uptake on C-S-H, from uptake experiments using eq. (7), it was assumed that the exchange for calcium at the C-S-H surface is the main uptake mechanism. A value of 1.2 eq. kg^{-1} for the CEC of C-S-H as derived by Tits et al. (2006b) was used here. Based on this, selectivity coefficients for the Ra/Ca exchange of log Kc = 2.2 for C-S-H0.9 and log Kc = 1.8 for C-S-H1.4 in the alkali free systems were calculated.

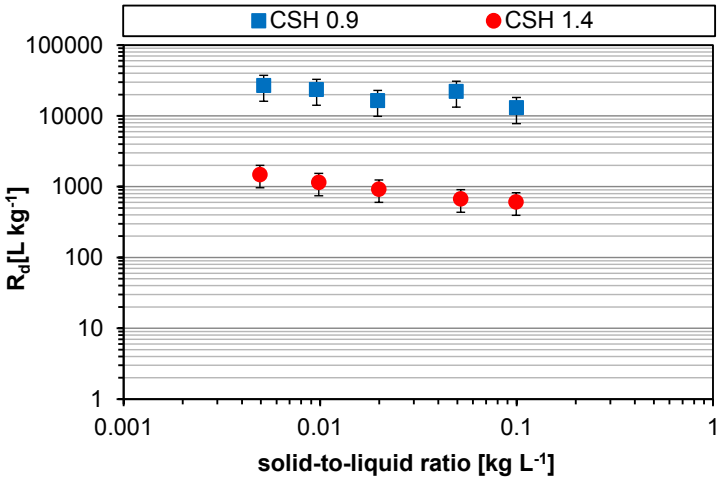

Figure 31 *Uptake of radium by C-S-H0.9 and C-S-H1.4 depending on variable solid-to-liquid ratio.*

These values are higher than the overall value of log Kc = 0.78 ± 0.6 determined by Tits et al. (2006a) for the Ra/Ca exchange on C-S-H under similar conditions. Comparison of the selectivity coefficients for the sorption of barium and strontium by C-S-H due to cation exchange reveals a decreasing affinity for uptake by C-S-H in the order Ra > Ba > Sr (Ba: log Kc = 1.05, Missana et al., 2017; Sr: log Kc = 0.08, Tits et al., 2006b). The significantly lower selectivity coefficient in particular for Sr suggests that Sr cannot be used as meaningful analogue for the uptake of radium in cementitious systems.

Incorporation of bivalent cations into the C-S-H interlayer as an additional uptake mechanism has been discussed previously by various authors (e.g. Komarneni et al., 1986; Komarneni and Tsuji, 1989; Missana et al., 2017; Shrivastava and Glasser, 1986; Shrivastava and Komarneni, 1994; Tits et al., 2006a; Tits et al., 2006b). It was concluded that cations smaller than calcium (e.g. Ni, Co or Zn) as well as strontium can replace calcium in the C-S-H interlayer in general, whereas the uptake of cations larger than calcium was limited to sorption at surface sites. However, more recent investigations on the uptake of Np(VI/V) and U(VI) by C-S-H suggested that also large cations can be incorporated into the C-S-H interlayer spacing (Gaona et al., 2011; Gaona et al., 2012; Tits et al., 2014; Tits et al., 2011).

5.2.2.2. Other phases

The uptake of radium by other cement hydration phases was low compared to C-S-H. The distribution ratios were generally below 50 L kg^{-1}; the higher R_d value (~140 L kg^{-1}) obtained for ettringite in an equilibrium solution can most probably be attributed to precipitation of $RaSO_4$, which was found to be oversaturated (Saturation index SI = 0.8) under the specific experimental conditions according to thermodynamic calculations. On the other hand, the R_d values for the radium uptake by ettringite in ACW (pH 13.3), and portlandite saturated solutions (pH 12.4) were obtained in solutions undersaturated with respect to $RaSO_4$. This indicates that ettringite may sorb some radium in young cementitious systems (R_d ~30 L kg^{-1}), whereas under stage II conditions, no significant uptake is to be expected. Similarly, a slight radium uptake by AFm-SO_4 and hydrogarnet was only found in alkali rich young cementitious water.

Additionally, experiments performed with calcite at pH 7.5, revealed a slightly more pronounced radium uptake (R_d ~220 L kg^{-1}). This outlines a potential retention mechanism for radium in carbonated cementitious materials. Jones et al. (2011) determined slightly lower distribution coefficients for radium sorption on natural calcite (R_d ~120 L kg^{-1}). According to Jones et al. (2011), the most likely mechanism for radium uptake onto calcite at low concentrations was thought to be co-precipitation within a Ca/Ra-carbonate at the calcite surface. However, the significantly larger size of radium compared to Ca (1.43 Å and 0.99 Å for coordination number CN = 6 (Shannon and Prewitt, 1969), makes an incorporation of radium in the calcite structure rather improbable. However, from DFT simulations by Liu et al. (2016) it was suggested that in the absence of sulfates, a formation of a barytocalcite-type phase ($CaRa(CO_3)_2$) might control the radium uptake in carbonate-rich systems.

5.2.3. Ab-initio calculations of radium uptake by C-S-H

Atomistic simulations were performed to investigate the potential of radium incorporation into the C-S-H interlayer, in addition to radium binding at C-S-H surface sites (see section 2.3.1). The structural uptake of radium into C-S-H was considered due to exchange with calcium at two different calcium positions (Figure 32). First, radium was substituted for calcium in the stable octahedral CaO_2 layers (A). Secondly, substitution of calcium

coordinated to silanol groups in the interlayer spacing by radium (B) was considered. The enthalpies of the respective configurations were computed and compared.

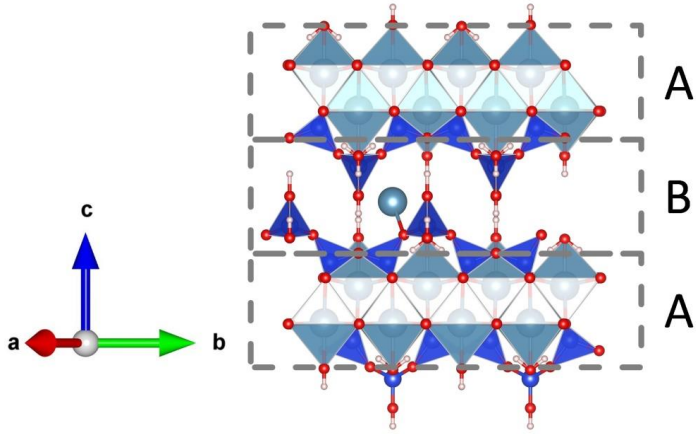

Figure 32 *Schematic representation of the C-S-H structure with octahedral CaO_2 layers (A) and the interlayer (B).*

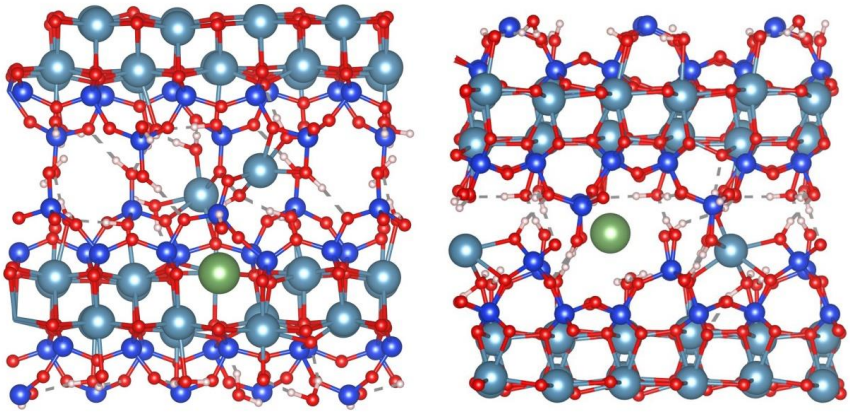

Figure 33 *Calculated final structures for radium incorporation into the CaO_2 octahedral layer (left) and the interlayer (right) of C-S-H0.75. Light blue: calcium, green: radium, blue: silicon, red: oxygen, white: hydrogen.*

The differences in the computed enthalpies (reaction enthalpies) for the two resulting super cells (Figure 33) revealed a large difference of 184 kJ mol^{-1} for C-S-H0.75. The lower enthalpy was obtained for the radium uptake into the interlayer. This was even more pronounced for C-S-H with Ca/Si- ratios of 0.9 and 1.0, with enthalpy differences of 260 kJ mol^{-1} and 202 kJ mol^{-1}, respectively. This strongly indicates that an uptake of radium by

substitution for interlayer calcium would be highly preferred over incorporation into the octahedral layer. The simulations show that the introduction of the large radium cation into this stable layer would induce an increase in the distance of the neighbouring calcium atoms along the crystallographic b axis from 7.43 Å to 7.64 Å. Thus presumably the increased strain and decreased length of Ca-O bonds along the a-b plane are the main contributors to the large energy differences.

In order to assess the potential of an exchange of radium from solution with an interlayer calcium in the C-S-H, the Gibb's free energy of this reaction was estimated. To compute $\Delta G=\Delta H-T\Delta S$ of the exchange reaction from the DFT-reaction-enthalpy (ΔH), an estimate of the reaction entropy ΔS is required. For the solid C-S-H phase it was assumed that the change in entropy due to Ra-Ca-exchange is given by the differences in Latimer entropies of elements in solid compounds (Latimer, 1951), corresponding to a $T\Delta S = 8.1$ kJ mol^{-1} at 300K in this case. For the entropies of the aqueous Ca^{2+} and Ra^{2+} ions, values of -56.484 J K^{-1} and +53.974 J K^{-1}, respectively, were used (Shock et al., 1997; SUPCRT98). The estimated ΔH, ΔS and ΔG of the exchange reaction of radium for calcium in the C-S-H interlayer are given in Table 14 for different C-S-H compositions. The error on the ΔG derived in this way was estimated to be ~20 kJ mol^{-1}, resulting in particular from uncertainties in the thermodynamic data (i.e. measured entropies and hydration enthalpies) used in the estimation of the Gibb's free energies (about 12 kJ mol^{-1} from uncertainties of Ca^{2+} and Ra^{2+} hydration enthalpies alone; Smith, 1977). Despite these uncertainties and the use of a simplified C-S-H model based on the tobermorite structure of Hamid (1981) for the derivation of the computed supercells, the computed data clearly show that the reaction enthalpy and the free energy increase significantly with increase of Ca/Si ratio. This is consistent with the observed decrease of the radium uptake with increasing Ca/Si ratio. The distinctively negative free energy of the exchange reaction for C-S-H0.75 suggests that the radium uptake in the interlayer is a plausible radium uptake mechanism, in particular for low Ca/Si-ratios.

Table 14 *Thermodynamic parameters for the exchange reaction of radium for calcium in the C-S-H interlayer at 300K for different C-S-H phases, estimated from DFT calculations.*

Ca/Si-ratio	ΔH_r [kJ mol^{-1}]	ΔS_r [J K^{-1}]	ΔG_r [kJ mol^{-1}]
0.75	-100.6	83.3	-75.6
0.9	-18.5	83.3	6.5
1.0	-10.8	83.3	14.2

5.2.4. Radium uptake by hardened cement paste

The uptake kinetics of radium by crushed HCP is shown in Figure 34. The radium uptake by the CEM I paste reached a steady state R_d value of ~60 L kg^{-1} after about 10 days. Leaching of the alkalis, due to the low S/L-ratio in the experiment, was indicated by the solution pH = 12.6, which was found to be constant throughout the sorption experiment. Therefore the experiment refers to a slightly degraded cementitious material in stage II, probably controlled by portlandite dissolution (Jacques et al., 2008; Ochs et al., 2016). Similar uptake kinetics while slightly higher R_d-values were observed by Tits et al. (2006a) for similarly degraded HCP made from sulfate-resisting Portland cement (CEM I 52.2 N HTS).

In the radium uptake experiments using the VTT low pH cement paste, equilibrium conditions were not attained within the experimental time frame of 100 days. The R_d value obtained at the end of the batch uptake experiment was 12,300 L kg^{-1}. During the experiment the solution pH dropped from initially 12.5 to 11.8. This suggests that hydration of remaining unreacted clinker phases, silica fume and blast furnace slag is ongoing, leading to formation of C-S-H with low Ca/Si-ratios. This is in agreement with the results of the hydration model of Idiart (2017). The significantly higher R_d value for the VTT cement paste can be attributed to the lower pH and lower Ca/Si ratio of the C-S-H as the main hydration phase contributing to radium retention, compared to CEM I based systems.

The results obtained of the radium uptake by the two composite HCP materials are in general agreement to the few published observations on the radium uptake by cementitious materials. Bayliss et al. (1989) found also a distinctively stronger uptake of radium by hydrated cement mixtures comprising BFS (R_d 900–1800 L kg^{-1}) compared to sulfate-resisting OPC (R_d 55–530 L kg^{-1}). However, they attributed the higher R_d-values in the BFS containing systems to the precipitation of $RaSO_4$. Similar to the findings of the study at hand,

Holland and Lee (1992) reported a R_d of ~50 L kg^{-1} for the sorption of radium by OPC based materials. Moreover, they observed that formulations leading to cementitious materials with C-S-H exhibiting lower Ca/Si ratios showed an enhanced radium uptake compared to OPC.

In general, the results obtained for the uptake of radium by HCP systems are in qualitative agreement with the uptake observed for the C-S-H phases. These results indicate that low pH cement formulations, obtained by i.e. high silica content, exhibiting C-S-H low in Ca/Si ratio possess a higher retention potential for radium.

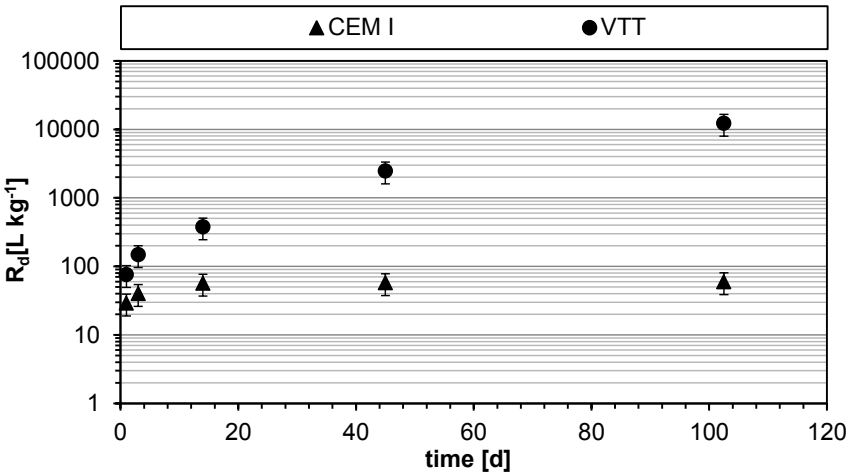

Figure 34 *Uptake kinetic of ^{226}Ra by CEM I and crushed VTT reference paste.*

5.2.5. Effects of carbonation

Carbonation by atmospheric CO_2 or carbonate-bearing groundwater is a common alteration process of cementitious materials (Taylor, 1997; Trägårdh and Lagerblad, 1998). Carbonation results in changes in the phase assemblage due to formation of calcite, first in expense of portlandite and second by decalcification of C-S-H. The subsequent formation of calcite is accompanied by decreasing alkalinity and pH of the pore solution. The uptake and therefore the retention potential for radium by calcite was found to be significant lower compared to C-S-H. So far the effects of carbonation and other alteration processes on the radionuclide migration behavior in cementitious materials have rarely been addressed.

Here, the fate of radium after carbonation of C-S-H1.4 under conditions expected in young cementitious materials was addressed, using CO_2 overpressure (Figure 35). In this

batch experiment, the initial distribution ratio of radium (R_d ~1,900 L kg^{-1}) was slightly higher compared to experiments using C-S-H with similar compositions in young cementitious pore water at pH 13.3. This might be due to a slightly lower Ca/Si-ratio, as consequence of the formation of minor amounts of calcite during sample preparation in this case (cf. Figure 36). A fast drop of solution pH from initially 13.3 to <10 occurred during the first hours of the experiment attributed to the precipitation of calcite and the increasing concentration of carbonate ions in solution. A final pH of about 8 was observed after one day and remained practically constant. Although a small amount of calcite occurred already in the initial sample, an increasing amount of calcite was observed in the solid phase by XRD.

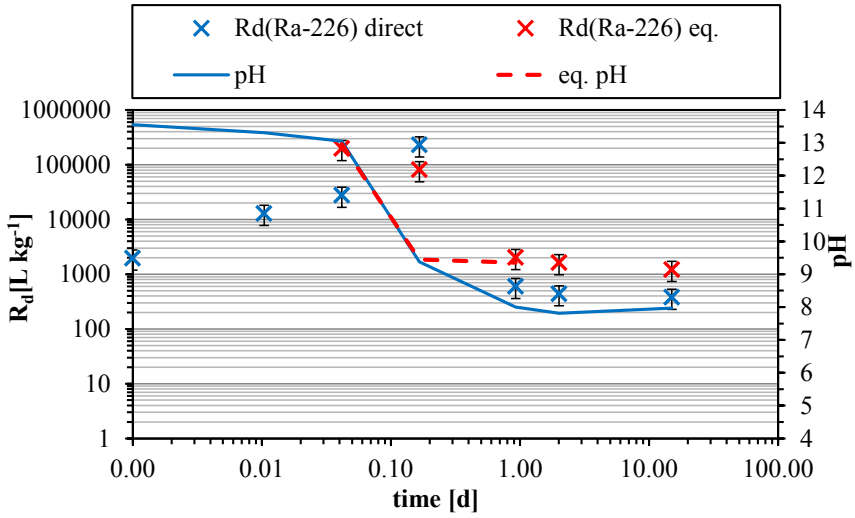

Figure 35 *Evolution of the distribution ratio R_d of radium and solution pH during continuous carbonation of C-S-H1.4 under CO_2 overpressure.*

The distribution ratio R_d of radium increased strongly during the first hours of the carbonation experiment with a maximum R_d (> 100,000 L kg^{-1}) observed after 4 hours of carbonation time at a solution pH of 9.4. This is attributed to the combined effects of the decreasing solution pH and the decrease in Ca/Si-ratio of the C-S-H phase, as well as radium entrapment in the precipitating calcite. After 1 day, the R_d approached values corresponding to those measured in batch experiments with calcite (~380 L kg^{-1}). This demonstrates that radium sorbed by C-S-H will be released during carbonation. However, some radium can be retained in the newly formed calcite. So far, the mechanism of the radium release from C-S-H

during carbonation has not been investigated. In general, carbonation of C-S-H is associated with the destruction of the tobermorite-like C-S-H structure resulting in the formation of calcite and amorphous SiO_2. Thus, the release of radium from the sorption sites followed by occlusion in the freshly formed calcite might be plausible uptake mechanism. An incorporation of radium into the calcite structure instead of calcium during precipitation is less likely, due to the large size of the radium ion.

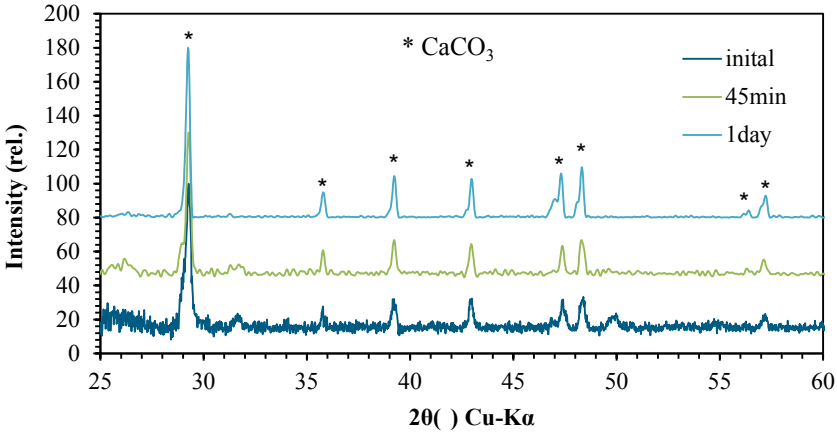

Figure 36 *Selected XRD patterns obtained during the carbonation of C-S-H.*

In contrast to a system using model phases, hardened cement pastes are much more complex in terms of phase assemblage and elemental composition. Thus for comparison, the fate of radium during carbonation of a cement monolith (CEM I) was investigated. It has to be noted that in this experiment the R_d was calculated using the total mass of the cement monolith, since the mass/volume of material responsible for the uptake of radium, which depends on the depth of diffusion into the monolith, could not be obtained in this experimental setup. Thus the concentration of radium in the supernatant solution is stated in addition to the calculated apparent R_d value.

The initial apparent distribution ratio of radium between solution and monolith was R_d ~35 L kg^{-1} ($c(^{226}Ra) = 1.2 \cdot 10^{-7}$ mol L^{-1}) at an equilibrium pH of 12.96. A fast drop of solution pH from initially 12.96 to 7.2 occurred during the first hours of carbonation, similar to the experiment using C-S-H, attributed to the precipitation of calcite and the increasing concentration of carbonate ions in solution. The solution concentration of radium finally decreased to $c(^{226}Ra) = 6.9 \cdot 10^{-9}$ mol L^{-1}, resulting in an apparent R_d ~820 L kg^{-1} at an

equilibrium pH of 7.2 after four weeks. Subsequently the cement monolith was cut perpendicular to the length axis in the middle to obtain the radial distribution of radium. The cross sections of the radium loaded monolith before and after carbonation and the corresponding autoradiography are shown in Figure 37.

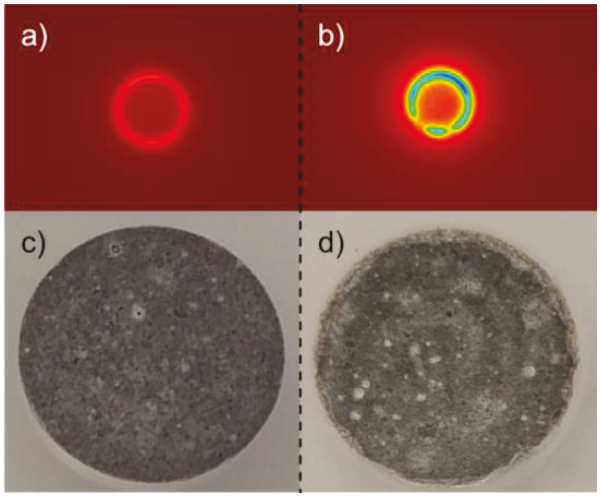

Figure 37 *Autoradiography image and photography of cut and polished cross sections for CEM I monoliths before (a and c) and after (b and d) carbonation.*

Due to the low diffusion rate of radium into the cement monolith, the activity measured was found to be located in a small zone close to the surface of the monolith that was in contact with the radium containing solution. Investigations by autoradiography showed that the diameter of the cylinder decreased from 12.1 mm to 12.0 mm, whereas the intensity of the autoradiography signal increased from 54 cpm to 983 cpm after carbonation (Figure 37). From the autoradiography it was noticed that the width of the rim containing the radium decreased slightly after carbonation, indicating an in-diffusion of radium.

The results of SEM/EDS investigations of the micro structure of the carbonated zone are shown in Figure 38. From the elemental distribution, three concentric zones can be identified from the outside to the inside of the monolith. The first zone comprises a a layer (400-500µm) consisting of calcite ("carbonate layer") containing larger pores, and remaining clinker phases rich in aluminum and iron, most likely calcium aluminates and calcium aluminum ferrites. The increased amount of pores observed in the outer zone may be attributed to the dissolution of clinker material during carbonation, leaving void zones and large pores (cf. Trägårdh and Lagerblad, 1998).

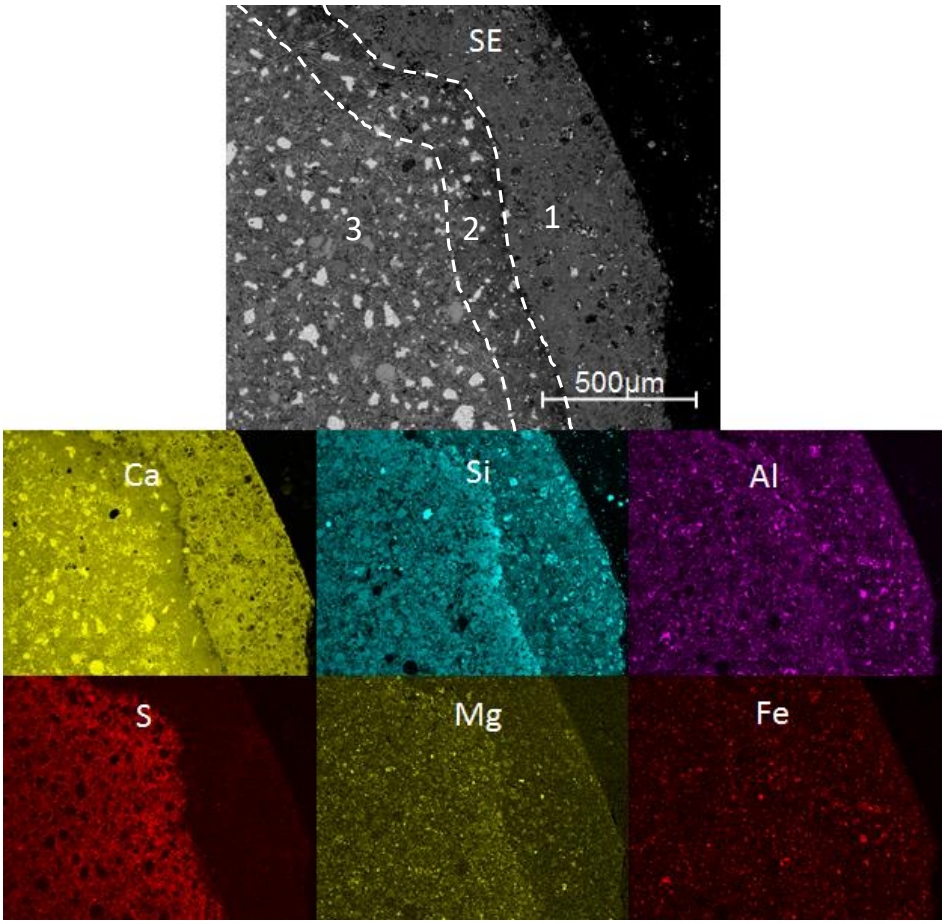

Figure 38 *SEM/EDS mapping of the polished cross sections for CEM I monoliths after carbonation. 1) carbonate layer, 2) alteration layer, 3) unaltered CEM I paste.*

Adjacent to the calcite layer a small alteration layer (thickness approx. 100 µm) is observed (Figure 39). Here, the concentration of calcium is slightly increasing with increasing depth, whereas the concentration of silicon peaked directly at the interface between layer 1 and 2. The concentration of sulfur was found to be slightly higher in the alteration layer 2. This effect was also observed by Trägårdh and Lagerblad (1998) and can be explained by a redistribution of sulfate and aluminium in calcium depleted areas, resulting in the formation of ettringite, monosulfate and, due to the higher CO_3^{2-} concentrations, probably also thaumasite (Trägårdh and Lagerblad, 1998). The calcium to silicon ratio was observed to be lowest in layer 2 in close proximity to the calcite layer. Hence, it can be assumed that the Ca/Si ratio of the C-S-H phases in this region is low.

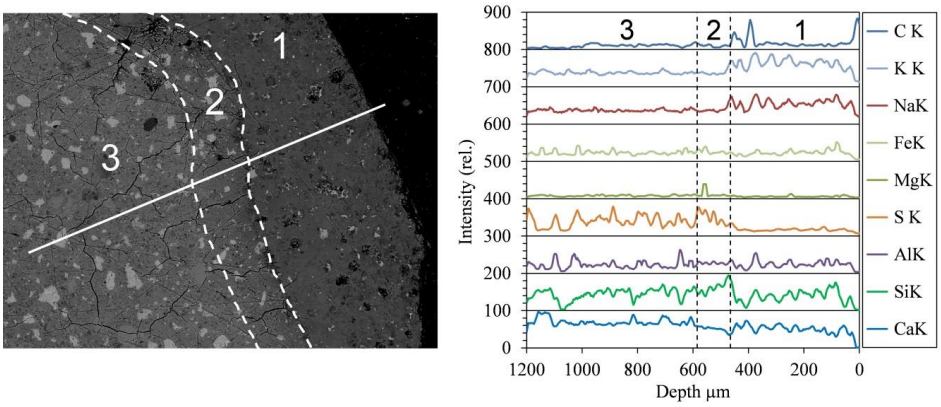

Figure 39 *Line scan of the polished cross sections for CEM I monoliths after carbonation. 1) calcite layer, 2) alteration layer, 3) unaltered CEM I paste. Dark area in upper right is epoxy resin.*

Furthermore, a slightly depletion of magnesium in the calcite layer was observed. The third region in the cylinder (layer 3) is assumed to consist of unaltered cement, which is continuing to the centre of the cross section. No traces of radium could be detected in EDS measurements and mappings, due to the detection limits of the EDS system. Therefore, the distribution of radium in the cross section could not be quantified, even though autoradiography indicated a small rim with elevated radium activity at and close to the surface. However, the EDS line scan indicated that the C-S-H close to the calcite layer has the lowest calcium to silicon ratio. It is thus to be expected that radium is sorbed stronger in this region, although none of the applied methods gave clear evidence. Moreover, it was observed that sulfate is moving inwards, resulting in a higher sulfate concentration at the interface between layer 2 and 3. Considering the solubility limitation of radium by $RaSO_4$, a correlation between the inwards moving sulfate and the solubility of radium may also be possible.

5.3. Technetium uptake in cementitious systems

5.3.1. Uptake kinetics and equilibrium distribution ratios

The kinetics of the Tc(VII) uptake by the model hydration phases were determined at a S/L-ratio of 0.005 kg L^{-1} in the various solutions for up to 100 days. The results of these experiments are depicted in Figure 40. In this set of experiments, the equilibrium concentrations were rather similar to the initial concentration of TcO_4^- within the experimental errors for all experiments. Therefore, calculated R_d-values occasionally reached negative values and could not be plotted. In Figure 41, the equilibrium R_d values determined at a S/L ratio of 0.04 kg L^{-1} are shown; the data are detailed in Table 15. As expected, the uptake of pertechnetate by the model phases was found to be generally rather low (Figure 41). The highest distribution ratio (R_d 4.5 L kg^{-1}) was obtained for C-S-H0.9, whereas 2.3 L kg^{-1} for C-S-H1.4. As previously mentioned, the surface charge of C-S-H depends on the calcium to silicon ratio, exhibiting negative surface charge at low Ca/Si ratio whereas at Ca/Si ratio (i.e. at Ca/Si > 1.2) the surface charge changes to positive. Hence, the negative charged pertechnetate was expected to exhibit a higher affinity to C-S-H1.4 which was not observed in the uptake experiments.

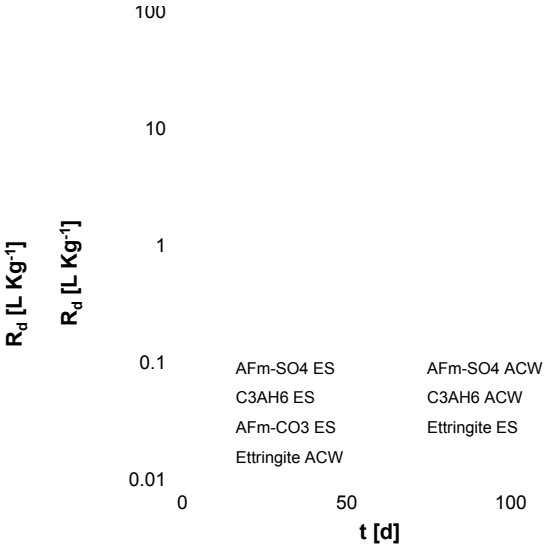

Figure 40 *Uptake kinetics of TcO_4^- by various model phases in different solutions (ES: equilibrium solution; ACW: artificial young cement water (pH 13.3); error bars are omitted for the sake of clarity.*

This result cannot be explained in terms of electrostatic sorption. Considering the low distribution ratios the higher affinity to C-S-H1.4 may be attributed to the difference in surface area of the synthetic C-S-H (C-S-H0.9 = 125 m^2 g^{-1}, C-S-H1.4 = 109 m^2 g^{-1}; see section 5.1.1). Furthermore, a slight uptake of pertechnetate by AFm-SO_4 (ES) (R_d = 4.0 L kg^{-1}) and AFm-CO_3 (ES) (R_d = 2.3 L kg^{-1}) was noticed, which indicates an effect of the pH in the supernatant solution. Uptake of pertechnetate by AFm-SO_4 and AFm-CO_3 could be due to surface sorption, edge sorption to the octahedral layers or exchange for the interlayer anion. Since the latter might lead to a change in basal spacing, a XRD study on the material was conducted. However, no changes in the interlayer spacing of the AFm phases or new reflexes attributable to the exchange of interlayer anions were observed. These findings are most probably due to the low uptake of pertechnetate by AFm, leading to no discernable change in the basal spacing. In principle, for the exchange of interlayer anions, divalent anions (e.g. CO_3^{2-} or SO_4^{2-}) are preferred to monovalent anions (TcO_4^-). However, the lower uptake by AFm-CO_3 compared to AFm-SO_4 might indicate that an exchange of TcO_4^- for the planar CO_3^{2-} is less favored compared to an exchange with the tetrahedral SO_4-anion. The uptake of TcO_4 by ettringite was found to be week, i.e. the R_d was generally < 1 L kg^{-1}, suggesting practically no uptake due to exchange for SO_4 groups in existing ettringite as proposed by Berner (1999). In contrast, Saslow et al. (2018) observed a slight incorporation of pertechnetate in ettringite precipitating in the presence of dissolved TcO_4^- ions.

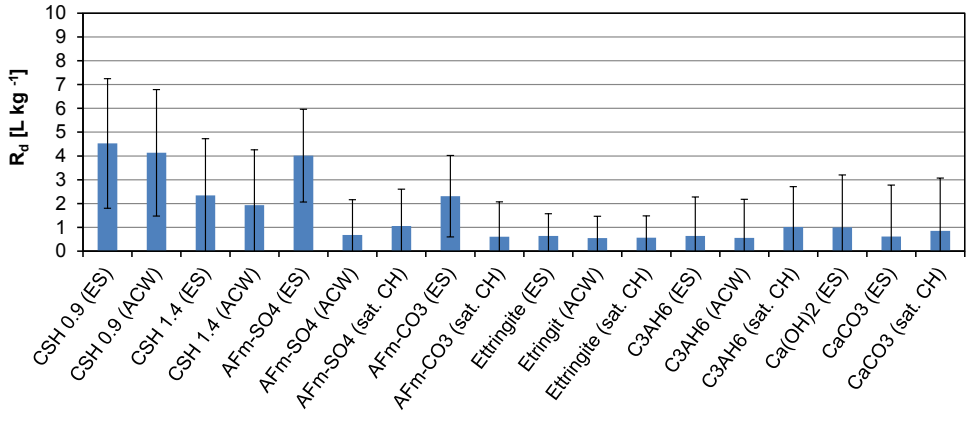

Figure 41 *Distribution ratios R_d for TcO_4^- uptake by various hydration phases in different solutions (ES: equilibrium solution; ACW: artificial young cement water (pH 13.3); CH: portlandite saturated solution (pH 12.3); C_3AH_6: hydrogarnet).*

Table 15 *Distribution coefficients R_d for the TcO_4^- uptake by cement hydration phases in different solutions (ES: equilibrium solution; ACW: artificial young cement water (pH 13.3); CH: saturated portlandite solution (pH 12.3)).*

Phase	R_d [L kg^{-1}]		
	ES	ACW	CH
C-S-H0.9	4.5 ±2.7	4.1 ±2.7	
C-S-H1.4	2.3 ±2.4	1.9 ±2.3	
AFm-SO_4	4.0 ±1.9	0.7 ±1.5	1.1 ±1.5
AFm-CO_3	2.3 ±1.7		0.6 ±1.5
Ettringite	0.6 ±0.9	0.6 ±0.9	0.6 ±0.9
C_3AH_6	0.6 ±1.6	0.6 ±1.6	1.0 ±1.7
Portlandite			1.0 ±2.2
Calcite	0.6 ±2.2		0.8 ±2.2

In general, these experiments investigating systematically the pertechnetate uptake by all major hydration phases in cementitious systems for the first time, elucidated the high mobility and low retention of TcO_4^- in cementitious environments in the absence of reductants able to produce the significantly less soluble Tc(IV) (cf. Ochs et al., 2016).

In order to investigate a potential dependency of the Tc(VII) uptake by the model phases on the concentration level of Tc in solution, sorption isotherms were measured for the pertechnetate uptake by the two different C-S-H phases and for AFm-SO_4 (Figure 42). Again, these investigations revealed a stronger uptake by C-S-H0.9, even though the positive surface charge of C-S-H1.4 should increase the electrostatically attraction of the pertechnetate anion. The linear trends observed in the log-log plots indicate a Freundlich-type sorption isotherm for all cases without any indications for sorption site saturation or (surface) precipitation, which would generally be improbable due to the high solubility of pertechnetate under the experimental conditions.

The deviations and uncertainties obtained for the slope and the value of the coefficient of determination reveal a low influence of the background and statistical errors of the LSC measurements on the distribution ratios.

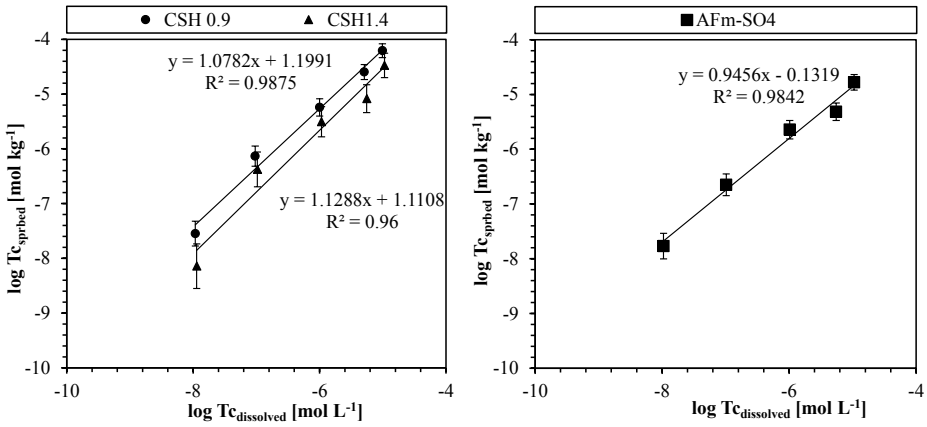

Figure 42 *Sorption isotherms of pertechnetate uptake by C-S-H0.9 and C-S-H1.4 (left) and AFm-SO_4 (right).*

5.3.2. Tc(VII) uptake by hardened cement paste

The uptake and sorption of pertechnetate by pure C-S-H and AFm phases was shown to play only a minor role in retention of pertechnetate in cementitious systems. Therefore batch-uptake experiments on crushed hardened cement paste were performed to study the potential accumulation of reduced Tc on reductive sites like Fe(II)-bearing inclusions or phases. These reductive sites in cementitious systems mainly originate from iron-containing educts used in the cement formulation, such as blast furnace slags.

The uptake experiments were conducted for 100 days for the CEM I paste and for 75 days for the VTT reference paste (Figure 43). The obtained distribution ratios are in equilibrium within the first day and show a low uptake of Tc by the crushed HCP. As expected from batch uptake experiments, distribution ratios of HCP based on CEM I are lower in general compared to the low-pH paste based on the VTT cement. This can be explained by the lower Ca/Si ratio of the C-S-H in the VTT cement paste and the higher content of Fe(II) and/or sulfides in this material due to the BFS used in the cement formulation. These findings are in good agreement with the stated high mobility and low retention of TcO_4^- in cementitious environments in the absence of reductants, according to Ochs et al. (2016).

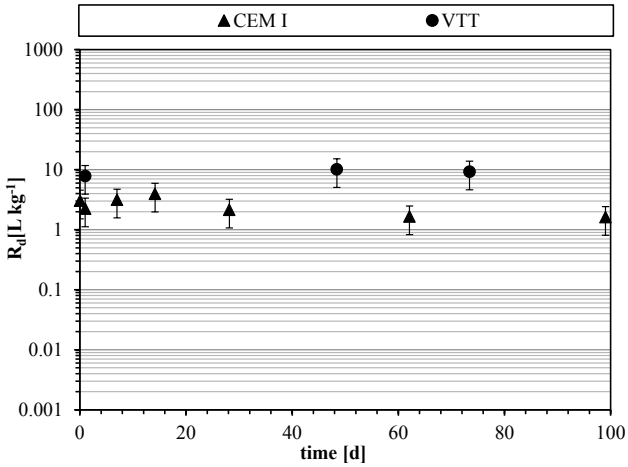

Figure 43 *Uptake kinetics of pertechnetate (TcO_4^-) on crushed CEM I paste and VTT reference cement paste.*

In addition to the batch-type experiments, the in-diffusion of Tc(VII) into cylindrical HCP monoliths was investigated. Subsequently, the monoliths were cut perpendicular to the length axis and the Tc-distribution on the obtained cross sections was investigated by autoradiography, to identify technetium hot spots and to record diffusion profiles. Figure 44 shows the intensity profiles for x and y-directions of the cross section of the CEM I monolith. The overall activity of technetium in this cement monolith was low and no Tc hot spots were observed (Figure 44a). From the intensity profiles a slight depth dependency can be observed. However, the obtained data quality was poor due to the small quantities of ^{99}Tc measured. Therefore, no diffusion profiles could be fitted to the data.

In-diffusion experiments performed with VTT cement monoliths revealed no measurable change in the aqueous Tc concentration over the course of 2 months, indicating practically no in-diffusion of pertechnetate. This may be attributed to the high contents of silica fume and quartzfiller used in the VTT cement formulation, resulting in a very low porosity and diffusivity. Generally, cement formulations containing larger amounts of BFS, like the VTT paste, can exhibit a higher retention potential for technetium(VII) due to formation of Tc(IV), according to the findings of Allen et al. (Allen et al., 1997a; Allen et al., 1997b). In the absence of reductants leading to the formation of Tc(IV) species, which sorb strongly on C-S-H (Ochs et al., 2016) or form sparingly soluble oxides or sulfides, the transport/migration of Tc as pertechnetate in cementitious systems is controlled by factors influencing the

effective diffusion coefficient, namely porosity, tortuosity and the state of hydration which are decreasing the overall diffusion properties.

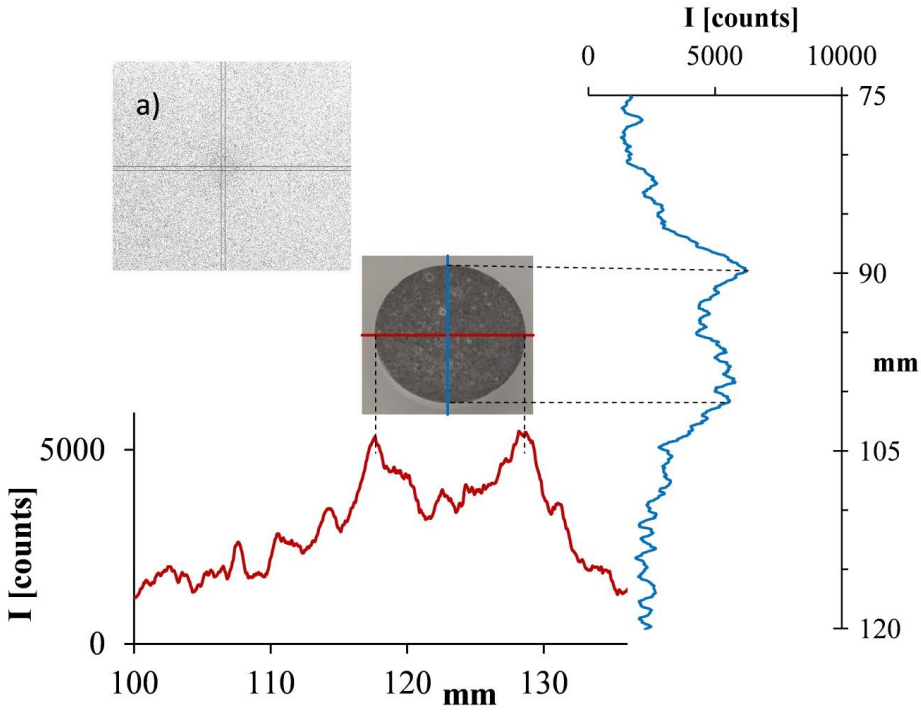

Figure 44 *Activity profiles for x and y direction (smoothed) of an autoradiography measurement of [^{99}Tc] pertechnetate in-diffusion in a hardened CEM I monolith; a) scanned autoradiograph plate and applied line scans.*

5.4. Molybdenum uptake in cementitious systems

5.4.1. Uptake kinetics

The results on the investigation of molybdate uptake kinetics by the various model phases performed at a S/L ratio of 0.005 kg L^{-1} are shown in Figure 45. Equilibrium was reached after 30 days at the latest. The most pronounced uptake was observed for C_3AH_6. It should be noted that in the 28 and 60 days sample of AFm-SO_4 measurable amounts (XRD) of mono carbonate and hemi carbonate were found. Furthermore, the measured equilibrium concentrations of molybdenum in these experiments were slightly above the initial concentration, due to the experimental error. Therefore, the calculated distribution ratios were negative and results are not included in this logarithmic plot. A similar issue was found in some batch uptake experiments for C-S-H0.9 and C-S-H1.4, where concentrations of molybdenum in the supernatant solution were very close to the initial value.

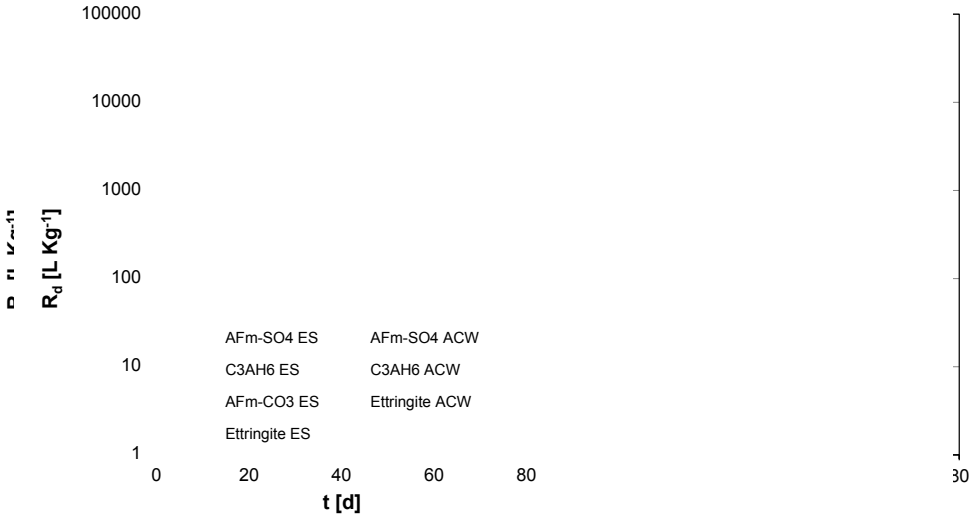

Figure 45 *Kinetics of molybdate (MoO_4^{2-}) uptake by various model phases in different solutions (ES: equilibrium solution; ACW: artificial young cement water (pH 13.3); C_3AH_6: hydrogarnet).*

5.4.2. Equilibrium distribution ratios

The R_d values for the molybdate uptake in the different systems determined at S/L-ratios of 0.04 L kg^{-1} are depicted in Figure 46 and detailed in Table 16. For C-S-H in equilibrium solutions distribution ratios of R_d = 750 L kg^{-1} for C-S-H1.4 and R_d = 420 L kg^{-1} C-S-H0.9 were observed. These findings are in agreement with the change in surface charge of C-S-H to positive values at Ca/Si ratios exceeding 1.2, suggesting an electrostatic sorption of the molybdate anion on C-S-H. In alkali-rich young cementitious water, distinctively lower R_d values were observed, which might be due to competition with OH^- ions for sorption sites, suggesting lower molybdate sorption and retention by C-S-H in young alkali-rich cementitious systems. These results show that C-S-H phases in cementitious materials play an important role with respect to the retention of molybdenum, in particular in aged systems (stage II and III).

As expected, a pronounced molybdate uptake (R_d ~1500 L kg^{-1}) by AFm-SO_4 and AFm-CO_3 was observed, indicating no preference of the uptake on the nature of the interlayer anion (i.e planar CO_3 or tetrahedral SO_4) in this case. However, the measured decrease of c(MoO_4^{2-}) in the supernatant solution was found to be significantly smaller in saturated portlandite solution and artificial cement pore water, respectively, suggesting a stronger retention under stage III conditions (portlandite stage pH 12.5).

Molybdate can substitute for sulfate in the AFm structure (Kindness et al., 1994). XRD studies on the AFm-SO_4 used in the batch sorption experiments showed an increase in the basal spacing compared to pure AFm-SO_4 indicating the structural incorporation of MoO_4^{2-} ions in the AFm-structure by anion exchange with the interlayer anion, since the size of the molybdate oxo-anions (Mo-O bond length ~1.77 Å) is larger than of SO_4^{2-}-ions (S-O bond length ~1.47 Å). However, the increase in the basal spacing could also be attributed to an increasing number of water molecules in the interlayer in the Mo substituted AFm.

Recent investigations by Ma et al. (2017) on the sorption of molybdate on AFm-SO_4 and AFm-Cl_2 by XRD and TEM/SAED had shown that an aqueous concentration of c(MoO_4^{2-}) ~ 1 mmol L^{-1} resulted in precipitation of Mo-bearing katoite. It was stated that the short bond length of Mo-O (~1.78 Å) is a possible reason of AFm-Cl_2 edge stabilization followed by Mo-bearing katoite precipitation, a comparison to AFm-SO_4

was not drawn here. Marty et al. (2018) demonstrated that molybdate exchanges for two chloride anions in AFm-Cl and that the competition between molybdate and OH^- results in a lower sorption capacity towards molybdate with increasing pH.

Ettringite, known for its capability to incorporate various monovalent and bivalent oxo-anions by solid-solution formation, showed a less pronounced affinity to incorporate molybdate compared to the AFm phases (R_d ~120 L kg^{-1} in equilibrium solution). Similar R_d values in young cement waters indicate a stronger retention of molybdate by ettringite in stage I compared to the later degradation stages. The retention of MoO_4^{2-} by portlandite (R_d 789 L kg^{-1}) might be attributed to the formation of surface precipitates of $CaMoO_4$, although the bulk solution was undersaturated with respect to powellite in the experiment.

The highest R_d values were observed for C_3AH_6 (up to 3000 L kg^{-1}); the uptake was found to be higher in more alkaline young cementitious waters compared to the portlandite saturated solution representing aged cementitious systems (cf. Table 16).

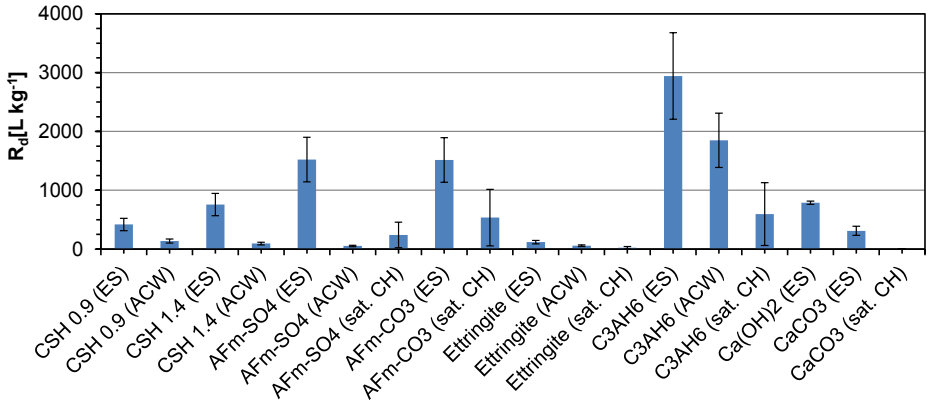

Figure 46 *Distribution coefficients R_d for the MoO_4^{2-} uptake by cement hydration phases in different solutions (ES: equilibrium solution; ACW: artificial young cement water (pH 13.3); CH: saturated portlandite solution (pH 12.3)).*

Table 16 *Distribution coefficients R_d for the MoO_4^{2-} uptake by cement hydration phases in different solutions (ES: equilibrium solution; ACW: artificial young cement water (pH 13.3); CH: saturated portlandite solution (pH 12.3)).*

Phase	R_d [L kg^{-1}]		
	ES	ACW	CH
C-S-H0.9	432 ±26	143 ±9	
C-S-H1.4	781 ±41	98 ±5	
AFm-SO_4	1571 ±115	55 ±1.5	240 ±220
AFm-CO_3	1564 ±90		535 ±481
Ettringite	122 ±4	122 ±3.6	23 ±21
C_3AH_6	3037 ±436	1909 ±142	594 ±436
Portlandite	789 ±28		
Calcite	321 ±18		

5.4.3. Uptake of molybdate in hydrogarnet-containing systems

Since the strongest uptake of molybdate was found in the systems with hydrogarnet (C_3AH_6), the solids used in these batch experiments were subsequently studied by XRD and SEM, to get insights into the uptake mechanism. However, no changes in the XRD patterns of the solids as consequence of the Mo-uptake were observed. In some XRD patterns the 003 reflexes of AFm-CO_3 and AFm-$OHCO_3$ were observed, which were found to be due to the drying and measuring procedure. No molybdenum was detected by EDS on the surface of the hydrogarnet, probably due to the limit of detection of the EDS. However, in some of the sorption experiments performed in ACW, small (6µm) newly formed (pseudo)hexagonal, sheet like crystals were observed (Figure 47).

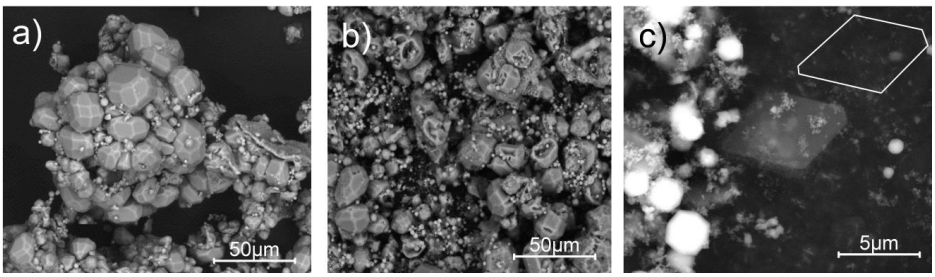

Figure 47 *SEM investigation of hydrogarnet before (a) and after uptake of molybdate (b and c) showing the formation of (pseudo?) hexagonal secondary phases (c).*

These very rare crystals contain measurable concentrations of Mo, Ca and Al, suggesting the potential formation of an AFm-MoO_4 phase. Moreover, it was found that the C_3AH_6 crystals exhibit evidence of dissolution and changes in the microstructure that took place after the addition of molybdate in the batch sorption experiments (Figure 47b). These results indicate that the observed uptake of molybdate in systems with hydrogarnet is due to the partial dissolution of hydrogarnet and the precipitation of small amounts of newly formed, AFm-like molybdate phase.

However, the amounts of the newly-formed Mo-bearing phase formed in the batch sorption experiments conducted at 10^{-7} mol L^{-1} MoO_4^{2-} were too low for further investigations. Therefore, the Mo concentration was increased in additional experiments until the precipitated phase contributed to the diffraction pattern of XRD (Figure 48). The interlayer spacing of the new phase was found to be 8.59 Å (d_{003}) and 4.29 Å (d_{006}), which is in good agreement with literature values for AFm-MoO_4 (Kindness et al., 1994; Marty et al., 2018), whereas no powellite formation was observed. Kindness et al. (1994) reported a spacing of 8.70 Å (d_{003}) and 4.3 Å (d_{006}) for AFm-MoO_4 comprising $14H_2O$ molecules in the interlayer. In contrast, Ma et al. (2017) observed interlayer distances of 10.3 Å and 10.4 Å for AFm-Cl_2 and AFm-SO_4 partially substituted by molybdate. The interlayer distances of AFm phases are strongly dependent on the state of hydration, thus the different interlayer spacing determined by Ma et al. (2017) can probably be attributed to a higher amount of water in the interlayer of the AFm-phases. Additional reflexes observed at 11.7°2Θ corresponding to d_{003} of AFm-CO_3 were probably due to carbonation during sample preparation, drying and measurement. This was confirmed by additional XRD measurements of the same substance performed without drying, conducting a fast measurement in the 2theta range up to 70°2Θ only. Due to the very small amounts of this newly formed, potentially AFm-like phase, which could not be separated, a further attempt was made for phase characterization, using a high concentration of MoO_4^{2-} (10^{-3} mol L^{-1}) in the sorption experiments with C_3AH_6 and prolonged reaction times. After 2 months of reaction, the aqueous MoO_4^{2-} concentration decreased to <0.1% of the initial concentration. Here, EDS spot measurements performed after termination of the experiments exhibited measurable amounts of molybdate present in the (pseudo)-hexagonal AFm-like crystals, whereas no MoO_4^{2-} could be found at the surface of the hydrogarnet (Figure 49). Thus, from these observations it can be concluded that the uptake of molybdate by hydrogarnet is most likely to take place due to formation of molybdenum bearing AFm-like phase.

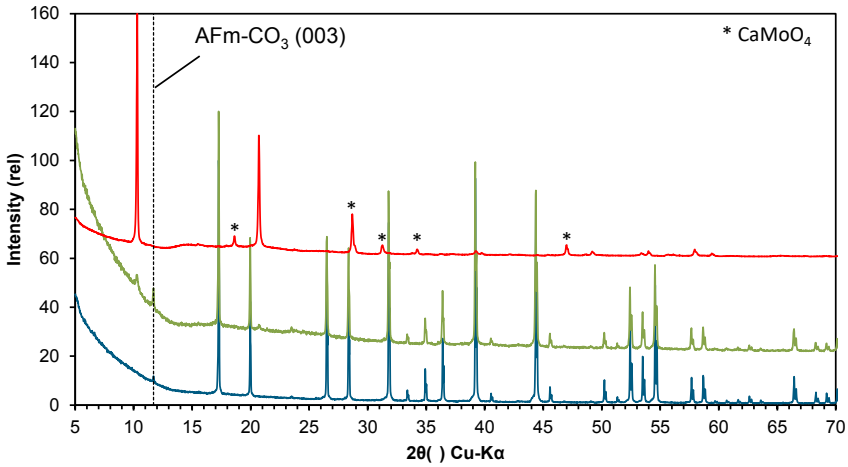

Figure 48 *Comparison of XRD pattern for sorption of MoO_4^{2-} by C_3AH_6 at 10^{-6} mol L^{-1} (blue), at 10^{-3} mol L^{-1} (green) and the pattern of AFm-MoO_4 (red).*

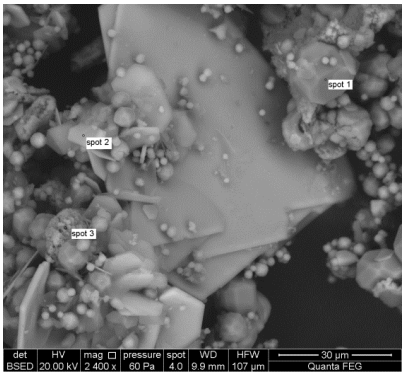

Figure 49 SEM of C_3AH_6 after batch sorption experiment of c(MoO_4^{2-}) = 10^{-3} mol L^{-1}. Marked are EDS spot measurements.

To gain additional insights into the nature of AFm-like Mo bearing phases forming under highly alkaline cementitious conditions, specific synthesis routes were used to obtain molybdate-bearing AFm-type phases either in sodium or potassium rich solutions, (cf chapter 4.1). The product obtained in the sodium-bearing system at pH 12.9 had a sheet like appearance similar to AFm (Figure 50). SEM/EDS measurements revealed a stoichiometric composition of Ca:Al:Mo of 4:2:1. Investigations by XRD indicated two different states of hydration of the interlayer anions of the AFm-type phase by peak splitting

for the d_{003} and d_{006} reflexes. The XRD pattern of the phase at highest hydration state (Figure 50) showed, beside the well-known reflex pattern for AFm-type structures, reflexes that cannot be attributed to molybdenum containing AFm phase. The reflexes of AFm-MoO_4 at 8.58 °2Θ and 17.26 °2Θ corresponding to distances of 10.3 A (d_{003}) and 5.13 A (d_{006}) for were also observed by Kindness et al. (1994) for molybdate bearing AFm with 10 water molecules in the interlayer.

The additional reflexes that cannot be attributed to AFm-MoO_4 fit to reflexes of the U-Phase ($4CaO{\cdot}0.9Al_2O_3{\cdot}1.1SO_3{\cdot}0.5Na_2O{\cdot}16H_2O$) first reported by Dosch and Zur Strassen (1967) and investigated by Li et al. (1997); Li et al. (1996). It was stated by these authors that the U-Phase exhibits a hexagonal or pseudo-hexagonal structure and can form in highly alkaline systems. The X-ray diffraction pattern of the U-Phase shows strong similarities compared to the additional phase obtained in the AFm-MoO_4 synthesis in the Na-rich system, although it contains sulfate as anion instead of molybdate. The U-Phase is a sodium substituted AFm phase that could exist in a wide range of alkali concentrations and exhibits reflexes at or close to those of AFm-MoO_4, thus peak overlapping could be the reason for the lack of reflexes referring to the structure of the observed impurity.

Considering the few reflexes at higher °2Θ to be not sufficient to distinguish between AFm-MoO_4 and the impurity, a more advanced technique was used to identify the obtained products. Thus a TEM study was performed to obtain more information on the structure of the synthesized layered material and to get an idea of its crystal structure. Electron diffraction patterns were obtained along the 001 zone axis, due to the preferred orientation of the platelets.

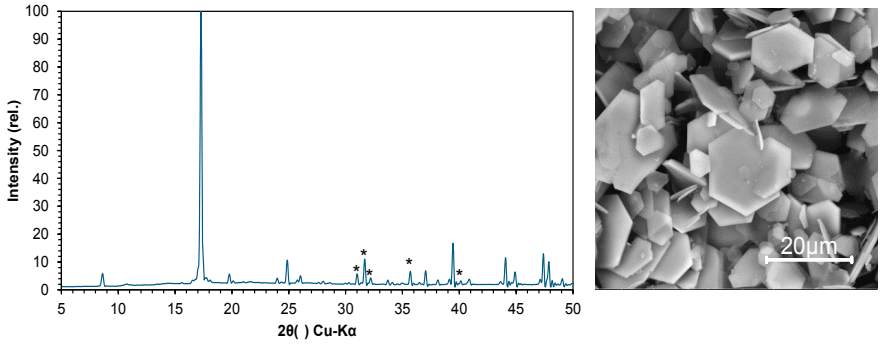

Figure 50 *XRD pattern (left) and SEM image (right) of impure AFm-MoO_4 synthesised in the Na-rich system under alkaline conditions. Reflexes marked with * potentially originate from the U-Phase.*

Despite the similarities in the SEM images of all platelets and their morphology, different electron diffraction patterns were obtained (Figure 51). A majority of the platelets exhibit a hexagonal or trigonal symmetry with a lattice constant a = 5.71 ± 0.06 Å (Figure 51, left), whereas the minority show a triclinic or monoclinic symmetry (Figure 51, center). Some platelets were found to overlap with a slight rotation; here the SAED patterns showed additional weak spots between the primary reflexes, indicating the presence of disorder in the crystal structure (Figure 51, right). Moreover, small amounts of powellite, one of the educts used in synthesis, were found.

The TEM study confirmed that the synthesized material was not single-phased AFm-MoO_4 and the observed unidentified XRD reflexes belong to a phase, probably with a structure similar to the U-Phase, with triclinic or monoclinic symmetry that exhibits a slightly smaller lattice constant a. However, due to the few triclinic platelets found, no discrete values for lattice constants for this phase could be obtained.

However, the results of the TEM study suggest a lower symmetry (i.e. triclinic or monoclinic) of the Mo-analogue of the U-Phase, compared to the higher symmetric hexagonal (or pseudohexagonal) structure of the sulfate-bearing U-Phase proposed by Li et al. (1997).

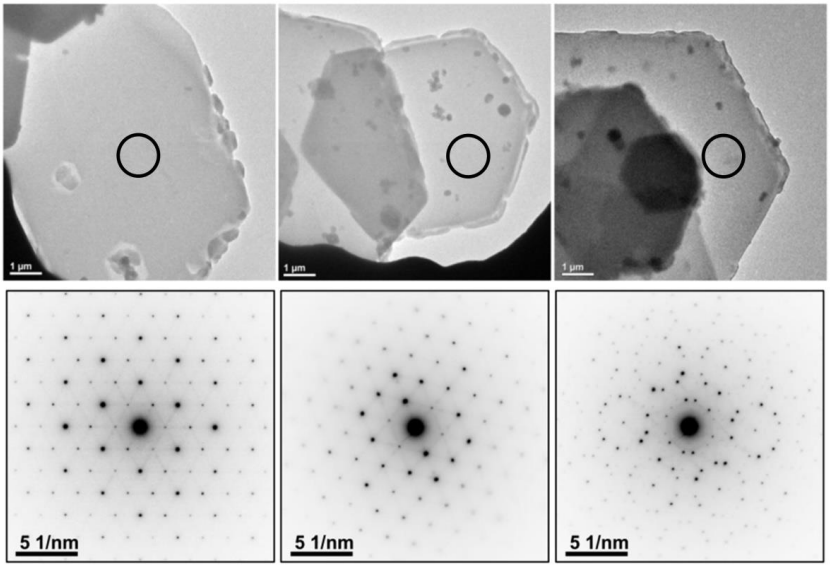

Figure 51 *TEM images and electron diffraction patterns of AFm-MoO_4 (left), a further molybdate-bearing phase (center), and overlay pattern of rotated trigonal phase.*

In the sodium-free systems, only some powellite impurities were observed besides the AFm-MoO_4, whereas no presence of an U-Phase analogue was observed. The diffraction patterns revealed a higher chemical yield of AFm-MoO_4 and less powellite impurities in the material synthesized at pH 13.5 (Figure 52). SEM investigations on the micro structure revealed the generally high crystallinity of the hexagonal sheet like AFm-MoO_4, exceeding a crystal size of 20 µm (Figure 53). The results indicate that in sodium-rich systems, besides AFm-MoO_4 and powellite, the formation of an analogue of the U-phase can contribute to the retention of molybdate, whereas in sodium-poor or potassium dominated conditions, only the AFm-MoO_4 (in combination with powellite) forms. In Addition, the synthesis without sodium or potassium gave a similar product compared to the potassium dominated conditions.

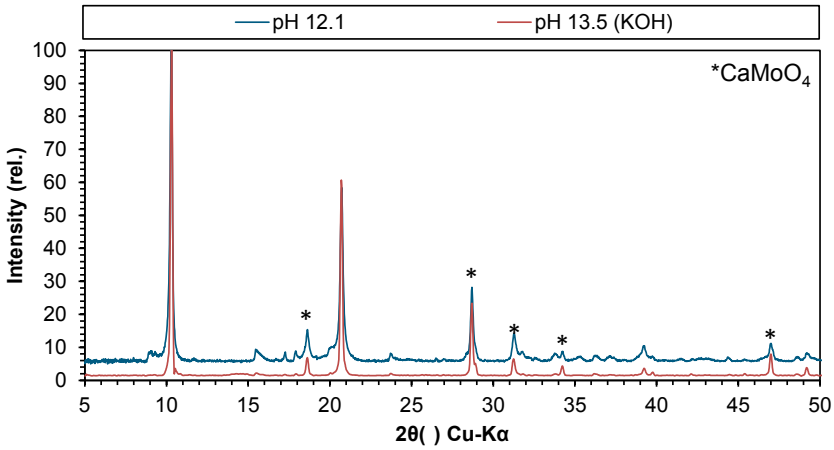

Figure 52 *Diffraction pattern of AFm-MoO_4 products synthesized in the Na-free system at pH 12.1 and 13.5 (KOH).*

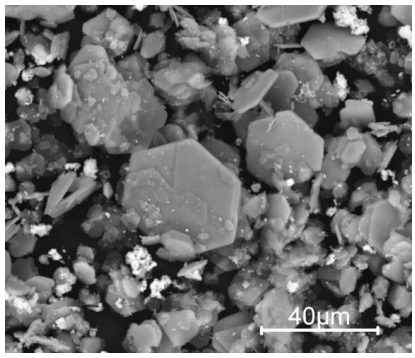

Figure 53 *SEM image of AFm-MoO_4 with powellite impurities.*

To investigate the coordination environment of molybdate in AFm, a Raman study was performed, using the material synthesized in the sodium-free systems. Raman spectra obtained for AFm-MoO_4 were compared to literature data on other hydrated molybdate phases published by Sejkora et al. (2014). The Raman shifts obtained for bands ν1 at 894 cm^{-1} (symmetrical stretching), ν3 at 833 cm^{-1} (triply degenerated antisymmetric stretching) and ν4 at 318 cm^{-1} (triply degenerated bending) refer to the tetrahedral symmetry of free MoO_4^{2-}, indicating a solution like environment of the hydrated MoO_4^{2-} in the interlayer of the AFm-MO_4 (Figure 54).

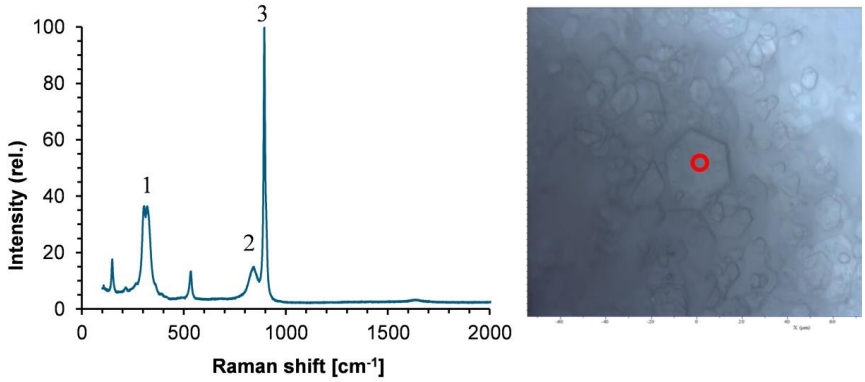

Figure 54 *Raman shifts of AFm-MoO_4, 1) triply degenerated bending vibrations ν_4, 2) triply degenerated antisymmetric stretching vibration ν_3, 3) symmetric stretching vibration ν_1.*

5.4.4. Uptake of molybdate by hardened cement paste

The uptake kinetics of molybdate by the CEM I paste reached a steady state R_d value of ~300 L kg^{-1} after about 15 days (Figure 55). Leaching of the alkalis, due to the low S/L-ratio in the experiment, was indicated by the solution pH = 12.6, which was found to be constant throughout the sorption experiment. Prior to the addition of molybdate, the initial equilibrium aqueous calcium concentration was found to be $c(Ca^{2+})$ = 21.2 mmol L^{-1} at a paste age of 30 days. As expected from batch uptake experiments, distribution ratios of CEM I are lower in general. The main contributors to retention of molybdenum in systems with HCP is the uptake by AFm or C_3AH_6 exhibiting distribution ratios of R_d > 1000 L kg^{-1} for the model phase systems. In addition, precipitation of powellite will contribute if the concentration of

molybdenum reaches the solubility limit of powellite. Therefore, the aqueous concentration of molybdate is very sensitive to differences in calcium concentrations in cementitious environments (pH > 9) (Grivé and Olmeda, 2015; Ochs et al., 2016).

The measured distribution ratios for the uptake of molybdate by CEM I are in good agreement with literature values by Kato et al. (2002). Further literature data on the uptake of molybdate is rare. Only one study was found addressing the uptake of molybdate by OPC (Kato et al., 2002). The data showed that uptake values for molybdate are in good agreement with values for selenite. Therefore, sorption data of selenite was use to derive sorption data for molybdenum (Ochs et al. 2016). Anyhow, literature values for the retention of molybdate in Stage II and Stage III conditions are still lacking.

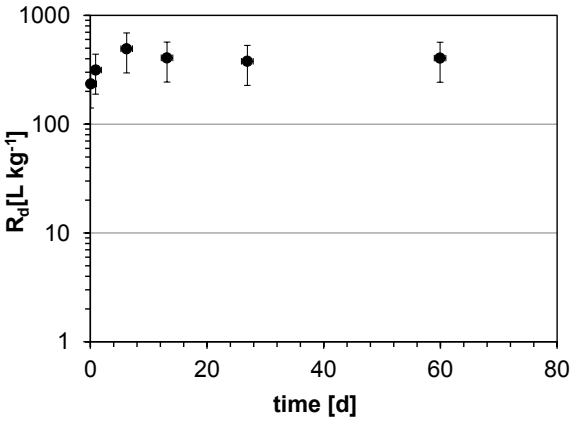

Figure 55 *Uptake kinetic of MoO_4^{2-} by crushed CEM I paste.*

5.5. Iodine uptake in cementitious systems

5.5.1. Uptake kinetics and equilibrium distribution ratios

The kinetics of the iodide and iodate uptake by the various cement hydration phases (at S/L ratio of 0.005 kg L^{-1}) are shown in Figure 56. Uptake was found to be in equilibrium within 30 day for the majority of model phases used. For the uptake of iodate by AFm-SO_4, equilibrium conditions were not reached within the experimental time frame of 60 days. The equilibrium R_d values determined at S/L = 0.005 kg L^{-1} are depicted in Figure 57 und summarized in Table 17. XRD measurements performed on the dried solids after the termination of the sorption experiments showed no significant phase changes, with exception of ettringite and hydrogarnet (ACW) samples in case of iodide and iodate after 60 days. Here, small amounts of AFm impurities were found as a result of carbonation during sample preparation and measurement.

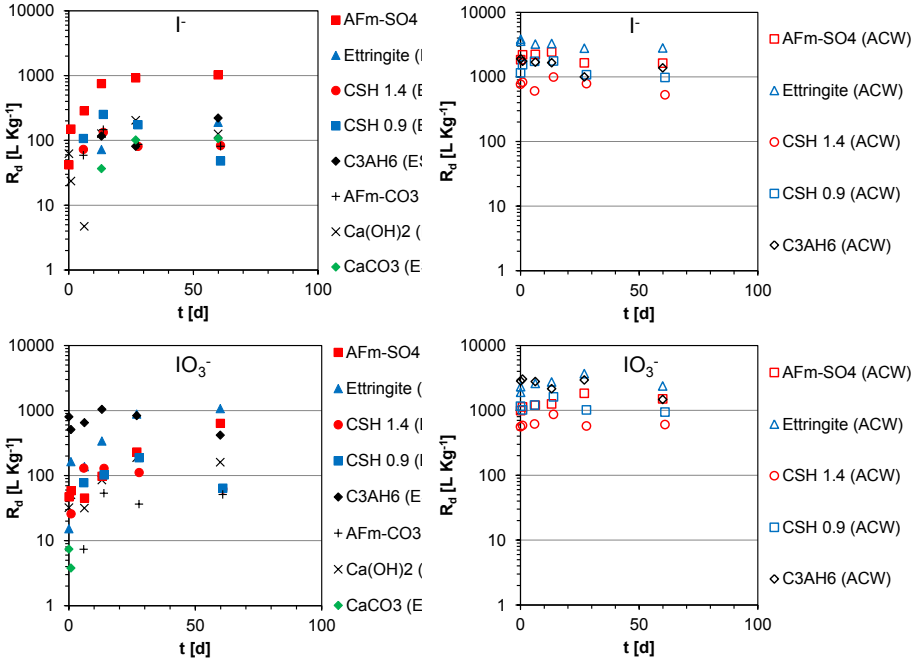

Figure 56 *Kinetics of iodide and iodate uptake by cement hydrates phases in equilibrium solution (ES) and artificial cement pore water (ACW).*

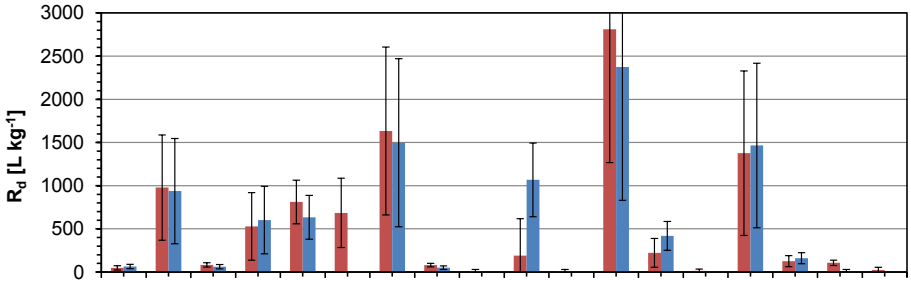

Figure 57 *Distribution coefficients R_d for I^- (red) and IO_3^- (blue) uptake by cement hydration phases in different solutions (ES: equilibrium solution; ACW: artificial young cement water (pH 13.3); CH: saturated portlandite solution (pH 12.3)).*

Table 17 *Distribution coefficients R_d for I^- and IO_3^- uptake by cement hydration phases in different solutions (ES: equilibrium solution; ACW: artificial young cement water (pH 13.3); CH: saturated portlandite solution (pH 12.3)).*

	R_d [L kg^{-1}]									
	Iodide						Iodate*			
	ES		ACW		sat. CH		ES		ACW	
C-S-H0.9	48	±19	978	±635			64	±25	937	±609
C-S-H1.4	83	±33	529	±343			62	±24	602	±391
AFm-SO_4	811	±324	1633	±1061	685	±413	634	±253	1497	±973
AFm-CO_3	81	±32			10	±15	51	±20		
Ettringite	190	±76	2810	±1826	10	±19	1068	±427	2374	±1543
C_3AH_6	222	±88	1376	±894	14	±18	418	±167	1466	±952
$Ca(OH)_2$	126	±50					161	±64		
$CaCO_3$	107	±30			24	±25	0	±22		

*Iodate in sat. CH solution was not determined

Highest uptake for iodide was observed for AFm-SO_4 (R_d = 811 L kg^{-1}) in equilibrium solution, whereas a slight uptake of iodide was observed for hydrogarnet (R_d = 222 L kg^{-1}), portlandite (R_d = 126 L kg^{-1}) and calcite (R_d = 107 L kg^{-1}). The observed equilibrium distribution ratios for the uptake of iodide by AFm-SO_4 are higher compared to literature values of Rd = 26 L kg^{-1} for an initial iodide concentration of $c(I^-)_{ini} = 10^{-11}$ M by Aimoz et al. (2012b). On the other hand, the strong uptake of iodide by AFm-SO_4, compared to the negligible uptake by AFm-CO_3 and ettringite are in good agreement with the

observation of Aimoz et al. (2012b), where it was concluded that an anion exchange of iodide for sulfate is suitable mechanism for the uptake by AFm-SO_4. However, compared to the literature values, these results do not support the stronger sorption of iodine by AFm or AFt compared to C-S-H as observed by Noshita et al. (2002). Distribution ratios for the uptake of iodine by C-S-H were found to be R_d = 83 L kg^{-1} and R_d = 48 L kg^{-1} for C-S-H1.4 and C-S-H0.9, respectively. The increasing uptake of iodine by increasing the Ca/Si- ratio of C-S-H is in agreement with the observations made by Aggarwal et al. (2000). The slightly higher uptake of iodine by C-S-H1.4 indicates higher retention in younger cementitious systems. In general, all model phases showed a higher uptake for iodine in ACW compared to the equilibrium solutions. This indicates a higher retention potential of iodine in young cementitious systems. The predicted uptake mechanism for the uptake of iodine by C-S-H is electrostatic sorption (Bonhoure et al., 2002; Ochs et al., 2016). The increasing uptake of iodine as observed in this study by increasing the Ca/Si- ratio of C-S-H, and therefore increasing positive surface charge of the C-S-H (cf. 2.3.1), is in good agreement with the predicted electrostatic sorption mechanism.

Distribution ratios for the uptake of iodate by C-S-H were found to be R_d = 64 L kg^{-1} and R_d = 62 L kg^{-1} for C-S-H1.4 and C-S-H0.9, respectively. Within the experimental error, no effect of the Ca/Si-ratio of C-S-H was found for uptake of iodate in equilibrium solution. The increasing uptake of iodide by increasing the Ca/Si- ratio of C-S-H is not fully in agreement with the conclusions made by Evans (2008). In general, all model phases showed a higher uptake for iodate in ACW compared to the equilibrium solutions. This indicates a higher retention potential of iodine in young cementitious systems. Moreover iodate was found to be taken up by hydrogarnet (R_d = 418 L kg^{-1}), AFm-SO_4 (R_d = 634 L kg^{-1}) and in particular by ettringite (R_d = 1068 L kg^{-1}). Idemitsu et al. (2013) showed in a synthetic approach that two iodate anions can be incorporated into ettringite structure by substituting for one sulfate anion. In contrast to reports on the incorporation of iodate into calcite (Feng and Redfern, 2018), no uptake of iodate by calcite was observed. Further investigations on the uptake of iodide in saturated portlandite solution exhibit strong sorption by AFm-SO_4 with a measured R_d = 685 L kg^{-1} in saturated portlandite solution (Table 17). Literature values on the uptake of iodate by cementitious materials are rare due to the large field of stability for iodine in cementitious environment (cf. section 2.8.4). Depending on the redox potential of the concrete and the iodine speciation in the waste, both species may persist in cementitious systems (Ochs et al., 2016).

5.5.2. Uptake of iodine by AFm-SO_4

From literature values the uptake of iodide by AFm phases was expected (cf. Aimoz et al., 2012b). However, in batch experiments an uptake of iodate by AFm was observed as well. Therefore, this interaction of iodide and iodate with AFm phases was investigated further with respect to changes in AFm solids used. Anyhow, the experiments performed on iodide uptake by AFm-SO_4 exhibit the expected high distribution ratios (R_d = 850 L kg^{-1}). Small amounts of needle like crystals were observed indicating the formation of ettringite, most probably as consequence of the increasing sulfate concentration in solution, due to the anion exchange of sulfate for iodide in the AFm phase (Figure 58, left). On the other hand, the uptake experiment conducted for 30 days at 10^{-3} mol L^{-1} iodate exhibits a phase transformation giving large quantities of a needle-like iodate containing phase (Figure 58, right).

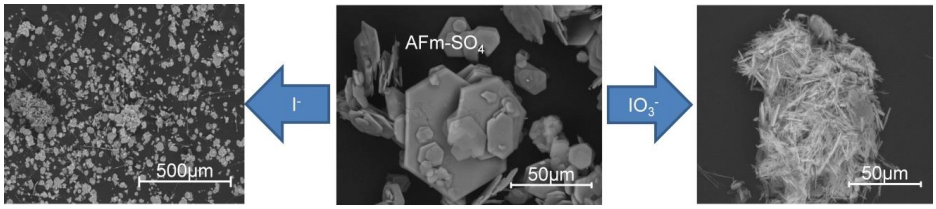

Figure 58 *SEM images of AFm-SO_4 after uptake of iodide (left) and iodate (right).*

Iodate is an oxoanion that can fit into the AFt structure and can exchange for sulfate (cf. Iwaida et al., 2001). The experimental results suggest that the elevated iodate concentrations in solution have the same effect as an increase of sulfate in solution, thus favoring the formation of an iodate-bearing AFt phase at the expense of AFm-SO_4.

To investigate the dependency of the phase transition of AFm-SO_4 to IO_3-bearing AFt on the iodate concentration, AFm-SO_4 was contacted with solutions possessing iodate concentrations between 0.1 and 100 mmol L^{-1}. Figure 59 shows the newly formed AFt needles and the corroded remains of AFm-SO_4 exposed to the highest IO_3^- concentration. XRD performed on the solids showed that first indications for the formation of an iodate containing AFt were observed at c(IO_3^-) = 10^{-4} mol L^{-1}, whereas at higher concentrations, AFt was the major phase (Figure 60). These findings are in good agreement with the changes in the phase assemblage observed on solidification of highly iodine bearing waste streams (Tanabe et al., 2010). Tanabe et al. (2010) reported that solidification of iodate with a cement

formulation that was enriched with calcium-aluminate ferrites resulted in an increase of the AFt fraction from 12% to approx. 80%.

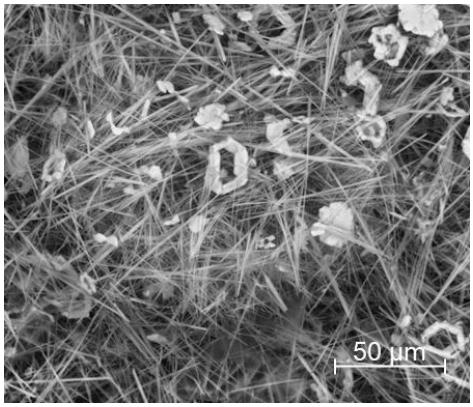

Figure 59 *SEM image of AFm-SO_4 contacted with 100 mM iodate solution.*

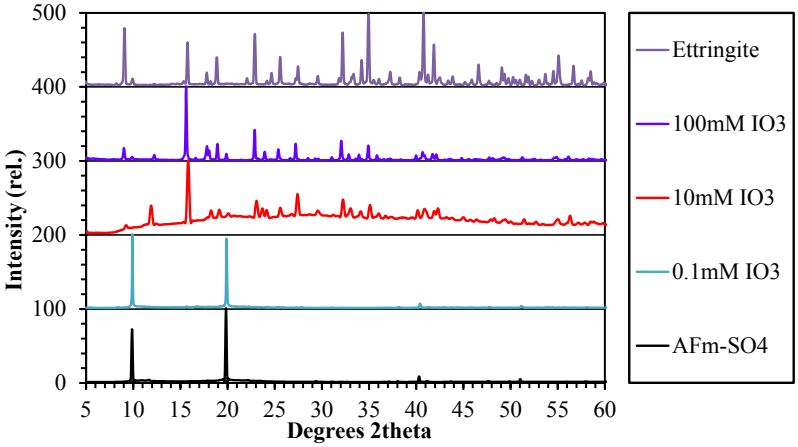

Figure 60 *XRD diffraction patterns of AFm-SO_4 contacted with solutions containing various concentrations of iodate compared to the diffraction patterns of AFm-SO_4 and ettringite.*

5.5.3. Iodine uptake of by hardened cement paste

The results of the experiments exploring the iodide and iodate sorption on crushed HCP based on CEM I are shown in Figure 61. For both iodine species a fast uptake was observed, with slightly higher sorption of IO_3^- (R_d ~140 kg L^{-1}) compared to I^- (R_d ~26 kg L^{-1}),

In general, the results obtained for the uptake of iodide and iodate by HCP systems are in qualitative agreement with the results obtained for the single hydration phases under equilibrium conditions, indicating that the major contribution to iodine uptake can be attributed to the minor cement hydration phases like AFm/AFt that exhibit slightly higher R_d values for IO_3^- than for I^-. Furthermore, distribution ratios for iodine are in good agreement with literature values of Pointeau et al. (2008) (R_d ~150 kg L^{-1}) and Bonhoure et al. (2002) (R_d ~200 kg L^{-1}).

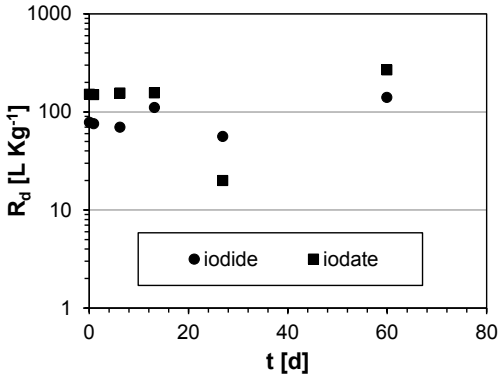

Figure 61 *Uptake kinetic of iodide and iodate by crushed CEM I paste.*

The uptake of iodide by hardened CEM I paste was additionally studied in terms of in-diffusion into cement monoliths. ToF-SIMS was used to obtain a depth profile of iodide starting at the contacted surface of the monolith (Figure 62). The results show that iodide is distributed unevenly on the surface of the hardened cement monolith. However, a connection between the distribution of iodide and specific features of the HCP could not be established. The depth profiles of selected elements obtained by ToF-SIMS are shown in Figure 63. Here, the relative intensities of the elements in the hardened cement paste are displayed as a function of the number of ion beam scattering shots. The scattering depth cannot be given as absolute value, due to the uneven scattering of the inhomogeneous material and the slightly

different scattering efficiencies of the various components in the HCP. The results indicate that the measured intensity of iodide reaches a maximum close to the surface of the monolith. Compared to the intensity of gold used for coating, it can be observed that the majority of iodine is contained within this gold layer. This leads to the conclusion that the very mobile iodide was mainly present in the pore solution and has probably diffused out of the cement matrix, due to the low pressure applied during coating and measuring. Therefore, the obtained ToF-SIMS data were inconclusive for elucidating the depth of iodide in-diffusion into the hardened CEM I paste.

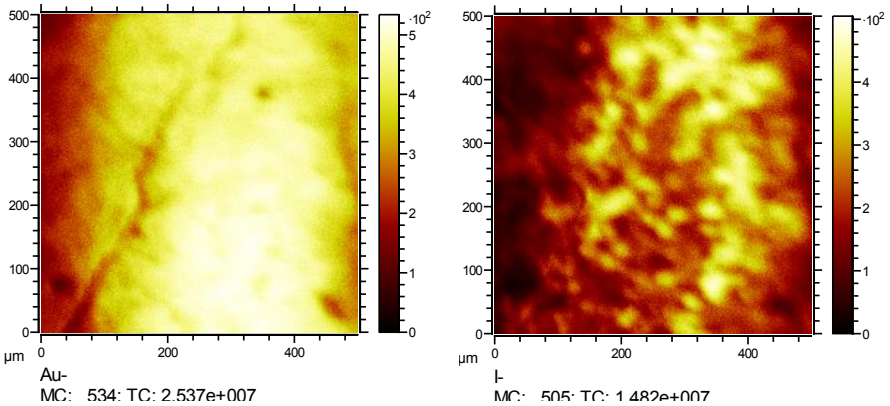

Figure 62 *ToF-SIMS total ion maps of gold (left) and iodide (right) on CEM I HCP.*

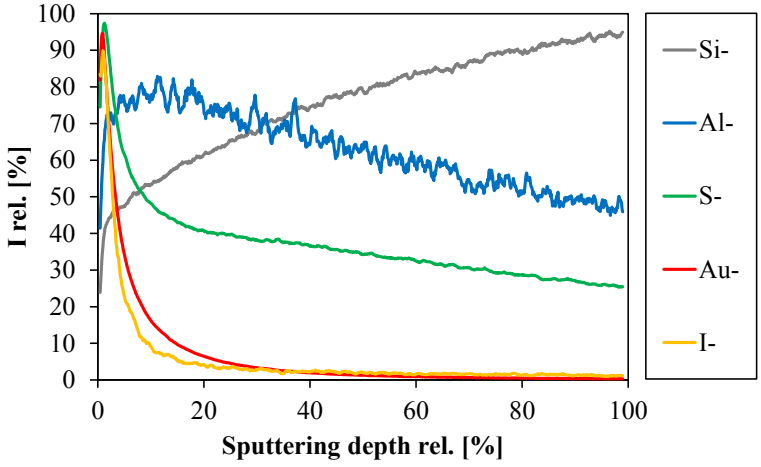

Figure 63 *(ToF-SIMS) depth profiles of selected elements of CEM I HCP contacted with iodide (Au coating was used to create a conductive surface layer).*

6. Conclusions

In this work the retention mechanism of radium, technetium, molybdenum and iodine in cementitious systems were investigated by batch sorption experiments. A systematic bottom-up approach was used to investigate radionuclide retention by single model phases, representative for the cement hydration phases, and various hardened cement pastes. Complementary, advanced microanalytical methods (e.g. TEM, ToF-SIMS) were used to improve the understanding for the investigated uptake and retention mechanisms. Experiments were conducted in different solutions to address the uptake and retention behavior in young, mature and altered cementitious systems. This study provides for the first time a systematic investigation of radium, technetium, molybdenum, and iodine uptake for all major CEM hydration phases. This work aims to close knowledge gaps, especially for the uptake of radium by other phases than C-S-H and the uptake of iodine, technetium and molybdenum by for the major CEM hydration phases. For the first time systematic studies on the uptake of these safety relevant radionuclides by cement model phases were conducted. The obtained distribution ratios for the main hydration phases can be used as a basis for a component additive approach to address the retention properties of complex cement-based materials in repository environment.

Uptake and retention was characterized in terms of distribution ratios referring to the different chemical environments expected for the various stages of the long-term alteration of cementitious materials. Microanalytical methods and atomistic simulations complemented the experimental approaches to understand/propose uptake mechanisms and to distinguish between surface sorption, structural uptake and secondary phase formation. Depending on the system, various, partially competing uptake mechanisms could be identified, such as electrostatic surface sorption (e.g. MoO_4^{2-} on C-S-H), cation exchange (e.g. radium uptake by C-S-H), anion exchange (e.g. MoO_4^{2-} uptake by AFm) or phase transformation (e.g. formation of IO_3^--AFt from AFm), which contribute to the radionuclide retention in cementitious systems. Below are the findings for the individual radionuclides summarized.

6.1. Radium

Uptake kinetics of radium were found to be fast and in equilibrium within 30 days. Strong uptake of radium by C-S-H (R_d up to 22,000 L kg^{-1}), depending on the pH, was observed. Distribution ratios were found to decrease with increasing Ca/Si ratio. Sorption equilibrium was reached in less than 30 days, with distribution ratios independent of the solid-to-liquid ratio. Ab-initio calculations performed on the uptake of radium in the C-S-H interlayer reveal negative free energies for the cation exchange reaction. These results suggest that radium uptake in the interlayer can occur/occurs (or is a competing mechanism to surface sorption) in particular at low Ca/Si ratios, in addition to surface sorption. The uptake of radium by AFm and ettringite was found to be negligible. Investigation on the effect of cement alteration exhibits a lower retention potential for young cement. With increasing cement aging and decreasing calcium to silicon ratio, the retention potential for radium increases. Atomistic simulations show that, in addition to surface sorption, uptake of radium by cation exchange with calcium in the interlayer of the C-S-H is a plausible uptake mechanism, especially for C-S-H with low Ca/Si ratio. Furthermore, a weak uptake of radium is obtained for calcite (R_d ~ 220 L kg^{-1}), a major product of cement alteration by carbonation. In contrast, a carbonation of C-S-H and the successive formation of calcite lead to a release of the previously bound radium.

In case of CEM I the mature cement paste will exhibit a weak retention potential for radium. The studied VTT reference cement paste, exhibits a strong retention potential based on the higher C-S-H contents and the lower Ca/Si ratios obtained by the addition of fumed silica and quartz. Carbonation of CEM I HCP reveals an increasing uptake of radium in the calcite layer formed on the materials surface. Whether the higher uptake of radium by the carbonation layer of hardened cement paste (CEM I) is based on the lower calcium to silicon ratio in the C-S-H close to the calcite alteration layer or if this migration is coupled to the migration of sulfate could not be resolved by the microanalytical methods applied.

The obtained data are, with respect to the contents and composition of C-S-H in the HCP, consistent with the distribution ratios measured for the model phases.

6.2. Technetium

The uptake of pertechnetate by cement model phases was found to be generally low. The highest distribution ratio (R_d = 4.5 L kg^{-1}) was obtained for C-S-H0.9, whereas R_d = 2.3 L kg^{-1} for C-S-H1.4. This result cannot be explained in terms of electrostatic sorption and could be attributed to the difference in surface area of the synthetic C-S-H. Furthermore, a slight uptake of pertechnetate by AFm-SO_4 (ES) (R_d = 4.0 L kg^{-1}) and AFm-CO_3 (ES) (R_d = 2.3 L kg^{-1}) was noticed. The lower uptake by AFm-CO_3 compared to AFm-SO_4 might indicate that an exchange of TcO_4^- for the planar CO_3^{2-} is less favored compared to an exchange with the tetrahedral SO_4-anion. The uptake of TcO_4 by ettringite, which was proposed in the literature as a potential retention mechanisms, was found to be weak, i.e. the R_d was generally < 1 L kg^{-1}, suggesting no uptake due to exchange for SO_4 groups.

The retention of pertechnetate by the studied cement model phases and alteration phases is very weak. Based on the distribution ratios determined for AFm phases and C-S-H, pertechnetate is expected to be mobile in cementitious materials, as long as no reducing agents are present to immobilize technetium in form of significantly less soluble and less mobile Tc(IV). Distribution ratios obtained for uptake by C-S-H phases unexpectedly revealed that the C-S-H phases with higher calcium to silicon ratios are weaker sorbents for pertechnetate despite their more positive surface charge which is expected to result in a higher anion sorption potential.

It is expected that mechanical, physical and chemical properties that influence diffusivity in general are of greater importance with respect to the mobility of pertechnetate compared to the retention/sorption to the hydration phases. However, the range of elements present in cement model phases was limited in this study. Further investigations should address the uptake and retention of pertechnetate by iron containing AFm/AFt and hardened cement pastes formulations containing high contents of reducing agents.

6.3. Molybdenum

Studies on the uptake and retention of molybdate were conducted to investigate the mechanisms decreasing the mobility of molybdate besides the formation of powellite, and at Mo concentrations below the solubility limit/constraint of powellite. Uptake for molybdate by

C-S-H exhibited distribution ratios of R_d = 750 L kg^{-1} for C-S-H1.4 and R_d = 420 L kg^{-1} C-S-H0.9. In young cementitious water, distinctively lower R_d values were observed. An enhanced molybdate uptake (R_d ~1500 L kg^{-1}) by AFm-SO_4 and AFm-CO_3 was observed. The highest R_d values were observed for C_3AH_6 (up to 3000 L kg^{-1}). Batch sorption experiments reveal strong uptake by AFm phases, due to anion exchange in the interlayer, and hydrogarnet. Furthermore, distribution ratios obtained for uptake by C-S-H exhibit a lower uptake by C-S-H0.9 than C-S-H1.4 and are in agreement with the electrostatic sorption mechanism regarding change in surface charge of C-S-H to positive values at Ca/Si ratios exceeding 1.2. Thus is could be shown that, besides the uptake of MoO_4^{2-} by AFm-phases due to anion exchange in the interlayer, C-S-H play a major role with respect to the retention of Mo migration in cementitious systems.

The strong uptake by hydrogarnet-bearing systems leading to formation of a molybdate bearing AFm phase indicate that cement pastes rich in AFm offering the highest potential on molybdenum retention. On the other hand, the observed uptake by hydrogarnet indicates that calcium aluminate cements could offer a high retention potential due to the high content of hydrogarnet.

6.4. Iodine

The highest distribution ratios for iodide were observed for AFm-SO_4 (R_d = 811 L kg^{-1}). Distribution ratios for hydrogarnet, portlandite and calcite were distinctively lower. The strongest uptake of iodate was observed for ettringite (R_d = 1068 L kg^{-1}).

The retention of iodide in cementitious material was attributed to the uptake by AFm-SO_4 and the AFt-SO_4/IO_3 formation, where the C-S-H phases contributed to the retention potential. In the portlandite stage, AFm-SO_4 was found to be the main contributor to iodide retention. Distribution ratios were found to be in equilibrium within 30 days. Uptake of iodate by AFm-SO_4 leads to a phase transformation into needle shaped iodate-AFt. Uptake and in-diffusion studies for hardened cement paste exhibit highest iodide concentrations at the surface of the HCP specimen, revealing the high mobility of iodide in cementitious environments. The obtained distribution ratios for the uptake of iodide by crushed hardened cement paste were, with respect to the contents of AFm/AFt, consistent with distribution ratios measured for model phases.

7. Outlook

Cementitious barriers in a final repository will undergo mineralogical changes in the long-term due to alteration processes. The matured, altered or chemically changed phase inventory of the cementitious material will be accountable for radionuclide retention in the post closure period. These changes and their effect on the retention on radionuclides need to be fully understood in order to create a model that can be used to evaluate the long-term safety of the disposal facility. The storage containers, packages and waste compartments considered for a deep geological repository are designed to last for several thousand years (IAEA, 2011). However, the long-term safety assessment needs to ensure the safe retention of the radionuclides for 1,000,000 years. In case of a canister failure, the retention of radionuclides is likely to be subject to mature or altered cementitious material. In fact, future studies need to address the retention of safety relevant radionuclides in altered cement pastes, comprising an experimental approach, to fit various possibilities of cement alteration, especially the alteration reactions of cement in contact with the various host rocks.

Comprehensive investigations regarding the uptake of radium by fully characterized hardened cement pastes, especially in terms of C-S-H content, are necessary to point out the transferability of model phase uptake experiments. Furthermore, due to the abundancy of barium, the formation of radiobaryte in and close to the cementitious barriers should be addressed to investigate additional retention mechanisms.

With respect to redox sensitive radionuclides like technetium, experiments referring to the conditions of cementitious material close to corroding containers could exhibit additional insights into the retention of pertechnetate. AFm and AFt phases are able to incorporate iron. However, in this study, no iron containing hydrated cement phases were used to limit the number of model phases. These iron containing AFm/AFt phases could affect the redox potential and may potentially exhibit a higher retention potential for redox sensitive radionuclides.

The hydrogarnet in HCP often contains silicon (Taylor and Newbury, 1984). Further investigation should address the effect of Si-hydrogarnet on the uptake of molybdate and the formation of AFm-MoO_4 in hardened cement pastes. Moreover, experiments addressing the thermodynamic properties and the solubility of AFm-MoO_4 are of major interest, with respect to thermodynamic modelling of molybdenum solubilities in cementitious systems. Uptake

data for molybdate by hardened cement pastes addressing the retention in Stage II and Stage III conditions are still lacking.

Experiments and analytical approaches regarding the uptake of iodine in artificial cement pore water suffered from bad statistics. Particularly, the uptake of iodine in ACW needs to be readdressed to limit the experimental error.

Advanced microanalytical methods used to investigate the uptake of radionuclides by hardened cement pastes gave evidence that radionuclides solved in the cement pore water were able to diffuse to the surface of the specimen under vacuum which was required for the measurement. Freezing the specimen and immobilizing the pore water could preserve the concentration profiles of the analyte. Therefore, cryo-techniques (e.g. cryo-SEM, cryo-ToF-SIMS) could be used to evaluate diffusion and concentration profiles of the analyte in hardened cement pastes. Furthermore, investigations by EXAFS could provide complementary insights into the uptake of radium by C-S-H phases as well as for molybdate uptake by AFm phases.

The pursued systematic bottom-up approach gave insights into retention responsible cement model phases and mechanisms. This data provides a basis for a component additive approach or could be used by computational models to predict radionuclide mobility in cementitious systems (Lattice-Boltzmann codes) and optimization of cement formulation to obtain minimum radionuclide mobility.

8. Acknowledgement

Ich möchte mich bei meinem Doktorvater Herrn Professor Dirk Bosbach für die Möglichkeit diese Doktorarbeit anzufertigen bedanken. Bei Herrn Professor Georg Roth möchte ich mich für die Übernahme der Zweitbegutachtung und eine konstruktive Diskussion zu dieser Arbeit bedanken.

Besonders herzlich möchte ich mich bei Herrn Dr. Guido Deissmann für die hervorragende Betreuung, stete Diskussionsbereitschaft und freundschaftliche Unterstützung bei der Erstellung dieser Arbeit bedanken. Besonders bedanken möchte ich mich auch bei Stephan Rohmen für die anregenden Diskussionen zu den verschiedensten Themen der Zementchemie.

Nachfolgend möchte ich mich bei meinen internationalen Kooperationspartnern Herrn Professor David Read und Herrn Dr. Matthew Isaacs von der University of Surrey für die vielen Diskussionen und Anregungen bedanken. Herrn Dr. Piotr M. Kowalski danke ich für die atomistischen Modellrechnungen. Bei Dr. Philip Kegler und Frau Simone Weigelt bedanke ich mich für die zahlreichen Röntgendiffraktometriemessungen und bei Herrn Dr. Juri Barthel für die TEM-Messungen. Herrn Dr. Uwe Breuer danke ich für den freundlichen Empfang, die Durchführung der ToF-SIMS-Messungen und die stetige Bereitschaft sein Wissen über Massenspektrometrie zu teilen.

Bei Herrn Fabian Sadowski möchte ich mich für unzählige ICP-MS Messungen bedanken. Für ihre Hilfe bei der Probenpräparation danke ich Dimitri Schneider, Daniel Assenmacher und Thomas Jonas. Für die gute Zusammenarbeit und Hilfestellung in diversen Belangen danke ich Herrn Dr. Stefan Neumeier, Herrn Dr. Andreas Wilden, Herrn Ralf König. Meinen Kollegen im IEK-6 danke ich für die gute Arbeitsatmosphäre.

Danken möchte ich auch der Europäischen Kommission, die im Rahmen der Horizon 2020 Programme diese Arbeit unter der Zuwendungsvereinbarung Nr. 662147 (Cebama) co-finanzierte.

9. List of figures

10. List of tables

11. References

Aggarwal, S., Angus, M.J., Ketchen, J., 2000. Sorption of radionuclides onto specific mineral phases present in repository cements. AEA Technology, NSS/R31, Windscale, Cumbria, p. 70.

Aimoz, L., Kulik, D.A., Wieland, E., Curti, E., Lothenbach, B., Mäder, U., 2012a. Thermodynamics of AFm-(I_2, SO_4) solid solution and of its end-members in aqueous media. Appl. Geochem. 27, 2117-2129.

Aimoz, L., Wieland, E., Taviot-Gueho, C., Dahn, R., Vespa, M., Churakov, S.V., 2012b. Structural insight into iodide uptake by AFm phases. Environ. Sci. Technol. 46, 3874-3881.

Allen, P.G., Shuh, D.K., Bucher, J.J., Edelstein, N.M., Reich, T., Denecke, M.A., Nitsche, H., 1997a. Chemical speciation studies of radionuclides by XAFS. J. Phys. IV 7, 789-792.

Allen, P.G., Siemering, G.S., Shuh, D.K., Bucher, J.J., Edelstein, N.M., Langton, C.A., Clark, S.B., Reich, T., Denecke, M.A., 1997b. Technetium speciation in cement waste forms determined by X-ray absorption fine structure spectroscopy. Radiochim. Acta 76, 77-86.

ANDRA, 2005. Andra Research on the geological disposal of highlevel long-lived radioactive waste – Results and perspectives. ANDRA, Dossier 2005.

ANDRA, 2008. Technological demonstrators. ANDRA, 310 VA.

Andreussi, O., Dabo, I., Marzari, N., 2012. Revised self-consistent continuum solvation in electronic-structure calculations. J. Phys. Chem. 136, 064102.

Atkins, M., Damidot, D., Glasser, F.P., 1994. Performance of cementitious systems in the repository. Mater. Res. Soc. Symp. Proc. 333, 315-326.

Atkins, M., Glasser, F.P., 1990. Encapsulation of radioiodine in cementitious waste forms. Mater. Res. Soc. Symp. Proc. 176, 15-22.

Atkins, M., Glasser, F.P., 1992. Application of portland cement-based materials to radioactive waste immobilization. Waste Manage. 12, 105-131.

Atkins, M., Glasser, F.P., Kindness, A., 1992. Cement hydrate phases: solubility at 25°C. Cem. Concr. Res. 22, 241-246.

Atkins, M., Glasser, F.P., Moroni, L.P., 1991a. The long-term properties of cement and concretes. Mater. Res. Soc. Symp. Proc. 212, 373-386.

Atkins, M., Macphee, D., Kindness, A., Glasser, F.P., 1991b. Solubility properties of ternary and quaternary compounds in the calcia-alumina-sulfur trioxide-water system. Cem. Concr. Res. 21, 991-998.

Atkinson, A., Nickerson, A., 1984. The diffusion of ions through water-saturated cement. J. Mater. Sci 19, 3068-3078.

Bach, T.T.H., Chabas, E., Pochard, I., Cau Dit Coumes, C., Haas, J., Frizon, F., Nonat, A., 2013. Retention of alkali ions by hydrated low-pH cements: Mechanism and Na+/K+ selectivity. Cem. Concr. Res. 51, 14-21.

Bamforth, P.B., Baston, G.M.N., Berry, J.A., Glasser, F.P., Heath, T.G., Jackson, C.P., Savage, D., Swanton, S.W., 2012. Cement materials for use as backfill, sealing and structural materials in geological disposal concepts, A review of current status. SERCO, Serco Report SERCO/005125/001 Issue 3.

Baquerizo, L.G., Matschei, T., Scrivener, K.L., Saeidpour, M., Wadso, L., 2015. Hydration states of AFm cement phases. Cem. Concr. Res. 73, 143-157.

Barcena, I., Garcia-Sineriz, J.-L., 2008. Full scale demonstration of shotcrete sealing plug under realistic working conditions, International Technical Conference on the Practical Aspects of Deep Geological Disposal of Radioactive Waste, Prague, pp. 1-10.

Baur, I., Keller, P., Mavrocordatos, D., Wehrli, B., Johnson, C.A., 2004. Dissolution-precipitation behaviour of ettringite, monosulfate, and calcium silicate hydrate. Cem. Concr. Res. 34, 341-348.

Baur, I., Ludwig, C., Johnson, C.A., 2001. The leaching behavior of cement stabilized air pollution control residues: a comparison of field and laboratory investigations. Environ. Sci. Technol. 35, 2817-2822.

Bayliss, S., Ewart, F., Howse, R., Lane, S., Pilkington, N., Smith-Briggs, J., Williams, S., 1989. The solubility and sorption of radium and tin in a cementitious near-field environment. Mater. Res. Soc. Symp. Proc. 127, 879-885.

Bel, J.J., Wickham, S.M., Gens, R.M., 2006. Development of the Supercontainer design for deep geological disposal of high-level heat emitting radioactive waste in Belgium. MRS Online Proceedings Library Archive 932.

Bennett, D.G., Read, D., Atkins, M., Glasser, F.P., 1992. A thermodynamic model for blended cements. II: cement hydrate phases; thermodynamic values and modeling studies. J. Nucl. Mater. 190, 315-325.

Berner, U., 1999. Concentration limits in the cement based Swiss repository for long-lived, intermediate-level radioactive wastes (LMA). PSI, PSI Bericht 99-10, 59 pp.

Berner, U.R., 1988. Modelling the incongruent dissolution of hydrated cement minerals. Radiochim. Acta 44-45, 387-393.

Berner, U.R., 1992. Evolution of pore water chemistry during degradation of cement in a radioactive waste repository environment. Waste Manage. 12, 201-219.

BfS, 2008. Hauptbetriebsplan für die Errichtung des Endlagers Konrad zugelassen.

BGE, 2018. Nr. 01/18 - Fertigstellung des Endlagers Konrad verzögert sich. www.bge.de/de/pressemitteilungen/2018/03/pm-0118-fertigstellung-des-endlagers-konrad-verzoegert-sich/.

Blanc, P., Bourbon, X., Lassin, A., Gaucher, E.C., 2010a. Chemical model for cement-based materials: Temperature dependence of thermodynamic functions for nanocrystalline and crystalline C-S-H phases. Cem. Concr. Res. 40, 851-866.

Blanc, P., Bourbon, X., Lassin, A., Gaucher, E.C., 2010b. Chemical model for cement-based materials: Thermodynamic data assessment for phases other than C-S-H. Cem. Concr. Res. 40, 1360-1374.

Bonaccorsi, E., Merlino, S., Kampf, A.R., 2005. The crystal structure of tobermorite 14 Å (plombierite), a C-S-H phase. J. Am. Ceram. Soc. 88, 505-512.

Bonhoure, I., Scheidegger, A.M., Wieland, E., Dahn, R., 2002. Iodine species uptake by cement and C-S-H studied by I K-edge X-ray absorption spectroscopy. Radiochim. Acta 90, 647-651.

Borkel, C., Montoya, V., Kienzler, B., 2014. Modeling long-term leaching experiments of full scale cemented wastes: effect of solution composition on diffusion, NEWCEM, Avignon, pp. 378-390.

Breval, E., 1976. C3A hydration. Cement and Concrete Research 6, 129-137.

Brisi, C., Lucco Borlera, M., Montanaro, L., Negro, A., 1986. Hydration of 5CaO · 3Al2O3. Cem. Concr. Res. 16, 156-160.

Brodda, B.G., Xu, M., 1989. Leaching of chlorine, cesium, strontium and technetium from cement-fixed intermediate level liquid waste. Mater. Res. Soc. Symp. Proc. 127, 481-487.

Chen, J.J., Thomas, J.J., Taylor, H.F.W., Jennings, H.M., 2004. Solubility and structure of calcium silicate hydrate. Cem. Concr. Res. 34, 1499-1519.

Chida, T., Sugiyama, D., 2008. Diffusion behavior of organic carbon and iodine in low-heat portland cement containing fly ash. MRS Online Proceedings Library Archive 1124.

Committee on Radioactive Waste Management, 2006. Managing our Radioactive Waste Safely. CoRWM, CoRWM Doc 700.

Corkhill, C.L., Bridge, J.W., Hillel, P., Gardner, L.J., Banwart, S.A., Hyatt, N.C., 2012. Technetium-99m transport and immobilisation in porous media: Development of a novel nuclear imaging technique. MRS Online Proc. Libr. 1518, 111, 117 pp.

Crossland, I.G., Vines, S.P., 2001. Why a cementitious repository? Nirex Report N/034.

Curtius, H., Kattilparampil, Z., 2005. Sorption of iodine on Mg-Al-layered double hydroxide. Clay Miner. 40, 455-461.

Damidot, D., Lothenbach, B., Herfort, D., Glasser, F.P., 2011. Thermodynamics and cement science. Cem. Concr. Res. 41, 679-695.

De Windt, L., Pellegrini, D., van der Lee, J., 2004. Coupled modeling of cement/claystone interactions and radionuclide migration. J. Contam. Hydrol. 68, 165-182.

Deutsches Atomforum e.V., 2015. Endlagerung hochradioaktiver Abfälle. http://www.kernenergie.de/kernenergie-wAssets/docs/service/061endlagerung-haw2015.pdf. Accessed August 2017

Dosch, W., Zur Strassen, H., 1967. Ein alkalihaltiges Calciumaluminatsulfathydrat (Natrium-Monosulfat). Zement-Kalk-Gips 20, 392-401.

Environment Agency, 2015. Decision Document: Low Level Waste Repository, UK.

European Union, 2011. Eestablishing a Community framework for the responsible and safe management of spent fuel and radioactive waste, Council Directive 2011/70/EURATOM.

Evans, N., Hallam, R., Aldridge, S., Warwick, P., 2008. The fate of Tc in a UK intermediate-level nuclear waste repository. WIT Trans. Ecol. Environ. 109, 579-588.

Evans, N.D.M., 2008. Binding mechanisms of radionuclides to cement. Cem. Concr Res. 38, 543-553.

Fairhall, G.A., Palmer, J.D., 1997. The immobilization and packaging of radioactive wastes for deep geological disposal in the UK - an integrated approach, WM Symposia.

Felipe-Sotelo, M., Hinchliff, J., Drury, D., Evans, N.D.M., Williams, S., Read, D., 2014. Radial diffusion of radiocaesium and radioiodide through cementitious backfill. Phys. Chem. Earth, Parts A/B/C 70, 60-70.

Feng, X., Redfern, S.A.T., 2018. Iodate in calcite, aragonite and vaterite $CaCO_3$: Insights from first-principles calculations and implications for the I/Ca geochemical proxy. Geochim. Cosmochim. Acta 236, 351-360.

Francois, M., Renaudin, G., Evrard, O., 1998. A cementitious compound with composition $3CaO.Al_2O3.CaCO_3.11H_2O$. Acta Crystallogr., Sect. C: Cryst. Struct. Commun. C54, 1214-1217.

Fuhrmann, M., Bajt, S., Schoonen, M.A.A., 1998. Sorption of iodine on minerals investigated by X-ray absorption near edge structure (XANES) and 125I tracer sorption experiments. Appl. Geochem. 13, 127-141.

Fujii, K., Kondo, W., 1981. Heterogeneous equilibrium of calcium silicate hydrate in water at 30 °C. J. Chem. Soc., Dalton Transactions, 645-651.

Gaona, X., Dähn, R., Tits, J., Scheinost, A.C., Wieland, E., 2011. Uptake of Np(IV) by C–S–H phases and cement paste: An EXAFS study. Environ. Sci. Technol. 45, 8765-8771.

Gaona, X., Kulik, D.A., Mace, N., Wieland, E., 2012. Aqueous-solid solution thermodynamic model of U(VI) uptake in C-S-H phases. Appl. Geochem. 27, 81-95.

Garbev, K., 2004. Struktur, Eigenschaften und quantitative Rietveldanalyse von hydrothermal kristallisierten Calciumsilikathydraten (C-S-H-Phasen), Forschungszentrum Karlsruhe. Ruprecht-Karls-Universität Heidelberg, Eggenstein-Leopoldshafen, p. 271.

Garcia Calvo, J.L., Hidalgo, A., Alonso, C., Fernandez Luco, L., 2010. Development of low-pH cementitious materials for HLRW repositories. Cem. Concr. Res. 40, 1290-1297.

Geckeis, H., Röhlig, K.J., Mengel, K., 2012. Endlagerung radioaktiver Abfälle. Chemie in unserer Zeit 46, 282-293.

Giannozzi, P., Andreussi, O., Brumme, T., Bunau, O., Nardelli, M.B., Calandra, M., Car, R., Cavazzoni, C., Ceresoli, D., Cococcioni, M., Colonna, N., Carnimeo, I., Corso, A.D., Gironcoli, S.d., Delugas, P., R. A. DiStasio, J., Ferretti, A., Floris, A., Fratesi, G., Fugallo, G., Gebauer, R., Gerstmann, U., Giustino, F., Gorni, T., Jia, J., Kawamura, M., Ko, H.Y., Kokalj, A., Küçükbenli, E., Lazzeri, M., Marsili, M., Marzari, N., Mauri, F., Nguyen, N.L., Nguyen, H.V., Otero-de-la-Roza, A., Paulatto, L., Poncé, S., Rocca, D., Sabatini, R., Santra, B., Schlipf, M., Seitsonen, A.P., Smogunov, A., Timrov, I., Thonhauser, T., Umari, P., Vast, N., Wu, X., Baroni, S., 2017. Advanced capabilities for materials modelling with Q uantum ESPRESSO. J. Phys. Condens. Matter 29, 465901.

Giannozzi, P., Baroni, S., Bonini, N., Calandra, M., Car, R., Cavazzoni, C., Ceresoli, D., Chiarotti, G.L., Cococcioni, M., Dabo, I., 2009. QUANTUM ESPRESSO: a modular and open-source software project for quantum simulations of materials. J. Phys. Condens. Matter 21, 395502.

Giffaut, E., Grivé, M., Blanc, P., Vieillard, P., Colàs, E., Gailhanou, H., Gaboreau, S., Marty, N., Madé, B., Duro, L., 2014. Andra thermodynamic database for performance assessment: ThermoChimie. Appl. Geochem. 49, 225-236.

Gilliam, T.M., Spence, R.D., Bostick, W.D., Shoemaker, J.L., 1990. Proceedings of the Gulf Coast Hazardous Substance Research Center Second Annual Symposium: Mechanisms and applications of solidification/stabilization of technetium in cement-based grouts. J. Hazardous Mater. 24, 189-197.

Glasser, F., 2011. 4 - Application of inorganic cements to the conditioning and immobilisation of radioactive wastes, in: Ojovan, M.I. (Ed.), Handbook of Advanced Radioactive Waste Conditioning Technologies. Woodhead Publishing, pp. 67-135.

Glasser, F.P., 1997. Fundamental aspects of cement solidification and stabilisation. J. Hazardous Mater. 52, 151-170.

Glasser, F.P., 2002. Characterization of the barrier performance of cements. Mater. Res. Soc. Symp. Proc. 713, 721-732.

Glasser, F.P., Atkins, M., 1994. Cements in radioactive waste disposal. MRS Bull. 19, 33-38.

Glasser, F.P., Macphee, D., Atkins, M., Pointer, C., Cowie, J., Wilding, C.R., Mattingley, N.J., Evans, P.A., 1989. Immobilisation of radwaste in cement based matrices. Department of the Environment.

Gougar, M.L.D., Scheetz, B.E., Roy, D.M., 1996. Ettringite and C□S□H Portland cement phases for waste ion immobilization: A review. Waste Manage. 16, 295-303.

Grivé, M., Duro, L., Colàs, E., Giffaut, E., 2015. Thermodynamic data selection applied to radionuclides and chemotoxic elements: An overview of the ThermoChimie-TDB. Appl. Geochem. 55, 85-94.

Grivé, M., Olmeda, J., 2015. Molybdenum behaviour in cementitious materials (AMPHOS). Amphos 21 Consulting, CEBAMA (662147) Deliverable n°D2.2.

Groll, N., Dreyszas, T., Kahl, H., 2015. Konrad final waste repository – modernisation of the shaft winding system and extension of adjacent shaft inset zones. Thyssen Mining, Thyssen Mining Report 2014/15.

Grutzeck, M., Benesi, A., Fanning, B., 1989. Silicon-29 Magic Angle Spinning Nuclear Magnetic Resonance study of calcium silicate hydrates. J. Am. Ceram. Soc. 72, 665-668.

Hamid, S.A., 1981. The crystal structure of the 11 Å natural tobermorite $Ca_{2.25}[Si_3O_{7.5}(OH)_{1.5}].1 H_2O$. Z. Kristallogr. 154, 189-198.

Harris, A.W., Manning, M.C., Tearle, W.M., Tweed, C.J., 2002. Testing of models of the dissolution of cements—leaching of synthetic C-S-H gels. Cem. Concr. Res. 32, 731-746.

Heath, T.G., Ilett, D.J., Tweed, C.J., 2000. Development of a Near-field Sorption Model for a Cementitious Repository. United Kingdom Nirex Ltd, AEAT/R/ENV/0229.

Heinonen, J., Isaksson, R., 2016. STUK ruling: Posiva can commence construction of final disposal facility. Finnish Radiation and Nuclear Safety Authority's (STUK).

Henocq, P., Giffaut, E., Macé, N., Landesman, C., Madé, B., 2014. Radionuclide behaviour in the concrete backfill and waste inventory context of an IL-LLW disposal vault. Current state of knowledge and remaining issues., NUWCEM, Avignon, pp. 481-494.

Hinchliff, J., 2015. Diffusion and advection of radionuclides through a cementitious backfill with potential to be used in the deep disposal of nuclear waste. Loughborough University, Loughborough Institutional Repository, p. 331.

Holland, T.R., Lee, D.J., 1992. Radionuclide getters in cement. Cem. Concr. Res. 22, 247-258.

Hummel, W., Berner, U., Curti, E., Pearson, F.J., Thoenen, T., 2002. Nagra / PSI Chemical Thermodynamic Data Base 01/01. NAGRA, NTB 02–16.IAEA, 2009. Geological Disposal of Radioactive Waste: Technological Omplications for Retrievability. International Atomic Energy Agency, NW-T-1.19, Vienna.

IAEA, 2011. Disposal of Radioactive Waste. International Atomic Energy Agency, Specific Safety Requirements No. SSR-5, Vienna.

IAEA, 2013. The Behaviours of Cementitious Materials in Long Term Storage and Disposal of Radioactive Waste. International Atomic Energy Agency, IAEA-TECDOC-1701, Vienna.

Idemitsu, K., Matsuki, Y., Kishimoto, M., Inagaki, Y., Arima, T., Haruguchi, Y., Yamashita, Y., Sasoh, M., 2013. Migration of iodine solidified in ettringite into compacted bentonite. Ceram. Trans. 241, 23-34.

Idiart, A., 2017. Preliminary results and interpretation of the modelling of WP1 & WP2 experiments. CEBAMA, Deliverable D3.05, http://www.cebama.eu/Home/Deliverables, pp. 10 - 17.

Iwaida, T., Yano, K., Tanaka, S., Nagasaki, S., 2001. Synthesis and characterization of sulfate-iodate ettringite; and their potential role in immobilization of 129I. Genshiryoku Bakkuendo Kenkyu 7, 57-63.

Jacques, D., Wang, L., Martens, E., Mallants, D., 2008. Time dependency of the geochemical boundary conditions for the cementitious engineered barriers of the Belgian surface disposal facility, project near surface disposal of category: a waste at Dessel. NIRAS-MP5 DATA-LT (NF) Version 1, 2008-2024.

Jalilehvand, F., Spångberg, D., Lindqvist-Reis, P., Hermansson, K., Persson, I., Sandström, M., 2001. Hydration of the calcium ion. An EXAFS, large-angle X-ray scattering, and molecular dynamics simulation study. J. Am. Chem. Soc. 123, 431-441.

Jantzen, C., Johnson, A., Read, D., Stegemann, J.A., 2010. Cements in waste management. Adv. Cem. Res. 22, 225-231.

Jimenez, A., Prieto, M., 2015. Thermal stability of ettringite exposed to atmosphere: Implications for the uptake of harmful ions by cement. Environ. Sci. Technol. 49, 7957-7964.

Jones, M.J., Butchins, L.J., Charnock, J.M., Pattrick, R.A.D., Small, J.S., Vaughan, D.J., Wincott, P.L., Livens, F.R., 2011. Reactions of radium and barium with the surfaces of carbonate minerals. Appl. Geochem. 26, 1231-1238.

Kato, H., Mine, T., Mihara, M., Ohi, T., Honda, A., 2002. The sorption database of radionuclides for cementitious materials. JAEA, JNC-TN--8400-2001-029, Japan, p. 63.

Kim, J.-S., Kwon, S., Choi, J.-W., Cho, G.-C., 2011. Properties of low-pH cement grout as a sealing material for the geological disposal of radioactive waste. Nucl. Eng. Technol. 43, 459-468.

Kindness, A., Lachowski, E.E., Minocha, A.K., Glasser, F.P., 1994. Immobilization and fixation of molybdenum (VI) in portland cement. Waste Manage. (N. Y.) 14, 97-102.

Komarneni, S., Roy, R., Roy, D.M., 1986. Pseudomorphism in xonotlite and tobermorite with Co^{2+} and Ni^{2+} exchange for Ca^{2+} at 25°C. Cem. Concr. Res. 16, 47-58.

Komarneni, S., Tsuji, M., 1989. Selective cation exchange in substituted tobermorites. J. Am. Ceram. Soc. 72, 1668-1674.

Kommission Lagerung hoch radioaktiver Abfallstoffe, 2016. Abschlussbericht, K-Drs. 268.

Kronlöf, A., 2003. Development of Cement Based Materials for Grouting of Rock at Olkiluoto. VTT BUILDING AND TRANSPORT, Working Report 2003-29, Finland.

Kugel, K., Möller, K., 2017. An forderungen an endzulagernde radioaktive Abfälle - Endlager Konrad, Federal Office for Radiation Protection. BfS, BfS-Bericht SE-IB-29/08-REV-3.

Kursten, B., Smailos, E., Azkarate, I., Werme, L., Smart, N.R., Santarini, G., 2004. State-of-the-art document on the COrrosion BEhaviour of COntainer MAterials. EUROPEAN COMMISSION, FINAL REPORT FIKW-CT-20014-20138.

Labbez, C., Nonat, A., Pochard, I., Jönsson, B., 2007. Experimental and theoretical evidence of overcharging of calcium silicate hydrate. J. Colloid Interface Sci. 309, 303-307.

Labbez, C., Pochard, I., Jönsson, B., Nonat, A., 2011. C-S-H/solution interface: Experimental and Monte Carlo studies. Cem. Concr. Res. 41, 161-168.

Lachowski, E.E., Hong, S.Y., Glasser, F.P., 2000. Crystallinity in C-S-H gels: influence of preparation and cure conditions. RILEM Proc. PRO 13, 215-225.

Lager, G.A., Armbruster, T., Faber, J., 1987. Neutron and X-ray diffraction study of hydrogarnet $Ca_3Al_2(O_4H_4)_3$. Am. Mineral. 72, 756-765.

Latimer, W.M., 1951. Methods of Estimating the Entropies of Solid Compounds. J. Am. Chem. Soc. 73, 1480-1482.

Li, G., Le Bescop, P., Moranville-Regourd, M., 1997. Synthesis of the U phase ($4CaO_{0.9}Al_2O_3 \cdot 1.1SO_3 \cdot 0.5Na_2O \cdot 16H_2O$). Cem. Concr. Res. 27, 7-13.

Li, G., Le Bescop, P., Moranville, M., 1996. The U phase formation in cement-based systems containing high amounts of Na_2SO_4. Cem. Concr. Res. 26, 27-33.

Lidman, F., Källström, K., Kautsky, U., 2017. Mo-93 from the grave to the cradle, Report from a workshop on molybdenum in radioactive waste and in the environment. . SKB Report, P-16-22.

Liu, X., Vinograd, V.L., Bosbach, D., Winkler, B., 2016. Atomistic simulation study of ternary $(Ca,Ba,Sr)CO_3$ solid solutions, 24th Annual Conference of the German Crystallographic Society Z. Kristallog, Stuttgart, Germany.

Lothenbach, B., Le Saout, G., Ben Haha, M., Figi, R., Wieland, E., 2012. Hydration of a low-alkali CEM III/B-SiO2 cement (LAC). Cem. Concr. Res. 42, 410-423.

Lothenbach, B., Nonat, A., 2015. Calcium silicate hydrates: Solid and liquid phase composition. Cem. Concr. Res. 78, 57-70.

Lothenbach, B., Wieland, E., 2006. A thermodynamic approach to the hydration of sulphate-resisting Portland cement. Waste Manage. 26, 706-719.

Ma, B., Fernandez-Martinez, A., Findling, N., Koishi, A., Tisserand, D., Bureau, S., Charlet, L., Grangeon, S., Tournassat, C., Claret, F., Marty, N.C.M., Salas-Colera, E., Salas-Colera, E., Elkaim, E., Marini, C., 2017. Evidence of multiple sorption modes in layered double hydroxides using Mo as structural probe. Environ Sci Technol. 51, 5531-5540.

Martin, L.H.J., Leemann, A., Milodowski, A.E., Mäder, U.K., Münch, B., Giroud, N., 2016. A natural cement analogue study to understand the long-term behaviour of cements in nuclear waste repositories: Maqarin (Jordan). Appl. Geochem. 71, 20-34.

Marty, N.C.M., Grangeon, S., Elkaïm, E., Tournassat, C., Fauchet, C., Claret, F., 2018. Thermodynamic and crystallographic model for anion uptake by hydrated calcium aluminate (AFm): an example of molybdenum. Scientific reports 8, 7943.

Maruyama, I., Igarashi, G., Nishioka, Y., 2015. Bimodal behavior of C-S-H interpreted from short-term length change and water vapor sorption isotherms of hardened cement paste. Cem. Concr. Res. 73, 158-168.

Matschei, T., Lothenbach, B., Glasser, F.P., 2006. The AFm phase in Portland cement. Cem. Concr. Res. 37, 118-130.

Matschei, T., Lothenbach, B., Glasser, F.P., 2007. Thermodynamic properties of Portland cement hydrates in the system CaO-Al_2O_3-SiO_2-$CaSO_4$-$CaCO_3$-H_2O. Cem. Concr. Res. 37, 1379-1410.

Matsuda, A., Mori, H., 2014a. A quantum chemical study on hydration of Ra (II): Comparison with the other hydrated divalent alkaline earth metal ions. J. Comput. Chem., Japan 13, 105-113.

Matsuda, A., Mori, H., 2014b. Theoretical study on the hydration structure of divalent radium ion using Fragment Molecular Orbital–Molecular Dynamics (FMO–MD) simulation. J. Solution Chem. 43, 1669-1675.

Mattigod, S.V., Whyatt, G.A., Serne, J.R., Wood, M.I., 2004. Diffusion of iodine and technetium-99 through waste encasement concrete and unsaturated soil fill material. Mater. Res. Soc. Symp. Proc. 824, 391-398.

Mattigod, S.V., Whyatt, G.A., Serne, R.J., Martin, P.F., Schwab, K.E., Wood, M.I., 2001. Diffusion and leaching of selected radionuclides (Iodine-129, Technetium-99, and Uranium) through category 3 waste encasement concrete and soil fill material. Pacific Northwest National Laboratory (PNNL), , PNNL-13639, Richland, WA (US).

Mauke, R., Herbert, H.J., 2015. Large scale in-situ experiments on sealing constructions in underground disposal facilities for radioactive wastes – Examples of recent BfS- and GRS-activities. Prog. Nucl. Energy 84, 6-17.

Merlini, M., Artioli, G., Meneghini, C., Cerulli, T., Bravo, A., Cella, F., 2007. The early hydration and the set of Portland cements: In situ X-ray powder diffraction studies. Powder Diffr. 22, 201-208.

Minocha, A.K., Goyal, M.K., 2013. Immobilization of molybdenum in ordinary Portland cement. J. Chem. Eng. Process Technol. 4, 1000162/1000161-1000162/1000166, 1000166 pp.

Minocha, A.K., Kumar, P., Singh, J., Aggarwal, L.K., Verma, C.L., 2004. Effect of molybdate (II), chromium (III) and (VI) metal ions on the setting time of ordinary portland cement. Indian J. Environ. Prot. 24, 771-774.

Missana, T., García-Gutiérrez, M., Mingarro, M., Alonso, U., 2017. Analysis of barium retention mechanisms on calcium silicate hydrate phases. Cem. Concr. Res. 93, 8-16.

Mokka, J., 2015. Press releases. Posiva.

Mondal, P., Jeffery, J.W., 1975. The crystal structure of tricalcium aluminate, $Ca_3Al_2O_6$. Acta Cryst. Section B 31, 689-697.

NAGRA, 2002. Project Opalinus Clay: safety report: demonstration of disposal feasibility for spent fuel, vitrified high-level waste and long-lived intermediate-level waste (Entsorgungsnachweis). NAGRA, NTB 02–05.

NAGRA, 2006. Im Vergleich: Entsorgungskonzepte gestern und heute. http://www.nagra.ch/de/tiefenlager.htm. Accessed August 2018.

NAGRA, 2008. Entsorgungsprogramm 2008 der Entsorgungspflichtigen. Technischer Bericht 08-01.

NDA, 2017. Annual Report & Accounts 2016/17. NDA, HC269, UK.

Niibori, Y., Funabashi, T., Mimura, H., 2012. Some experiments on sorption behavior of iodide ions into C-S-H gel under the condition saturated with saline groundwater. MRS Online Proc. Libr. 1518, 2012.1715/2011-2012.1715/2016.

Nonat, A., 2004. The structure and stoichiometry of C-S-H. Cem. Concr. Res. 34, 1521-1528.

Noshita, K., Nishi, T., Yoshida, T., Fujihara, H., Saito, N., Tanaka, S., 2002. Categorization of cement hydrates by radionuclide sorption mechanism. Mater. Res. Soc. Symp. Proc. 663, 115-121.

Ochs, M., Mallants, D., Wang, L., 2016. Radionuclide and metal sorption on cement and concrete. Springer International Publishing Switzerland 2016, Switzerland.

Ojovan, M.I., Lee, W.E., 2014. An introduction to nuclear waste immobilisation, Second Edition ed. Elsevier, UK.

ONDRAF/NIRAS, 2001. Technical overview of the SAFIR 2 report. ONDRAF/NIRAS, NIROND 2001–05 E, Brussels.

Parkhurst, D.L., Appelo, C., 2013. Description of input and examples for PHREEQC version 3: a computer program for speciation, batch-reaction, one-dimensional transport, and inverse geochemical calculations. US Geological Survey, 2328-7055.

Perdew, J.P., Burke, K., Ernzerhof, M., 1996. Generalized gradient approximation made simple. Phys. Rev. Lett. 77, 3865-3868.

Pointeau, I., Coreau, N., Reiller, P.E., 2008. Uptake of anionic radionuclides onto degraded cement pastes and competing effect of organic ligands. Radiochim. Acta 96, 367-374.

Pommersheim, J., Chang, J., 1986. Kinetics of hydration of tricalcium aluminate. Cem. Concr. Res. 16, 440-450.

Poyet, S., 2006. The Belgian supercontainer concept: Study of the concrete buffer behaviour in service life, Journal de Physique IV (Proceedings). EDP sciences, pp. 167-175.

Ranft, M., Regenauer, U., Weiser, A., 2010. Notfallplanung für das Endlager Asse. BfS Federal Office for Radiation Protection

Rapin, J.-P., Walcarius, A., Lefevre, G., Francois, M., 1999. A double-layered hydroxide, $3CaO{\cdot}Al_2O_3{\cdot}CaI_2{\cdot}10H_2O$. Acta Crystallogr., Sect. C: Cryst. Struct. Commun. C55, 1957-1959.

Richardson, I., 2014. Model structures for C-(A)-S-H(I). Acta Crystallogr. Sect. B 70, 903-923.

Richardson, I.G., 2004. Tobermorite/jennite- and tobermorite/calcium hydroxide-based models for the structure of C-S-H: applicability to hardened pastes of tricalcium silicate, β-dicalcium silicate, Portland cement, and blends of Portland cement with blast-furnace slag, metakaolin, or silica fume. Cem. Concr. Res. 34, 1733-1777.

Richardson, I.G., 2008. The calcium silicate hydrates. Cem. Concr. Res. 38, 137-158.

Roller, P.S., Ervin, G., 1940. The system calcium-oxide-silica-water at 30°. The association of silicate* ion in dilute alkaline solution. J. Am. Chem. Soc. 62, 461-471.

Sarott, F.A., Bradbury, M.H., Pandolfo, P., Spieler, P., 1992. Diffusion and adsorption studies on hardened cement paste and the effect of carbonation on diffusion rates. Cem. Concr. Res. 22, 439-444.

Saslow, S.A., Um, W., Russell, R.L., Williams, B.D., Assmussen, R.M., Varga, T., Qafoku, O., Riley, B.J., Lawter, A.R., Snyder, M.M.V., Baum, S.R., Leavy, I.I., 2018. Effluent management facility evaporator bottoms: Waste streams formulation and waste form qualificationt testing. ; Pacific Northwest National Lab. (PNNL), Richland, WA (United States), RPT-SWCS-012, Rev 1.0; PNNL-26570, Rev 1.0 United States 10.2172/1460056 PNNL English, p. Medium: ED; Size: 138 p.

Schatz, T., Martikainen, J., 2012. Laboratory tests and analyses on potential Olkiluoto backfill materials. B+TECH Oy, Working Report 2012-74, Finland.

Scrivener, K.L., Juilland, P., Monteiro, P.J.M., 2015. Advances in understanding hydration of Portland cement. Cem. Concr. Res. 78, 38-56.

Sejkora, J., Čejka, J., Malíková, R., López, A., Xi, Y., Frost, R.L., 2014. A Raman spectroscopic study of a hydrated molybdate mineral ferrimolybdite, $Fe_2(MoO_4)_3 \cdot 7–8H_2O$. Spectrochim. Acta A, 130, 83-89.

Soyer-Usun, S., Chae Sejung, R., Benmore, C. J., Wenk H. R., Monteiro, P.J.M., 2012. Compositional evolution of calcium silicate hydrate (C–S–H) structures by Total X-Ray Scattering. J. Am. Ceram. Soc. 95, 793-798.

Shannon, R.D., Prewitt, C.T., 1969. Effective ionic radii in oxides and fluorides. Acta Crystallogr. Sect. B 25, 925-946.

Shirai, K., Niibori, Y., Kirishima, A., Mimura, H., 2011. Sorption behavior of iodine on calcium silicate hydrates formed as a secondary mineral. American Society of Mechanical Engineers, pp. 237-242.

Shock, E.L., Sassani, D.C., Willis, M., Sverjensky, D.A., 1997. Inorganic species in geologic fluids: Correlations among standard molal thermodynamic properties of aqueous ions and hydroxide complexes. Geochim. Cosmochim. Acta 61, 907-950.

Shrivastava, O.P., Glasser, F.P., 1986. Ion-exchange properties of 11-Å tobermorite. Reactivity of Solids 2, 261-268.

Shrivastava, O.P., Komarneni, S., 1994. Cesium selectivity of (Al+Na)-substituted tobermorite. Cem. Concr. Res. 24, 573-579.

SKB, 2010. Radionuclide transport report for the safety assessment SR-Site. SKB, TR-10-50.

SKB, 2011. Long-term safety for the final repository for spent nuclear fuel at Forsmark. SKB, Technical Report TR-11–01.

Smith, D.W., 1977. Ionic hydration enthalpies. J. Chem. Educ. 54, 540.

Smith, R.W., Walton, J.C., 1993. The role of oxygen diffusion in the release of technetium from reducing cementitious waste forms. Mater. Res. Soc. Symp. Proc. 294, 247-253.

Stumm, W., 1992. Chemistry of the solid-water interface: Processes at the mineral-water and particle-water interface in natural systems. John Wiley & Son Inc.

Sugiyama, D., 2008. Chemical alteration of calcium silicate hydrate (C–S–H) in sodium chloride solution. Cem. Concr. Res. 38, 1270-1275.

Sugiyama, D., Fujita, T., 1999. Sorption of radionuclides onto cement materials altered by hydrothermal reaction. Mater. Res. Soc. Symp. Proc. 556, 1123-1130.

Tallent, O.K., McDaniel, E.W., Cul, G.D.D., Dodson, K.E., Trotter, D.R., 1987. Immobilization of technetium and nitrate in cement-based materials. MRS Online Proceedings Library Archive 112.

Tanabe, H., Sakuragi, T., Yamaguchi, K., Sato, T., Owada, H., 2010. Development of new waste forms to immobilize iodine-129 released from a spent fuel reprocessing plant. Adv. Sci. Technol. 73, 158-170.

Taylor, H.F.W., 1950. Hydrated calcium silicates. I. Compound formation at ordinary temperatures. J. Chem. Soc., 3682-3690.

Taylor, H.F.W., 1997. Cement Chemistry. Thomas Telford Publishing, London, UK.

Taylor, H.F.W., Newbury, D.E., 1984. An electron microprobe study of a mature cement paste. Cem. Concr. Res. 14, 565-573.

Terai, T., Mikuni, A., Nakamura, Y., Ikeda, K., 2007. Synthesis of ettringite from portlandite suspensions at various Ca/Al ratios. Inorg. Mater. 43, 786-792.

The Federal Office for Radiation Protection, 2009. Schachtanlage Asse II–Beschreibung und Bewertung der Stilllegungsoption Vollverfüllung. AF-Colenco AG, Gesellschaft für Anlagen- und Reaktorsicherheit (GRS) mbH, IfG Institut für Gebirgsmechanik GbH, Baden-Dättwil/Braunschweig/Leipzig 1, 2009.

Thoenen, T., Hummel, W., Berner, U., Curti, E., 2014. The PSI/Nagra Chemical Thermodynamic Database 12/07, NAB 14-49.

Tits, J., Gaona, X., Laube, A., Wieland, E., 2014. Influence of the redox state on the neptunium sorption under alkaline conditions: Batch sorption studies on titanium dioxide and calcium silicate hydrates. Radiochim. Acta 102, 385-400.

Tits, J., Geipel, G., Mace, N., Eilzer, M., Wieland, E., 2011. Determination of uranium(VI) sorbed species in calcium silicate hydrate phases: A laser-induced luminescence spectroscopy and batch sorption study. J. Colloid Interface Sci. 359, 248-256.

Tits, J., Iijima, K., Wieland, E., Kamei, G., 2006a. The uptake of radium by calcium silicate hydrates and hardened cement paste. Radiochim. Acta 94, 637-643.

Tits, J., Wieland, E., Mueller, C.J., Landesman, C., Bradbury, M.H., 2006b. Strontium binding by calcium silicate hydrates. J. Colloid Interface Sci. 300, 78-87.

Toyohara, M., Kaneko, M., Mitsutsuka, N., Fujihara, H., Saito, N., Murase, T., 2002. Contribution to understanding iodine sorption mechanism onto mixed solid alumina cement and calcium compounds. J. Nucl. Sci. Technol. 39, 950-956.

Trägårdh, J., Lagerblad, B., 1998. Leaching of 90-year old concrete mortar in contact with stagnant water. Svensk kärnbränslehantering AB/Swedish Nuclear Fuel and Waste Management, TR-98-11.

Tuerker, P., Yesilkaya, A., Yeginobali, A., 2003. The hydration process and the microstructure development of Portland limestone cements. Thomas Telford Ltd., pp. 93-102.

Van Cotthem, A., Van Humbeeck, H., Biurrun, E., 2012. Underground Architecture and Layout for the Belgian High-Level and Long-Lived Intermediate-Level Radioactive Waste Disposal Facility-12116, Proceedings of the WM2012 Conference. Proceedings of the WM2012 Conference.

Vanderbilt, D., 1990. Soft self-consistent pseudopotentials in a generalized eigenvalue formalism. Phys. Rev. B 41, 7892-7895.

Vehmas, T., Schnidler, A., Löija, M., Leivo, M., Holt, E., 2017. Reference mix design and castings for low-pH concrete for nuclear waste repositories, in: Altmaier, M., Montoya, V., Duro, L., Valls, A. (Eds.), Proceedings of the First Annual Workshop of the HORIZON 2020

CEBAMA Project. KIT Scientific Publishing, KIT Scientific Reports 7734, Karlsruhe, pp. 101-111.

Verein Deutscher Zementwerke, 2008. Taschenbuch Zement, Verein Deutscher Zementwerke e.V. (Hrsg.), Düsseldorf.– Düsseldorf: Verlag Bau+Technik.

Wacquier, W., 2012. Summary of the Safety Report for the Surface Repository of Category A Waste in Dessel. ONDRAF/NIRAS, NIROND-TR, NIROND-TR 2012-17 E.

Wang, L., 2009. Near-field chemistry of a HLW/SF repository in Boom Clay - scoping calculations relevant to the supercontainer design. SCK-CEN, SCK-CEN-ER-17, Belgium.

Wang, L., 2013. Solubility of radionuclides in Supercontainer concrete. SCK-CEN, SCK-CEN ER-239.

Wei, Y., Yao, W., 2013. Quantitative characterization of hydration of cement pastes by Rietveld phase analysis and thermoanalysis. Key Eng. Mater. 539, 19-24, 17 pp.

Wersin, P., Johnson, L.H., Schwyn, B., Berner, U., Curti, E., 2003. Redox Conditions in the Near Field of a Repository for SF/HLW and ILW in Opalinus Clay. NAGRA, TECHNICAL REPORT 02-13.

Wieland, E., 2014. Sorption data base for the cementitious near field of L/ILW and ILW repositories for provisional safety analyses for SGT-E2. NAGRA, Technical Report 14-08.

Wieland, E., Tits, J., Kunz, D., Daehn, R., 2008. Strontium uptake by cementitious materials. Environ. Sci. Technol. 42, 403-409.

Wieland, E., Tits, J., Spieler, P., Dobler, J.P., 1998. Interaction of Eu(III) and Th(IV) with sulfate-resisting portland cement. Mater. Res. Soc. Symp. Proc. 506, 573-578.

Wieland, E., Van Loon, L., 2002. Near-field sorption database for performance assessment of a ILW repository in Opalinus clay and crystalline host rock. Paul Scherrer Institut, Technical Report 02-20.

Wilson, J., Benbow, S., Metcalfe, R., 2017. Understanding the long-term evolution of cement backfills: alteration of NRVB due to reaction with groundwater solutes, RWM/03/043 ed. AMEC, 202387/002 Issue A, United Kingdom.

WNA, 2018. Radioactive Waste Managem http://www.world-nuclear.org/information-library/nuclear-fuel-cycle/nuclear-wastes/radioactive-waste-management.aspx ent. Accessed July 2018.

Yalcintas, E., Scheinost, A.C., Gaona, X., Altmaier, M., 2016. Systematic XAS study on the reduction and uptake of Tc by magnetite and mackinawite. Dalton Trans. 45, 17874-17885.

Yang, X.N., Zhou, W.Y., Wang, R.S., 1995. Study of the immobilization of ^{226}Ra. II. Predictive model of radionuclide leaching behavior in a cement-based solid. J. Radioanal. Nucl. Chem. 198, 287-294.

Zhang, M., 2000. Incorporation of oxyanionic boron, chromium, molybdenum, and selenium into hydrocalumite and ettringite: application to cementitious systems. University of Waterloo, Ontario, Canada, p. 172 pp.

Zhou, Q., Glasser, F.P., 2000. Kinetics and mechanism of the carbonation of ettringite. Adv. Cem. Res. 12, 131-136.

12. Already published parts of this PhD thesis

Publications

Lange, S., Kowalski, P.M., Pšenička, M., Klinkenberg, M., Rohmen, S., Bosbach, D., Deissmann, G., 2018. Uptake of ^{226}Ra in cementitious systems: A complementary solution chemistry and atomistic simulation study. Applied Geochemistry 96, 204-216.

Conference presentations

Kowalski, P.M., Lange, S., Burek, K., McGee, S., Pšenička, M., Vinograd, V., Klinkenberg, M., Rohmen, S., Kumke, M., Bosbach, D., Deissmann, G. 2018. Uptake of Ra and Eu in cementitious systems by joint solution chemistry and atomistic modeling studies. MRS Fall Meeting, November 25 – 30, 2018, Boston, MA, USA.

Lange, S., Isaacs, M., Klinkenberg M., Read D., Bosbach D., Deissmann G., 2018. Uptake mechanisms of radionuclides in cementitious systems: Insights from atomistic simulations. Cebama 3rd Annual Workshop, Nantes, France.

Isaacs, M., Lange, S., Deissmann, G., Bosbach D., Rastrick, E., Felipe-Sotelo, M., Read D., 2018, Retention and mobility studies of safety relevant radionuclides in cementitious materials. Cebama 3rd Annual Workshop, Nantes, France.

Lange, S., Isaacs, M., Klinkenberg M., Read D., Bosbach D., Deissmann G., 2017. Retention mechanisms for safety relevant radionuclides in cementitious materials. Goldschmidt Conference 2017, Paris, France.

Lange, S., Isaacs, M., Klinkenberg M., Read D., Bosbach D., Deissmann G., 2017. Structural investigations on the uptake of long-lived safety relevant radionuclides by cementitious materials. Cebama 2nd Annual Workshop, Helsinki, Finland.

Poster

Lange, S., Klinkenberg, M., Bosbach, D., Deissmann, G. 2019. Retention of molybdenum in cementitious systems. 5th International Workshop on "Mechanisms and Modelling of Waste/Cement Interactions", 25. – 27. March 2019, Karlsruhe, Germany.

Lange, S., Klinkenberg, M., Kowalski, P.M., Bosbach, D., Deissmann, G. 2018. Uptake and retention of ^{226}Ra by cementitious materials: A complementary solution chemistry and atomistic simulation study. NUWCEM 2018, 24 – 26 October 2018, Avignon, France.

Kittnerová, J., Lange, S., Drtinová, B., Deissmann, G., Bosbach, D., Vopálka, D. 2018. Impact of carbonation on the uptake of radium by cementitious materials. NUWCEM 2018, 24 – 26 October 2018, Avignon, France.

Burek, K., Lange, S., Baaske, J., McGee, S., Kumke, M., Kowalski, P.M., Bosbach, D., Deissmann, G. 2018. Eu(III) uptake by cementitious materials: A combined TRLFS and atomistic simulation study. NUWCEM 2018, 24 – 26 October 2018, Avignon, France.

Lange, S., Isaacs, M., Klinkenberg M., Read D., Bosbach D., Deissmann G., 2017. Uptake of long-lived safety relevant radionuclides by cementitious materials and hardened cement pastes. 16th International Conference on the Chemistry and Migration Behaviour of Actinides and Fission Products in the Geosphere (Migration 2017), Barcelona, Spain.

Lange, S., Deissmann, G., Bosbach D., 2017. Interaction of long-lived safety relevant radionuclides with cementitious materials. Tagung der Deutsche Arbeitsgemeinschaft Endlagerforschung (DAEF 2016), Cologne, Germany.

Lange, S., Deissmann, G., Bosbach D., 2016. Structural uptake and retention of safety relevant radionuclides in cementitious systems. 4th International Workshop on Mechanisms and Modelling of Waste / Cement Interactions, Murten, Switzerland.

13. Eidesstattliche Erklärung

Hiermit versichere ich eidesstattlich, dass ich die Dissertation selbstständig verfasst und alle in Anspruch genommenen Hilfen in der Dissertation angegeben habe.

Unterschrift | Ort, Datum

Die Dissertation wurde außerhalb der RWTH-Aachen an der Forschungszentrum Jülich GmbH angefertigt.

Hiermit erkläre ich, dass mit Veröffentlichung der Dissertation keine bestehenden Betriebsgeheimnisse verletzt werden.

Unterschrift | Ort, Datum

Band / Volume 466
Initialinfrastruktur für Wasserstoffmobilität auf Basis von Flotten
F. Grüger (2019), V, 209 pp
ISBN: 978-3-95806-413-3

Band / Volume 467
Techno-ökonomische Analyse alternativer Wasserstoffinfrastruktur
M. E. Reuß (2019), 205 pp
ISBN: 978-3-95806-414-0

Band / Volume 468
Study on a miniaturized satellite payload for atmospheric temperature measurements
J. Liu (2019), 153 pp
ISBN: 978-3-95806-415-7

Band / Volume 469
Partitioning Water Vapor Fluxes by the Use of Their Water Stable Isotopologues: From the Lab to the Field
M. E. Quade (2019), XVI, 113 pp
ISBN: 978-3-95806-417-1

Band / Volume 470
Entwicklung von Reparaturmethoden für Nickel-Superlegierungen mittels thermischer Spritzverfahren
T. Kalfhaus (2019), VI, 126, XXX pp
ISBN: 978-3-95806-418-8

Band / Volume 471
Entwicklung von korrosionsstabilen Schutzschichten für oxidische Faserverbundwerkstoffe
C. S. Gatzen (2019), II, 143 pp
ISBN: 978-3-95806-422-5

Band / Volume 472
Coatings for Metallic Bipolar Plates in High-Temperature Polymer Electrolyte Fuel Cells
R. Li (2019), II, 119 pp
ISBN: 978-3-95806-425-6

Band / Volume 473
Thermochemische Eigenschaften von kombinierten Katalysator- und Sauerstoffträgersystemen für die partielle Oxidation von Teeren aus der Biomassevergasung
M. Ma (2019), VII, 157 pp
ISBN: 978-3-95806-426-3

Band / Volume 474
Einfluss der klimatischen Fertigungsumgebung auf die Mechanik und Rissstrukturierung der elektrodenbeschichteten Membran einer PEM-Brennstoffzelle
B. Wienk-Borgert (2019), IV, 141 pp
ISBN: 978-3-95806-428-7

Band / Volume 475
Reversible wasserstoffbetriebene Festoxidzellensysteme
M. H. Frank (2019), 187 pp
ISBN: 978-3-95806-430-0

Band / Volume 476
Partitioning of carbon dioxide exchange in rapidly and slowly changing ecosystems
P. Ney (2019), xvi, 95 pp
ISBN: 978-3-95806-431-7

Band / Volume 477
Massentransportphänomene in Schichtsystemen eines Elektrolyseurs
U. Panchenko (2019), 107 pp
ISBN: 978-3-95806-433-1

Band / Volume 478
Mechanische Eigenschaften von Polymer-Elektrolyt-Membran-Brennstoffzellen
P. Irmscher (2019), vii, 177 pp
ISBN: 978-3-95806-435-5

Band / Volume 479
Morphology and Degradation of High Temperature Polymer Electrolyte Fuel Cell Electrodes
S. Liu (2019), III, 162 pp
ISBN: 978-3-95806-436-2

Band / Volume 480
Structural uptake and retention of safety relevant radionuclides by cementitious materials
S. Lange (2019), 133 pp
ISBN: 978-3-95806-437-9

Energie & Umwelt / Energy & Environment
Band / Volume 480
ISBN 978-3-95806-437-9

Mitglied der Helmholtz-Gemeinschaft

JÜLICH
Forschungszentrum